Internal Report
DESY F41-76/06
July 1976

Dielectric and Optical Properties

by

B. Sonntag

DIELECTRIC AND OPTICAL PROPERTIES

by

B. Sonntag

II. Institut für Experimentalphysik der Universität Hamburg

and

Deutsches Elektronen-Synchrotron DESY, Hamburg, Germany

Chapter 17 of Rare Gas Solids (Eds. M.L. Klein and J.A. Venables),
Academic Press 1976

Contents

Abstract

The dielectric and optical properties of the rare gas solids (RGS) are reviewed. The experimental techniques used for the determination of the dielectric constants, the low frequency refractive indices, for absorption, reflection, electron energy loss, photoconductivity and photoemission measurements are discussed. Experimental results are presented for all RGS. Emphasis is given to the data obtained in the VUV and soft x-ray region, which give detailed information on the electronic states of the RGS. The spectra are compared to the spectra of the corresponding free rare gas atoms and are discussed in terms of atomic excitations, excitons and interband transitions.

1. Introduction

1.1 Electronic structure of the rare gases and optical experiments

The rare gas solids (RGS), which are formed from closed shell atoms bound by weak van der Waals forces, can in many respects be considered as model substances for insulating crystals. Therefore great interest has been shown in the electronic structure of the solid rare gases by both theoreticians and experimentalists. A review of the theoretical calculations of the electron states in solid rare gases has been presented in chapter 8 in Vol. I of this book.

In spite of this great interest, the first systematic investigations were performed less than two decades ago due to the great difficulties encountered. For experiments in the visible region, considerable care has to be taken with crystal growth to prevent unwanted scattering and absorption of light, and the first successful work was that by Jones and coworkers in the 1960's. For absorption and reflection measurements, which probe the excited electronic states, the measurements have to be carried out in the vacuum ultraviolet (VUV) and at even shorter wavelengths and at these wavelengths most other substances show strong absorption. For solid He, Ne and Ar even the absorption threshold lies above the LiF cut off (11.8 eV) where no transparent windows exist. The windowless connection of the gas discharge sources, commonly used in this spectral region, to the spectrometer and the sample chamber causes considerable problems. In particular the heavier RGS (Ne, Ar, Kr and Xe) are usually prepared by vacuum deposition at temperatures below 60 K. An excellent review of the techniques of vacuum ultraviolet spectroscopy has been presented by Samson (1967).

These requirements on specimen preparation cause special problems for the study of solid He, which only exists at high pressure. Accordingly studies of

solid He have been confined to the visible region. There are only some preliminary results on the dielectric constant and low frequency refractive index of solid He and Ne (Haase and Meyer, 1974; Meyer, 1975). The birefringence of hcp He has been determined by Vos et atl. (1967) and by Heybey and Lee (1967). The dielectric constants and low frequency refractive indices of solid Ar, Kr and Xe are discussed in section 2.

Up to now the reflection measurements performed by Surko et al. (1969) on liquid He at 12 K are the only optical investigations of condensed He in the VUV. Surko et al. found a small structure around 20.8 eV followed by strong reflectivity maximum at 21.6 eV. The latter probably originates from the $1s^2\ ^1S_o \rightarrow 1s2p\ ^1P_1$ transition of atomic He shifted towards higher energies by the interaction with the neighbouring atoms. There are no optical data on solid He in the VUV; thus in sections 3, 4 and 5 which deal with the optical, electron-energy loss, photoconductivity and photoemission measurements in the VUV and beyond we are only dealing with Ne, Ar, Kr and Xe, which crystallize in the fcc structure. The microstructure of vapour-deposited films is often far from perfect; although this is rarely determined in optical experiments, examples of the probable microstructure are given by Venables and Smith in chapter 10.

Since the RGS are transparent in such a large photon energy range, they are ideal host crystals for the investigation of impurities imbedded in solid matrices. Matrix isolation spectroscopy using RGS is itself a large subject which is not touched on here. Irradiation of RGS by VUV light, x-rays or γ-rays or bombardement by charged particles produces excited states which can decay by emitting photons. This luminescence of the RGS, especially the fascinating possibilities of high power VUV RGS lasers have brought about a vast amount of interesting results. A review of all the experimental and theoretical aspects of the luminescence of RGS would fill a separate chapter and therefore is not included in the present chapter. It is interesting to note that the first optical experiments on RGS were concerned with the luminescence of solid Ar. McLennan and Shrum (1929), Vegard (1930, 1934)).

The optical properties of rare gas atoms have been studied extensively, starting with the refractive index measurements of Cuthbertson (1911) and extended into the ultraviolet in the 1920's by Lyman and Saunders (1925), Saunders (1925, 1927) Dargelo and Abbink (1926, 1927), Cuthbertson (1927) and Hertz and Abbink (1926). In more recent years the properties in the VUV and soft x-ray region have been thoroughly investigated both experimentally (Samson (1966), Codling et al. (1967), Deslattes (1968), Madden et al. (1969), Krause (1969), Watson and Morgan (1969), Wuilleumier and Combet Franoux (1969), Wuilleumier (1970), Wuilleumier and Bonnelle (1970), Hubbel (1971), Codling and Madden (1972), Hudson and Kiefer (1971), Wuilleumier and Krause (1971)) and theoretically (Brandt et al. (1967), Fano and Cooper (1968), McGuire (1968), Starace (1970), Amusia et al. (1971), Amusia (1973, 1974), Kennedy and Manson (1972), Lin (1974), Kelly and Simons (1973), Wendin (1973, 1974)). This opens the possibility of a detailed comparison of the spectra of the rare gases in the solid and the gaseous phase. We will see later that this comparison turns out to be an excellent tool for understanding the spectra of the RGS. This does not only hold for the gross features of the spectra but also in part for the sharp excitonic structures which show up at the onset of transitions from the valence band and inner shells. For reference, the binding energies of the occupied levels of the rare gas atoms are compiled in Table I.

1.2 Optical Constants

The linear response of a solid to an electromagnetic wave can be described by the frequency dependent complex dielectric function

$$\tilde{\varepsilon}(\omega) = \varepsilon_1(\omega) + i\varepsilon_2(\omega) \tag{1.1}$$

An entirely equivalent representation is obtained by the use of the complex index of refraction

$$\tilde{n}(\omega) = n(\omega) + i\kappa(\omega) \tag{1.2}$$

Maxwell's relation connects the dielectric function $\tilde{\varepsilon}(\omega)$ to the index of refraction $\tilde{n}(\omega)$

$$\tilde{\varepsilon}(\omega) = \tilde{n}^2(\omega) \tag{1.3}$$

Inserting (1.1) and (1.2) into (1.3) leads to the following relations for the components

$$\varepsilon_1 = n^2 - \kappa^2, \tag{1.4}$$

$$\varepsilon_2 = 2n\kappa\,, \tag{1.5}$$

The dispersion of the wave propagating through a solid is given by n, the damping by κ. The intensity I transmitted through a thin slab of thickness d is determined by

$$I = I_o\, e^{-\mu d}, \tag{1.6}$$

where I_o is the intensity of the incoming wave. The linear absorption coefficient μ is therefore connected to κ and ε_2 by the relation:

$$\mu = \frac{2\omega\kappa}{c} = \frac{\omega\varepsilon_2}{nc} \tag{1.7}$$

where c is the velocity of light in vacuo.

The well-known Fresnel equations (see, for example, Wolter, 1956) give the complex reflectivity $\tilde{r}$ at a vacuum solid interface. At normal incidence they reduce to

$$\tilde{r} = \frac{\tilde{n}(\omega)-1}{\tilde{n}(\omega)+1} = r\cdot e^{i\Theta} \tag{1.8}$$

The intensity of the reflected light is determined by $R = r^2$. The real part $\varepsilon_1(\omega)$ and the imagninary part $\varepsilon_2(\omega)$ of the dielectric function are connected by the Kramers-Kronig relations

$$\varepsilon_1(\omega) - 1 = \frac{2}{\pi} P \int_0^\infty \frac{\omega'\varepsilon_2(\omega')d\omega'}{\omega'^2-\omega^2}$$

$$\varepsilon_2(\omega) = \frac{2\omega}{\pi} P \int_0^\infty \frac{\varepsilon_1(\omega')d\omega'}{\omega^2-\omega'^2} \tag{1.9}$$

where P indicates the Cauchy principle value of the integral. Corresponding relations exist for an and κ.

$$n(\omega) - 1 = \frac{2}{\pi} P \int_0^\infty \frac{\omega'\kappa(\omega')}{\omega'^2-\omega^2}\, d\omega'$$

$$\kappa(\omega) = \frac{2\omega}{\pi} P \int_0^\infty \frac{n(\omega')-1}{\omega^2-\omega'^2}\, d\omega' \tag{1.10}$$

The phase Θ of the reflection is connected to r by the Kramers-Kronig relation

$$\Theta(\omega) = \frac{2\omega}{\pi} \int_0^\infty \frac{\ell n r(\omega') - \ell n\, r(\omega)}{\omega^2-\omega'^2}\, d\omega' \tag{1.11}$$

For the determination of the dielectric constants from energy loss spectra the following Kramers-Kronig relation is used frequently:

$$1 - \mathrm{Re}\,\frac{1}{\varepsilon(\omega)} = \frac{2}{\pi}\,P\int_0^\infty -\mathrm{Im}\,\frac{1}{\varepsilon(\omega')}\;\frac{\omega'}{\omega'^2-\omega^2}\,d\omega' \qquad (1.12)$$

Various sum rules have been derived, which are very valuable in analyzing and testing data (e.g. Altarelli et al.,1972). Equations (1.13) to (1.16) give sum rules which have been proven to be of great practical importance.

$$\int_0^\infty (n(\omega)-1)\,d\omega = 0 \qquad (1.13)$$

$$\int_0^\infty \omega\kappa(\omega)\,(n(\omega)-1)\,d\omega = 0 \qquad (1.14)$$

$$\int_0^\infty \omega\kappa(\omega)\,d\omega = \frac{1}{4}\,\pi\,\omega_p^{\,2} \qquad (1.15)$$

$$\int_0^\infty \omega\varepsilon_2(\omega)\,d\omega = \frac{1}{2}\,\pi\omega_p^{\,2} \qquad (1.16)$$

Here ω_p is the plasma frequency given by

$$\omega_p = \left(\frac{4\pi Ne^2}{m}\right)^{1/2} \qquad (1.17)$$

where N is the electron density and m the electron mass.

By rewriting (1.15) and (1.16) in terms of the number n_{eff} of electrons per atom which contribute to the optical properties in the photon energy range from E_1 to E_2 we can derive equations (1.18) and (1.19) which have turned out to be very useful:

$$n_{eff}(E_1,E_2) = \frac{2mA}{N_A\rho e^2\hbar^2}\int_{E_1}^{E_2} E\;\varepsilon_2(E)\,dE \qquad (1.18)$$

$$n_{eff}(E_1,E_2) = \frac{mcA}{N_A\rho\pi e^2}\int_{E_1}^{E_2} n(E)\mu(E)\,dE \qquad (1.19)$$

where A is the atomic weight, N_A Avogadro's number and ρ the density of the material. These formulae will be used in the following sections.

2. Dielectric constants and refractive indices at frequencies below the valence band transitions

The polarizability of the homogeneous, nonpolar solid such as a RGS is entirely electronic. In a simple model the polarization of the crystal produced by an applied electric field is

$$\vec{P} = Nq\vec{d} \tag{2.1}$$

where q is the magnitude of the charge of the outer electrons of each atom that are displaced a distance $\vec{d}$ with respect to the remaining positive cores (N/unit volume). Furthermore we assume the core itself is rigid and unpolarized. For this simple model the effective field which acts on the atoms in the crystal can be written

$$\vec{E}_{eff} = \vec{E} + (4\pi/3)\gamma\vec{P} \tag{2.2}$$

where $\vec{E}$ is the macroscopic average field in the medium. Guertin and Stern (1964) have shown that for cubic materials $\gamma=1$ if the overlap between the electron distributions of neighbouring atoms is small. This leads to the Lorentz-Lorenz formula for the relation between the dielectric constant ε or the index of refraction n respectively and the atomic polarizability α

$$\frac{(\varepsilon-1)}{(\varepsilon+2)}\frac{1}{\rho} = \frac{(n^2-1)}{(n^2+2)}\frac{1}{\rho} = \frac{4\pi N_A \alpha}{3M} = F_{LL} \tag{2.3}$$

where M is the molecular weight and F_{LL} is termed the Lorentz-Lorentz function. Taking into account the possibility that the polarizability of a rare gas atom in the solid may differ from the free atom value because of the interaction with the neighbouring atoms, the dielectric behaviour of the cubic RGS should be described adequately by Eq. (2.3). For a detailed discussion of the dielectric properties of gases, fluids and solids and their relation to thermodynamic properties the reader is referred to an article by Smith (1974) and to the references cited therein.

2.1 Measurements on the RGS

The low frequency dielectric constant of solid Ar, Kr, and Xe near the melting point have been experimentally determined by Smith and Pings (1963), by Amey and Cole (1964) and by Marcoux (1970a). Lefkowitz et al. (1967) measured the dielectric constant of solid Ar at 77° K. They also studied the influence of some crystal growth parameters on the dielectric constant ε. In all these measurements ε was determined by measuring the ratio of the capacity of a cylindrical condenser filled with the RGS to the capacity of the same condenser in vacuum. The results of these measurements are given in Table II. By reducing the growth rate of the Ar crystal inside the condenser by about a factor of ten Lefkowitz et al. (1967) obtained $\varepsilon = 1.7036$. This clearly demonstrates that the dielectric properties of a RGS sample, as has been shown in many experiments, critically depend on the treatment the sample has undergone, and particularly on the crystal growth parameters, as discussed in Chapter 10, §6.

The refractive indices of condensed Ar, Kr, and Xe have been determined at various wavelengths in the spectral region between 3500 Å and 7000 Å, by Jones and Smith (1960), by Eatwell and Jones (1964), by Sinnock and Smith (1967, 1968), by Smith and Pings (1968), and by Marcoux (1969, 1970 b). Most of the available experimental data are given in a paper by Sinnock and Smith (1969) where the authors also discuss the experimental results in terms of theoretical models. The experimental procedure has been discussed by Smith

(1963). In most of these measurements the spectroscopic method of minimum deviation was employed. In this method a prism-shaped specimen is confined in an optical cell contained in a cryostat and located at the axis of rotation of a spectrometer mounted outside the cryostat on a coaxial turntable. The refractive index n is found from the angle of minimum deviation β and the angle of the prism α by means of the classical relation

$$n = \sin \tfrac{1}{2} (\alpha+\beta)/\sin \tfrac{1}{2} \alpha \qquad (2.4)$$

In the experiments of Marcoux (1969,1970b) the gas to be studied was condensed in a Pyrex tube attached to a Dewar. Light passing through the filled Pyrex tube was focussed by this complex cylindrical lense. By determining the position of the focal line the refractive index could be obtained. The apparatus was calibrated with liquids whose indices are well known.

In all these measurements care was taken to minimize the amount of impurities and defects present in the sample. Specimen free of visual defects were grown from the liquid or the vapor phase near the triple point. The variation of the refractive index with temperature has been carefully studied in several experiments. Even with care, however, it is probable that the solids do not have the equilibrium internal pressure at temperatures far below the triple point, due to adhesion to the walls of the cell.

Kruger and Ames (1959) determined the refractive indices of thin films of Ne, Ar, and Kr condensed on copper or gold mirrors cooled to liquid He temperature by using an ellipsometer. Most of the values obtained by them are lower than the values reported by other authors, almost certainly due to the lower density of crystals vapour deposited at low temperature. The experimentally determined refractive indices for solid Ar, Kr and Xe are given in Figs. 1a, b, c and table III.

According to the theory of dielectric materials based on the Lorentz local field model the Lorentz-Lorenz function F_{LL} (Equ. 2.3) should be constant. The variation of F_{LL} with density measures the variation of the atomic polarizability and should give detailed information on the interatomic forces in RGS. Employing the densities of the solid rare gases given in the literature the Lorentz-Lorenz function F_{LL} has been calculated as a function of density from the refractive indices measured at different temperatures (Jones and Smith,1960; Eatwell and Jones,1964; Sinnock and Smith,1967,1968,1969; Smith and Pings,1968). In all measurements a decrease of the Lorentz-Lorenz function F_{LL} with increasing density has been found. The rate of the decrease increases with increasing density. Only close to the triple point, where the behaviour of the Lorentz-Lorenz function has not been established unambiguously an initial increase of the Lorentz-Lorenz function with increasing density has been reported in some measurements. One of the major problems in this respect are uncertainties in the density of the samples which critically depend on the way the samples have been prepared. The variation of F_{LL} with density for solid Ar is shown in Fig. 2.

Additional information on the dielectric properties, the atomic polarizabilities and the interatomic forces can be obtained by the study of magneto-optical effects. Until now only the Faraday effect of RGS has been studied by Molgaard (1971), who has carried out a careful investigation of the Verdet constant of the RGS in the visible. The Verdet constant describes the rotation of the plane of polarization of linearly polarized light propagating through a medium in the direction of an applied magnetic field. In a simple classical model for free atoms the Verdet constant V can be related to the photon energy $\hbar\omega$ and the refractive index n by the Becquerel equation (see e.g. Born, 1965)

$$V = \frac{e}{2mc^2} \omega \cdot \frac{dn}{d\omega} \qquad (2.5)$$

For the RGS Molgaard found considerable discrepancies between the temperature dependence of the Verdet constant calculated from the refractive index values of Sinnock and Smith (1969) using relation (2.5) and the Verdet constant determined experimentally. The limitations of the model underlying the Becquerel equation are an obvious explanation for these discrepancies. But there is, as has been pointed out by Smith (1974), also the possibility that the discrepancies are partially due to uncertainties of the experimental data.

In the visible far below the lowest electronic transitions in the ultraviolet, which determine the optical properties of the RGS at longer wavelengths, the magnetooptical effects are small and difficult to interpret. More information on these lowest transitions and their dependence on density should be obtained by extending the measurements into the ultraviolet region.

2.2 Theoretical interpretations

Three theoretical approaches, all based on a tight-binding model, have been proposed in order to explain the behaviour of the dielectric constant and F_{LL} respectively (Mazo, 1964; Doniach and Huggins, 1965; Keil, 1967).

Mazo (1964) calculated F_{LL} by using the formalism of thermodynamic Green's function and second quantization. Tightly bound excitons, corresponding to the lowest ultraviolet absorption peaks in the spectra of the RGS, were used to describe the excitations of the crystal. According to Mazo's result the polarizability of a rare gas atom is reduced by a factor (1-2f) when

the atom is built into a solid. The constant f is the probability that a given atom is excited in the true many body ground state of the system. f increases with increasing density. From this model F_{LL} for the solid can be obtained by estimating the difference ΔF_{LL} between a low-pressure gas and a solid. Sinnock and Smith (1968, 1969) found reasonable agreement between the theoretical and the experimental values of ΔF_{LL} for Ar , whereas the values for Kr and Xe are inconsistent.

Doniach and Huggins (1965) described the dielectric properties of rare gas solids by a semiphenomenological shell model, in which the atoms are represented by localized oscillators. Each oscillator consists of the outer shell of electrons which oscillates relative to the core consisting of the nucleus and the remaining electrons. These oscillators are coupled by dipole-dipole and nearest neighbour forces. Like Mazo, Doniach and Higgins assumed that the dielectric properties result mainly from the lowest ultraviolet excitons originating from the spin-orbit doublet $^1S_o - {}^{3,1}P_1$ of the free atoms. In this case F_{LL} is given by

$$F_{LL} = \frac{\varepsilon-1}{\varepsilon+2}\frac{1}{\rho} = \frac{1}{\rho}\left(\frac{1}{3}\,\frac{\omega_p^2}{\omega_o^2+V_o-\omega^2} + \chi_1\right) \qquad (2.6)$$

where ω_p is the plasma frequency of the outer electron shells, ω_o is the frequency of the non-interacting atomic oscillator, and V_o corresponds to the shift in ω_o observed with increasing density. The term χ_1 was assumed to be frequency-independent; it was introduced to take account of the polarizability of the core and of the contribution from higher excited atomic states. Since ω_p^2 and χ_1 are proportional to the density ρ the density dependence of the right hand side of equation (2.6) is determined by the density dependence of V_o. Thus the observed density dependence of the Lorentz-Lorenz function F_{LL} can be interpreted in terms of the effect of the density dependence of the interatomic

exchange interaction on the energy position of the lowest ultraviolet absorption peaks. Setting ω_o equal to the mean of the spin-orbit-split lowest absorption frequencies for atomic Ar and equal to the lowest absorption frequency of atomic Kr and Xe reasonable fits to the experimental results for solid Ar, Kr and Xe have been obtained (Sinnock and Smith,1967, 1969; Doniach and Higgins,1965). For the fit a value of V_o was chosen at the triple point $V_o(TP)$ and evaluated for other temperatures by assuming that

$$V_o = V_o(TP) \exp\left(-\frac{12(a_T - a_{TP})}{a_o}\right) \qquad (2.7)$$

where a_o, a_{TP} and a_T are the appropriate lattice parameters. The theoretical results are included in Figs. 1a,b,c. In agreement with the experimental results the theory predicts a blue shift of the exciton frequencies with increasing density or decreasing temperature respectively (Steinberger and Asaf,1973).

Keil (1967) calculated the static polarizability α of an Ar atom in solid Ar as a function of the lattice constant, by estimating the contribution to α of each electron shell by means of a linear variation techniques. His calculations confirm the assumption, made in the theoretical models discussed above, that most of the polarizability is due to the outer electron shell. The effect of overlap and interatomic exchange reduce the polarizability of an Ar atom in solid Ar below the free-atom value. The reduction of the polarizability as calculated by Keil (1967)is larger than that found experimentally (Sinnock and Smith, 1968, 1969; Smith and Pings, 1968).

The variation of the Lorentz-Lorenz function of solid Ar with density according to Keil's theory and experiment (Sinnock and Smith,1969) is shown in Fig. 2. In view of the difficulties encountered by Keil in calculating absolute polarizabilities the theoretical values have been normalized such that they coincide with the experimental results at $\rho = 0.0417$ (Mole cm^{-3}).

3. Fine structure at the onset of valence band transitions

3.1 Absorption measurements

The first measurements of the optical properties of RGS in the UV were reported by Nelson and Hartman (1959), who measured the absorption of solid Ar from 7.5 eV to 13 eV. By solidifying the Ar on a sodium salicylate phosphor and observing the visible light emitted by the phosphor the need for a ultraviolet transmitting substrate was obviated. Nelson and Hartman observed two absorption bands centered at 8.75 eV and at 12.3 eV. Later experiments showed that the absorption threshold for pure Ar lies above 12 eV and therefore the maximum at 8.75 eV was probably due to impurities.

Schnepp and Dressler (1960) performed absorption measurements on solid Ar, Kr and Xe in the energy range from 3.6 eV to 10.6 eV using a 2 m vacuum spectrograph with photographic recording of the spectra. The continuous light was provided by Ar and Kr discharge sources. High purity rare gases were condensed within a few seconds on a LiF window in thermal contact with a liquid He container. The films (estimated thicknesses 10 Å - several thousand Å) were not annealed. Two additional LiF windows separated the vacuum in the He Dewar from the source and the spectrometer. Schnepp and Dressler found strong absorption bands centered at 8.35 eV and 9.50 eV in solid Xe and at 10.015 eV in solid Kr. Weaker absorption bands showed up at 9.1 eV and at 8.22 eV in solid Xe and at 9.95 eV in solid Kr. The bands at 8.22 eV and at 9.95 eV lie below the threshold for electronic transitions and have not been confirmed in most of the later experiments, although Steinberger et al. (1970) detected a weak maximum at 8.19 eV in the reflectance spectrum of an unannealed film of solid Xe. No absorption of solid Ar was observed in the photon energy range below the LiF cut off.

Similar photographic absorption measurements on solid Kr and Xe have been performed by Roncin et al. (1964) and by Roncin and Moorjani (1967) using cleaved LiF crystals as substrates for the solid rare gas films. Using this technique they were able to obtain reproducible spectra up to 11.6 eV. The energy positions of the absorption maxima reported by Roncin et al. (1964) will be found in Tables VI and VII. Only a rough estimate of the ratio of the oscillator strengths of the main absorption bands was obtained in the experiments discussed so far.

The first detailed investigations of the ultraviolet absorption spectra of solid Ar, Kr and Xe were reported by Baldini (1962). Improving the technique applied by Nelson and Hartman (1959), which is based on the use of a phosphor, he was able to expand the photon energy range up to 14 eV. This upper limit was determined by the short wavelength limit of the line spectrum emitted by the hydrogen lamp used, and the wavelength resolution achieved with the normal incidence monochromator (40 cm grating) was 1 Å. Figure 3 gives a schematic representation of the film holder used by Baldini. A sapphire rod, previously coated on both flat ends with a phosphor (liumogen) was cooled to 20 °K by thermal contact with a liquid He reservoir. The phosphor converts the ultraviolet radiation into visible light, with almost constant quantum efficiency in the wavelength range under consideration. The phosphor films were a few microns thick and thus totally absorbed the UV light, and the emitted visible light was measured by a photomultiplier. High purity Ar, Kr and Xe were vapour-deposited in a few seconds on the phosphor coated sapphire holder. A thin film was condensed on one side and a thicker film deposited on the other side. The sapphire holder could be rotated and thus the absorption of both films could be determined. The absorption spectra of solid Ar, Kr and Xe shown in Figs. 4 - 6 correspond to films whose thicknesses are the difference between

the two, and were obtained by dividing the absorption of the thicker film by that of the thinner. Baldini assumed that the reflectivity of both films was the same and therefore did not apply any reflection corrections. The technique also tends to cancel out the absorption due to the residual gas in the vacuum system which condenses on the surface of the rare gas films. Before the measurement the films were annealed for several minutes (Ar at a few degrees above 20 K, Kr at 44 K and Xe at 53 K). Annealed films of Kr and Xe showed more and much sharper absorption maxima than unannealed films. For example the three small peaks between 9 eV and 9.3 eV found in the spectra of annealed Xe films only show up as one weak shoulder in the spectrum of a film not thermally treated Annealing also causes a slight red shift of the absorption maxima. Spectra taken at elevated temperature (40 °K for Kr, 53 °K for Xe) show somewhat broader structures which are shifted towards lower energies (a few hundredths of an eV for Kr, up to 0.1 eV for Xe). The energy positions of the absorption maxima detected by Baldini are included in Tables V, VI, and VII.

Steinberger and Schnepp (1967) repeated Baldini's absorption measurements on solid Xe using a Tanaka type (Tanaka, 1955) Kr lamp emitting a continuum in the spectral region under discussion. The wavelength resolution of their 1 m McPherson spectrometer was about 0.5 Å. The samples were condensed at 4 °K on cleaved LiF. The results reported pertain to samples which have been heated up to 50 K and recooled to 4 K. The peak positions are given in Table VII. By a technique similar to Baldini's, but extending the accessible energy range towards higher energies by using a triggered vacuum spark source Boursey et al. (1970) obtained the absorption spectrum of solid Ne at 4 K. Table IV gives the energy position of the absorption maxima detected in this experiment. Further transmission measurements on solid Kr and Xe have been performed in connection with reflectance measurements by Scharber and Webber (1971). We will discuss these measurements in section 3.2.

Most recently Saile et al. (1976a) clearly demonstrated the existence of surface excitations for solid Ar, Kr and Xe. The surface excitations are clearly to be seen in transmission and reflection spectra at energies below the corresponding bulk excitations. The measurements have been performed under ultra-high-vacuum conditions using the synchrotron radiation of the electron storage ring DORIS (Koch et al., 1976; Saile et al.,1976b). The dotted line in Fig. 7 shows the absorption spectrum of a clean Xe film deposited on a LiF substrate. Depositing a thin layer of Ar on top of this sample results in the spectrum given by the solid line. The Ar surface layer quenches the maximum at 8.21 eV and shifts the maximum at 8.28 towards higher energies. Gently heating the sample to temperatures above the sublimation temperature of Ar, and thus removing the Ar surface layer, restores the spectrum of the clean Xe sample (dashed line). The high sensitivity of the maximum at 8.21 eV to surface layers (monolayers of adsorbed residual gas already lead to the disappearance of the peak) strongly supports its assignment to surface excitations.

No absolute data for the dielectric function $\varepsilon(\omega)$ have been obtained in the measurements discussed so far. Baldini (1962,1965) only gives a rough estimate for the order of magnitude of the absorption coefficient μ. The main reason for this lies in the difficulties encountered in an exact determination of the thickness of the solid rare gas films. But even if we assume that these difficulties can be overcome the determination of absolute values of the optical constants in this energy range by absorption measurements remains a difficult task. As we shall see later the reflectivity of the solid rare gases in the energy region under consideration is high and therefore interference effects in the thin films should be taken into account.

In the case of transmission measurements using LiF substrates both the thin solid rare gas film and the substrate have to be considered at least in principle. This problem is discussed by Wolter (1956). Due to the great thick-

ness of the LiF substrate and the low reflectivity of LiF (Roessler and Walker 1967) we are allowed to neglect interference effects due to the substrate. Thus the problem reduces to the determination of the intensity I of the light transmitted through a thin film backed by a substrate. For normal incidence I is given by: (Wolter 1956)

$$I = I_o \frac{n_s(1+2r\cos\theta+r^2)(1+2r_s\cos\phi+r_s^2)e^{-\mu d}}{1+r^2r_s^2e^{-2\mu d} + 2r\cdot r_s\cos(\theta+\phi+\alpha)e^{-\mu d}} \tag{3.1}$$

For the intensity of the reflected light R the following relation holds:

$$R = I_o \frac{r^2 + 2rr_s\cos(\theta-\phi+\alpha)\cdot e^{-\mu d} + r_s^2e^{-2\mu d}}{1 + r_s^2r^2e^{-2\mu d} + 2rr_s\cos(\theta+\phi+\alpha)e^{-\mu d}} \tag{3.2}$$

where I_o is the intensity of the incoming light; n,κ are the optical constants of the solid rare gas film; n_s,κ_s the optical constants of the substrate; d the thickness of the solid rare gas film; $\mu = \frac{4\pi\kappa}{\lambda}$ is the absorption coefficient of the solid rare gas; λ the wavelength of the light $\alpha = \frac{4\pi dn}{\lambda}$. The reflectivity of the vacuum - rare gas interface is given

$$\tilde{r} = \frac{n+i\kappa-1}{n+1\kappa+1} = re^{i\theta} \; ; \quad R = r^2, \tag{3.3}$$

and the reflectivity at the rare gas-substrate (or phosphor) interface is

$$\tilde{r} = \frac{n_s+i\kappa_s-n-i\kappa_s}{n_s+i\kappa_s+n+i\kappa} = r_se^{i\phi} \; ; \quad R_s = r_s^2 \; . \tag{3.4}$$

Equation (3.1) shows that the intensity of the transmitted light depends on the optical constants of both the film and the substrate (or the phosphor) respectively and on the thickness of the film. Only if r_s is negligibly small can the absorption coefficient μ be determined from the difference of the intensity of the light transmitted through films of different thicknesses. One way to get

around this problem would be to make the films thick enough that $r^2 \cdot r_s^2 e^{-2\mu d} \ll 1$ and $2r \cdot r_s \cos(\theta+\phi+\alpha) e^{-\mu d} \ll 1$ hold. But this may at the same time reduce the intensity of the transmitted light considerably, so limiting the accuracy of the measurement. As we shall see in section 3.2 the optical constants of the RGS vary drastically in the energy range under consideration, and this makes it almost impossible to find a film thickness for which these criteria hold over the whole energy range. If we can neglect interference effects for example, due to surface roughness, equation (3.1) reduces to

$$I = I_o \frac{(1-R)(1-R_s) \cdot e^{-\mu d}}{1-R \cdot R_s e^{-2\mu d}} \qquad (3.5)$$

In this case the thickness only has to be such that $R \cdot R_s e^{-2\mu d} \ll 1$. But on the other hand the surface roughness might cause considerable errors due to light scattering and the uncertainties involved in the determination of the thickness.

These considerations explain why almost all the available absolute data on the optical constants of the solid rare gases have been obtained from reflectance measurements. If the problems connected with surface contamination and surface roughness can be mastered reflection measurements are, in cases where the reflectivity is high, the easiest way to obtain reliable absolute optical data. We will discuss the reflection measurements in the following section.

3.2 Reflection Measurements

The first reflection measurements on solid rare gases were performed by Beaglehole (1965). He determined the reflectivity near normal incidence of solid and liquid Xe condensed in a LiF cell in the energy range from 7.8 eV to 11 eV. Taking into account the reflectivity of the empty cell and using the known optical data for LiF, Beaglehole calculated the reflectivity of the sample from the measured reflectivity of the LiF-Xe interface. The main interest of this experiment lay in the comparison of the spectra of solid and liquid Xe; no attempt has been made to obtain absolute values for the optical constants. The reflectance spectra showed the same structures already found in absorption measurements. The most interesting result was that in going from the solid to the liquid Xe the maxima get broader and shift towards lower energies but do not disappear. In liquid Xe the small peaks found in the solid between 9.0 eV and 9.3 eV are smeared out to a weak and broad shoulder, but the maxima found in the solid at 8.4 eV and around 10.3 eV are still seen.

Steinberger et al. (1970) studied very carefully the reflectance spectrum of solid Xe near normal incidence in the energy range from 7.8 eV to 10.5 eV. They used the continuum emitted by either a Tanaka-type closed Kr source (for $h\nu < 9.4$ eV) or a Hinteregger-type Ar lamp (for $h\nu > 9.4$ eV) (Samson, 1967). In both cases a LiF window separated the source from the 1 m McPherson vacuum monochromator. A photomultiplier coated with sodium salicylate served as detector. Great care was taken to avoid contamination of the surface of the Xe films. The pressure in the sample chamber was 10^{-7} Torr with the liquid N_2 traps filled and dropped to 10^{-9} Torr when the liquid He container was filled too. But still a slight decrease of the reflectivity with time (of the order of hours) was noticed and subsequently corrected for. The Xe films

were deposited at 6 K on LiF windows, annealed at ∿50 K for a few minutes and cooled down again to ∿6 K for the measurement. To obtain the absolute reflectivity the measured relative reflectance spectrum was calibrated at one wavelength by comparison to the known reflectivity of LiF (Roessler and Walker, 1967). The absolute valuesobtained that way were in excellent agreement with the values determined by using a freshly cleaved NaCl crystal as the reflectivity standard (Roessler and Walker, 1968). Changes in the spectral distribution and intensity of the light are responsible for an error of the absolute reflectivities which amounts to ±5 % for the Kr lamp and to ±10 % for the Ar lamp. Figure 8a shows the reflectance spectrum of solid Xe thus obtained.

The films used were thick enough to be able to exclude interference effects. Assuming normal incidence the intensity of the reflected light is given by r^2 where relation (3.3) for r holds. The phase Θ of the reflection was determined using the Kramers-Kronig relation (1.11). From r and Θ the optical constants n and κ were calculated by means of the formulae

$$n = \frac{1-r^2}{1+r^2-2r\cos\Theta} \quad , \tag{3.6}$$

$$k = \frac{2r\sin\Theta}{1+r^2-2r\cos\Theta} \tag{3.7}$$

As a first step to evaluating (1.11) the measured reflectivity spectrum was extrapolated towards lower and higher energies by representing the lowest-energy and the highest-energy absorption bands by damped harmonic oscillators. In the next step the ε_2 spectrum obtained by means of the formulae (1.11, 3.6, 3.7, and 1.5) was resolved into a sum of 9 resonance bands, represented by damped harmonic oscillators. This set of resonance bands was used to determine new extrapolated reflectivities. By successively repeating the

preceding steps to achieve self-consistency the parameters of these resonance bands were varied in such a way that the reflectance spectrum calculated from this model approximated the experimental spectrum. Figures 8b,c show the resulting spectra of $\varepsilon_2=2n\kappa$ and $\varepsilon_1 = n^2-\kappa^2$. The energy positions of the maxima are included in Table VII.

Further reflection measurements on solid Xe were reported by Steinberger and Asaf (1973). They investigated the temperature dependence of the reflection maxima of solid and liquid Xe in the energy range from 7.8 eV to 10.3 eV, and observed a linear shift of the maxima towards lower energies with increasing temperature. The maxima get broader at higher temperature but most of them are still to be seen even in liquid Xe. This result confirms the findings of Beaglehole (1965). Figure 9 shows the peak positions as a function of temperature. A representation of the peak positions as a function of density also yields linear plots. In this case the values for the liquid also lie on the same straight lines. From the linear dependence of the peak positions on temperature and density the authors conclude that the red shift is not due to phonon interaction but can be explained in terms of the deformation potentials.

In the past few years a group at the Deutsches Elektronen-Synchrotron DESY in Hamburg has studied the optical properties of the RGS from the onset of electronic transitions up to 500 eV. In the course of these investigations the reflectance spectra of solid Ne, Ar, Kr and Xe have been measured from the absorption threshold up to about 30 eV. (Haensel et al. 1969c, 1970c,d). The intense synchrotron radiation emitted by the electrons circulating in the high energy electron accelerator was used as a light source. The synchrotron

radiation is concentrated in a narrow cone tangential to the electron orbit. The spectrum of the synchrotron radiation is continuous, completely smooth and spans the whole spectral range from the infrared to the x-ray region. The characteristics of the synchrotron radiation and details of the experimental arrangement used in these measurements have been discussed by Haensel and Kunz (1967), Godwin (1969), Hayes (1972), Codling (1973), Brown (1974), Madden (1974), Kunz (1976) and Koch and Otto (1976).

Figure 10 shows a schematic representation of the experimental set up used for the reflection measurements for photon energies up to 30 eV and for the absorption measurements performed above 30 eV. The latter will be discussed in section 4.1. For the low energy range, the continuous synchrotron radiation was monochromatized by a normal incidence monochromator in a modified Wadsworth mounting (Skibowski and Steinmann, 1967). The 2m concave grating forms an image of the source, (electron beam) in the accelerator 40 m away on the exit slit; there is no entrance slit. The resolution, determined by the focussing properties of the grating and the dimensions of the electron beam in the synchrotron was about 2 Å over the whole energy range. The high purity gases were evaporated either on cleaved KCl crystals or on polished LiF, glass or Au. During the evaporation and the subsequent measurements the substrates were kept at 6 °K for Ne, 20 °K for Ar and Kr and at 40 °K for Xe by a liquid helium cryostat. An open magnetic type photomultiplier detected the light reflected from the solid rare gas films. Cryostat and multiplier were mounted inside a modified commercial ultrahigh vacuum system. After baking of the vacuum chamber a basic pressure of the order of 10^{-9} torr was obtained and could be sustained during the cooling of the cryostat and during evaporation. The reflectance of a freshly evaporated film remained constant within 10 % over an hour. During evaporation oscillatory changes of the intensity of the reflected light with increasing thickness were observed for photon energies

below the onset of absorption due to interference effects. The evaporation was stopped when these oscillations in intensity disappeared. Further increase of the thickness resulted in a slow decrease of the reflectivity of the sample probably due to increasing surface roughness. No significant influence of the different substrates on the reflectance spectra could be observed. From the relative reflectance spectra measured at an angle of incidence of 15° the absolute reflectance spectra were obtained by using gold as a reference standard. Figures 11 and 12 show the reflectance spectra of solid Ne, Ar, Kr and Xe obtained in this way.

A word of caution should be inserted here. The determination of absolute reflectivities in the vacuum ultraviolet is a very difficult task even with a source offering as many advantages as synchrotron radiation. The spectral distribution of the synchrotron radiation is stable. The main reason for instabilities of the intensity are current fluctuations in the accelerator and these fluctuations can generally be well compensated for. The fact that the pressure in the synchrotron is better than 10^{-7} Torr eliminates the problems caused by gas from the source leaking into the sample chamber, one of the major difficulties encountered with the commonly used gas discharge sources. However, great care has to be taken in the optical alignment. Inhomogeneities of the cathode of the photomultiplier can give rise to considerable errors if it is not always the same area of the cathode that is illuminated. By using filters and choosing the proper grating the influence of background due to stray light and light of higher orders reflected from the grating can be minimized. But the latter can be a nontrivial problem with the continuous spectrum of the synchrotron radiation extending up to much higher photon energies. For normal incidence instruments this is less serious, than for instruments working at grazing incidence, due to the strong decrease of reflectivity at higher energies.

One of the major problems encountered in all reflectivity measurements is related to the sample itself. Besides surface contamination, surface roughness

and the structure of the film all of which depend critically on the way the sample has been prepared (e.g. the speed of evaporation and the nature of the substrate), the thickness of the film and the temperature can seriously influence the reflectivity. Rare gas films rapidly evaporated on to smooth substrates at temperature far below the sublimation point show the highest reflectivity. This way of preparation obviously minimizes the surface roughness of the film. On the other hand the great number of lattice defects present in these samples (cf. chapter 10, § 5.1) give rise to considerable broadening of the structures in reflectivity spectra. Annealing of the samples makes the reflectivity bands narrower but at the same time often results in a marked drop of the reflectivity probably due to increased surface roughness (see e.g. Steinberger et al., 1970). Light reflected at the backside of absorbing samples does not influence the measured reflectivities if thick films are used. But for photon energies where the absorption is very small (below the onset of absorption and around 18 eV for Ne, 13 eV for Ar and 10.5 eV for Kr) even films of several microns thickness may be too thin. Around 13 eV prominent interference effects have been observed recently even for 20,000 Å thick Ar films rapidly evaporated ($\sim$ 80 Å/sec) onto gold substrates kept at 10 K (Harmsen et al., 1974).

The fact that such drastic effects were not observed in the measurements discussed above itself indicates a considerable roughness and inhomogeneity of the samples. Especially at energies above 20 eV the measured reflectivities are often too low, probably due to light scattering at the rough surfaces. This might be one of the reasons for the discrepancies encountered at energies around 30 eV between data determined by reflectance measurements and those determined by absorption measurements. Furthermore the surface roughness can for example couple the electromagnetic field to surface excitations

thus causing additional structures in the spectra. At the present time it is almost impossible to determine the errors of the absolute reflectivity with precision over the whole spectral region covered by the measurements. The comparison of the reflectance spectrum of solid Xe given in Fig. 12b to the spectrum determined by Steinberger et al. (1970) shown in Fig. 8a gives a fair idea of the uncertainties involved in the data. As can be seen the absolute value of the reflectance R at given energy is much more uncertain than the energy position of a peak in R. For this reason we give more weight to the peak positions, which are listed in tables IV to VII.

From the reflectance spectra shown in Figs. 11 and 12 Skibowski (1971) calculated the dielectric constants by means of the Kramers-Kronig relation given in equation (1.11). For that purpose Skibowski extrapolated the measured reflectance spectra towards higher energies by setting $R \propto (h\nu)^{-4}$. At lower energies the reflectance spectra were smoothly joined to the reflectivities in the visible range determined from the data reported by Sinnock and Smith (1969) and by Kruger and Ames (1959). The slope and the magnitude of the reflectivity between the visible and the onset of electronic transitions were varied in such a way that ε_2 became approximately zero for energies below the absorption threshold. Though the extrapolations have been carried out with utmost care the possibility that they give rise to considerable errors cannot be excluded. Figures 13 and 14 show the ε_1 and ε_2 spectra of solid Ne, Kr, and Xe determined by Skibowski. For Ne and Ar, Keitel (1970) also varied the extrapolation to higher energies using the agreement between the absorption coefficients around 30 eV calculated from the reflectance spectra with those determined by absorption measurements as a further criterion. In principle this is a step in the right direction, but since neither the reflectivity measurements nor the absorption measurements give reliable data in the energy range around 30 eV there is also a lot of arbitrariness involved

in this procedure. The optical constants obtained by Keitel are similar to those obtained by Skibowski.

Recently Saile (1974), using a new data processing system (Nielsen, 1974; Klucker and Nielsen, 1973), redid the Kramers-Kronig analysis for Ne and Ar. Saile extrapolated the measured reflectance spectra to lower photon energies in the same way as Skibowski. For photon energies above 30 eV reflectivity data determined via Kramers-Kronig analysis from absorption spectra (see section 4) were used. Since there are no reliable data for photon energies between 20 eV and 30 eV the measured reflectance spectra below 20 eV were smoothly joined to those above 30 eV obtained from absorption data. From the overall reflectance spectra thus constructed the dielectric constants were calculated by means of the Kramers-Kronig relation (1.11). Varying the extrapolation of the reflectance spectra towards lower energies and the interpolation between 20 eV and 30 eV this analysis was repeated until the following criteria could be fullfilled: i) the phase θ of the reflection does not become negative below the onset of absorption, ii) ε_2 is zero below the onset of absorption, iii) the absorption and reflectance spectra calculated from the dielectric constants are in agreement with the experimental results. For Ne Saile corroborated Skibowski's results. Saile's ε_2 values for Ar are up to 40 % higher than those determined by Skibowski. Figure 13b presents the ε_1 and ε_2 spectra of solid Ar given by Saile.

In the regions of low absorption strong interference effects can be used to determine the optical constants accurately. For Ar Harmsen (Harmsen et al., 1974; Harmsen, 1975) determined the real part n of the complex index of refraction $\tilde{n}$ by comparing simultaneously the oscillations of the reflectivity with increasing film thickness at a fixed wavelength in the ultraviolet and at 6330 Å (He-Ne Laser, value of n at 6330 Å taken from Sinnock and Smith 1969). The imaginary part κ was determined from the damping of the interference amplitudes with increasing film thickness (see equ. 3.2). Since only the relative amplitudes of the reflectivity enter the evaluation the difficulties encountered in the determination of absolute reflectivities can be avoided. This is the great advantage of this method. The values of ε_1 and ε_2 obtained from these data are included in Fig. 13a. Except for photon energies close to 13 eV the ε_1 values thus determined are somewhat higher than those reported by Saile. The ε_2 values below the onset and above the first excitons around 13 eV are markedly lower than the values obtained by Saile. For photon energies just above the first excitons around 18 eV for Ne and 13 eV for Ar the absorption coefficient is extremely low. This indicates that also for Kr and Xe the ε_2 values given in Figs. 8b and 14 for energies just above the first excitons may be to high.

Scharber and Webber (1971) measured the reflectance spectra of Kr and Xe films deposited on a gold plated sapphire substrate kept at 20.4 K. The wavelength resolution of the spectrometer used was approximately 2 Å. The

intrinsic vacuum in the reflectometer was 10^{-8} Torr. But during the experiment the gas leaking into the system from the hydrogen lamp caused a pressure increase up to $\sim 3 \cdot 10^{-6}$ Torr. This fact casts some doubt on the cleanliness of the surfaces, though the authors state that they did not observe changes in the reflectance or absorption spectra over 20 - 30 minutes required for a complete scan of the region of interest. In order to minimize the influence of surface contaminations the authors measured the spectra of the samples kept a 20.4 °K immediately after evaporation without annealing. The films used for reflection measurements were thick enough to exclude interference effects. The same authors also determined the absorption spectra by measuring the transmission of thin films successively deposited on a LiF substrate. The experimental results for Kr and Xe are presented in Fig. 15. The main features of the absorption spectra agree with Baldini's (1962) data (Figs. 5 and 6), though the relative oscillator strengths differ considerably. Also the marked asymmetry of the strong absorption peaks reported by Scharber and Webber is not present in the spectra of Baldini.

From the transmission spectra of films of different thicknesses Scharber and Webber constructed a relative absorption (κ) spectrum. It was assumed that all films showed the same front surface reflection and scattering losses. The LiF substrate was not optically polished and therefore essentially no interference effects in the transmitted beam could be observed during the deposition of the gas. Since the film thickness could not be determined, the absolute values of κ could not be obtained directly, and the relative κ spectra had to be scaled into absolute κ spectra. Therefore the absolute values of κ have been determined at selected wavelengths by observing the oscillations in the intensity of the reflected light due to interference effects occuring during the deposition of the film (see equation 3.2). The pair of equations for n and κ

established by the value of the reflectivity at the first interference minimum and maximum was solved graphically (Scharber and Webber, 1971). Subsequently n was determined from the κ and reflectivity spectra. The resulting spectra of ε_1 and ε_2 are shown in Fig. 16.

There are considerable discrepancies between the reflectance spectra of Kr and Xe reported by the different authors (see Figs. 8a, 12, 15). Not only the absolute reflectivities differ by more than a factor of two but also the relative heights of the reflectance maxima vary drastically, although the main features and the energy positions of the peaks are fairly well reproduced. This clearly demonstrates the difficulties encountered in these experiments. Under these circumstances the discrepancies between the ε_1 and ε_2 spectra reported by the three groups are by no means surprising. The ε_1 values reported by Scharber and Webber for solid Kr don't seem realistic. They are up to a factor of five higher than those of Skibowski. Because of this large discrepancy, we must regard the agreemet between the ε_2 values (Figs. 14a, 16a) at the first exciton peak as fortuitous. Towards higher energies the ε_2 data of Scharber and Webber are too low. Between 8.5 eV and 9.5 eV there is reasonable agreement between the Xe ε_2 spectra of Steinberger et al. (Fig. 8b) and of Skibowski (Fig. 14b). Outside this region the ε_2 values obtained by Skibowski seem to be too low. Skibowski's values for ε_1 are considerably lower than those reported by Steinberger et al. The ε_1 values determined by Scharber and Webber (1971) are up to a factor of three larger than those of Steinberger et al. Except for energies between 8.6 eV and 9.4 eV, where the values obtained by Scharber and Webber are much lower than those reported by the two other groups, there is reasonable agreement between the ε_2 spectra of Scharber and Webber and of Steinberger et al. Part of the discrepancies between the data of Scharber and Webber and those of the two other groups may be due to errors in the absolute reflectivity at the interference

extrema. The method by which Scharber and Webber determined the absolute values of κ can give rise to considerable errors in κ if the absolute reflectivities are not determined very accurately (Scharber and Webber 1971). Steinberger (1973) has pointed out that another reason for the discrepancies may lie in the method used to find n from the observed R and κ values. Steinberger applied his self-consistent method of Kramers-Kronig analysis to the reflectivity data reported by Scharber and Webber. The ε_1 and ε_2 curves thus obtained are also presented in Fig. 16b. In comparison to the data of Scharber and Webber the ε_1 values are reduced by this method whereas the ε_2 values are increased. No satisfactory agreement between these modified results and the results of Steinberger et al. (1970) was achieved.

In section 4 we will show that, except for photon energies close to the onset of transitions from inner shells, the absolute cross sections for the solid and the gaseous phase agree within the error limits of the measurements. Figs. 20 and 21 show the absorption spectra of solid and gaseous Ne, Ar, Kr and Xe for photon energies up to 1000 eV. At threshold the absorption coefficients determined from reflectance spectra by Skibowski (Ne and Kr), Saile (Ar) and Steinberger (Xe) are included. The Xe absorption spectrum calculated from the dielectric constants which Steinberger (1973) obtained by the application of his self-consistent Kramers-Kronig analysis to the reflectance spectrum reported by Scharber and Webber (1971) is also given. At 22 eV for Ne, 16 eV for Ar and 14 eV for Kr the cross sections determined from reflectivity measurements join onto the values reported for the corresponding free atoms. (There are no reliable absorption data on RGS for photon energies between 20 eV and 30 eV.) This strengthens the confidence in these reflectance data. In the light of these arguments the absorption coefficients of solid Xe calculated from the

dielectric constants reported by Steinberger (1970) seem to be too low. The same holds for the absorption coefficients obtained by Skibowski (1971). The absorption spectrum based on Steinberger's (1973) analysis of the reflectance data reported by Scharber and Webber is in better agreement with the data for atomic Xe. This absorption spectrum is also in fair agreement with absolute absorption coefficients obtained by scaling Baldini's (1962) absorption spectrum of solid Xe by means of the absolute oscillator strength of the first exciton (Baldini 1965).

The author is well aware that the agreement between the absolute absorption coefficients of the RGS and those of the corresponding free atoms can only be considered as a guideline. Up to now the agreement has only been verified for photon energies above 30 eV. But it seems reasonable to assume that the oscillators strengths integrated from threshold up to 30 eV are approximately the same for both phases, although solid state effects can give rise to considerable fluctuations of the oscillator strength for photon energies less than 20 eV above threshold. On the basis of the present knowledge the author does not feel competent to decide finally which data are most reliable, but he tends to place more confidence in the reflectance data reported by Scharber and Webber (1971) and the dielectric constants derived from these data (Steinberger 1973).

3.3 Electron energy loss measurements

In addition to optical measurements, investigations of the electronic structure of the RGS have been made by electron energy loss measurements. A detailed discussion of the determination of optical constants by electron spectroscopy is given by Daniels et al. (1970).

3.3.1 Energy losses of high energy electrons

All the experiments discussed in this section have the following principle in common. Electrons thermally emitted from a hot cathode are accelerated up to about 60 keV and subsequently monochromatized. The energy of the electrons transmitted through the sample is analyzed. Figure 17a shows a schematic representation of the apparatus used by Schmidt (1971,1972).The apertures determine the angular acceptance of the monochromator and the analyzer respectively. The monochromator and the analyzer consist of a Wien filter and lenses and the energy aperture transmits only electrons with energies in a narrow energy band. Schmidt registered the electron energy loss spectra directly on photographic plates.

The samples investigated were thin films (thicknesses ranged from 100 Å to several 1000 Å) condensed on collodion, carbon, beryllium or aluminum substrates kept a low temperature by thermal contact with a He cryostat. The samples were surrounded by a radiation shield also cooled to low temperatures, which helped to prevent the condensation of the residual gas present in the high vacuum systems on the surface of the cold specimen. A schematic representation of the sample chamber and the cryostat used by Schmidt is shown in Figure 17b.

If the samples are sufficiently thin that one can neglect multiple energy losses, the intensity of electrons which have suffered an energy loss $\hbar\omega$

and a momentum transfer $\hbar q$ is proportional to the energy loss function

$$-\frac{1}{q^2}\,\mathrm{Im}\,\frac{1}{\varepsilon(\omega)} \qquad (3.8)$$

Taking the energy- and angular spread of the electron beam and the characteristics of the analyzer into account, the energy loss function can be calculated from the energy loss spectrum (see for example Daniels et al., 1970).

Hörl and Suddeth (1961) performed the first electron energy loss measurements on solid Xe. They found a weak loss at 7.9±0.6 eV. Probably due to the low energy resolution (because the electron beam was not monochromatized) no further structure was detected. Boersch et al. (1965) determined the energy loss spectra of solid Ne, Ar, Kr and Xe, with an energy resolution of 70 meV. Continuing these investigations Schmidt (1971,1972) determined the energy loss spectra of solid Ne, Ar, Kr and Xe from the onset of electronic transitions up to about 30 eV with an improved energy resolution of 40 meV. These spectra are shown in Figs. 18a,b,c,d. The variation of the sample temperature between 3 K and the sublimation temperature did not affect the spectra of Ne and Ar to within the accuracy of the experiments.

The energy loss spectra of solid Ar, Kr and Xe have also been obtained by Colliex and Jouffrey (1971). The relatively poor resolution ($\sim$1 eV) achieved in these experiments resulted in considerably smeared out structures and thus only the most prominent maxima found in other experiments could be detected. More detailed structures were reported by Keil (1966, 1968) who determined the electron energy loss spectrum of solid Xe and by Daniels and Krüger (1971) who performed the same measurements on solid Ne and Ar. The only authors who have determined the dielectric constants from the electron energy loss spectra are Keil (1968) for solid Xe and Daniels and Krüger (1971) for solid Ne.

As in the case of the optical absorption measurements the thickness of the films used in the electron energy loss experiments could not be determined. Therefore only relative spectra of $-\mathrm{Im}\frac{1}{\varepsilon}$ could be obtained. Keil (1968) and Daniels and Krüger (1971) constructed absolute values of $-\mathrm{Im}\frac{1}{\varepsilon}$ by calibrating the relative spectra with the help of the low frequency dielectric constant. Keil also proposed an alternative procedure based on the fact that the energy positions of the sharp maxima in the absorption spectra calculated from the electron energy loss data depend on the absolute values of $-\mathrm{Im}\frac{1}{\varepsilon}$. Thus the agreement between the calculated energy positions and those reported by Baldini can be used as a criterion for the absolute value of $-\mathrm{Im}\frac{1}{\varepsilon}$. Using the Kramers-Kronig relation (1.12), the real part $\mathrm{Re}\frac{1}{\varepsilon}$ was obtained. The dielectric constants ε_1 and ε_2 were subsequently determined with the help of the relations

$$-\mathrm{Im}\frac{1}{\varepsilon} = \frac{\varepsilon_2}{\varepsilon_1^2+\varepsilon_2^2} \tag{3.9}$$

$$\mathrm{Re}\,\frac{1}{\varepsilon} = \frac{\varepsilon_1}{\varepsilon_1^2+\varepsilon_2^2} \tag{3.10}$$

The ε_2 values obtained in this way by Keil (1968) and by Daniels and Krüger (1971) are much higher than those determined by reflection measurements (Figs. 8b, 13a, 14b, 16b), especially at the threshold of electronic transitions. The oscillator strength of the first exciton line in solid Xe calculated from Keil's data is more than twice as large as the oscillator strength of the corresponding $5p^6 \rightarrow 5p^5(3/2)6s$ transition of atomic Xe. The oscillator strengths extracted from the reflection data are all smaller than the corresponding value for free Xe atoms. In the framework of existing theoretical models (see chapter 8 Vol I) it seems hard to understand such a drastic

increase of the oscillator strength. Also Keil's ε_1 values for solid Xe differ markedly from those reported by the other groups. Part of this discrepancy may be due to the procedure used to calibrate the $-\mathrm{Im}\frac{1}{\varepsilon}$ spectra. Also uncertainties in the relative spectral behaviour of $-\mathrm{Im}\frac{1}{\varepsilon}$, which according to Keil (1968) could not be excluded, and the difficulties involved in extrapolating the measured $-\mathrm{Im}\frac{1}{\varepsilon}$ spectra towards lower and higher energies may contribute to the discrepancies. The latter problems we have already encountered in the discussion of the reflectance measurements.

3.3.2 Energy losses of low-energy electrons

Farrell and Strongin (1972) investigated the characteristic energy loss spectra of low-energy electrons (primary energy between 40 eV and 250 eV) from thin crystals of Ne, Ar, Kr, and Xe grown on the (100) face of a niobium singly crystal held near 7 K. Low energy electron diffraction patterns (LEED) (Farrell et al. 1972) verified that Neon, Argon and Krypton epitaxially grew either as single-crystals or polycrystalline films with the (111) face parallel to the niobium surface. The Xe structure was more complicated but could be annealed to the (111) orientation. The experiment was housed in an ultrahigh-vacuum system. The primary electrons hit the sample normal to the surface. The energy of the electrons backscattered into a solid angle of about 43° to the normal was analyzed by a standard four-grid LEED system. Using a modulation technique Farrell and Strongin attained the derivative of the energy loss spectra. The rapid desorption of the lighter rare gas crystals (Ne, Ar, Kr) by the electron beam severely complicated the experiment.

The energy positions of the characteristic energy loss features up to 60 eV are listed in Tables IV, V, VI, VII. The data agree fairly well with those obtained by optical or high-energy electron loss spectra, though due to the

inferior energy resolution not all details could be detected. Structures not previously reported were observed for energies above 30 eV for Kr and between 25 eV and 56 eV for Xe. At even higher energies maxima due to excitations of the Xe 4d electrons could be detected. Farrell and Strongin noticed shifts of the energy positions of the loss maxima up to 1 eV when the energy of the primary electrons was changed.

Recently Nuttall et al. (1975) studied the electron energy loss spectra of solid Ar, Kr and Xe for electron energies between 100 eV and 1000 eV. The incoming electron beam was incident on the rare gas film, condensed on a copper finger cooled to 10 K, at an angle of 70° to the surface normal. The electrons passing into the retarding hemispherical electron spectrometer travelled normal to the surface. Spectrometer and cold stage were situated in an ultra-high vacuum system. Any contamination of the specimen could easily be detected by scanning the Auger spectra. Due to the higher resolving power of the spectrometer Nuttall et al. were able to detect structures not reported by Farrell and Strongin (1972). Nuttall et al. also noticed changes of the spectra with primary energy. There is good correspondence between the energy positions of the maxima with those reported by Farrell and Strongin and those obtained by optical and high-energy electron loss experiments (see Tables IV, V, VI, VII). The general shape of the loss spectra at low primary energies differ from those at higher energies. The low energy spectra show a stronger high energy tail and a steeply rising background underneath the discrete loss maxima. However, at low electron energies the optical selection rules break down and the energy loss spectra cannot be described by the electron energy loss function given by equation (3.8).

Spectroscopy in $\vec{k}$-space ($\vec{k}$ is the wave vector of the crystal electrons) is one of the fascinating possibilities offered by electron energy loss measurements. The shift of the structures in the loss spectra as a function of the momentum $\hbar\vec{q}$ transferred to the crystal electrons can give detailed information on the $\vec{k}$-dispersion of the energy states of the crystal. The effort necessary to overcome the problems due to the $1/q^2$ decrease (see equ. 3.8) of the intensity of the scattered electrons will be outweighed by the information thus obtained. For solid rare gases the only attempt in this direction has been undertaken by Daniels and Krüger (1971).

Before leaving the subject of electron energy loss experiments we want to mention briefly the $M_{4,5}\,N_{4,5}\,N_{4,5}$ Auger spectrum of solid Xe determined by Nuttall and Gallon (1974) with the same apparatus used for the electron energy loss measurements by Nuttall et al. (1975). Comparison with the gas phase data shows that a considerable broadening of the Auger lines occurs in the solid which they suggest might be due at least partially to interaction with phonons.

3.4 Energy positions of maxima detected in various experiments below about 70 eV

The energy positions of the maxima found in the spectra of solid Ne, Ar, Kr and Xe are compiled in Tables IV, V, VI and VII.

3.4.1 Neon

Table IV gives the energy positions of the maxima reported for solid Ne. For comparison the energies of the 2p→ns (n≥3) lines of atomic Ne are included (Moore, 1949). There is reasonable agreement between the results of different experiments. The spin-orbit splitting of valence bands (0.10 eV for atomic Ne) has not been detected in most experiments, though for example in the reflectance measurements of Haensel et al. (1970d) the energy resolution at 18 eV was about 0.05 eV. Webber et al. (1964) predicted a broadening of the lines in the solid which might cause the spin-orbit partners to coalesce into a single broad line. Recently Pudewill et al. (1976a) observed a splitting of the lowest line of approximately 0.2 eV, which is very close to the 0.17 eV splitting of the 2p-3s line of atomic Ne.

3.4.2 Argon

The peak positions reported for solid Ar are listed in Table V . As for solid Ne we find reasonable agreement between the energy positions given by different authors. However, the energies of the maxima are slightly different in the ε_2, absorption, reflectance and electron energy loss spectra and also the width and the strength of the maxima may vary considerably. The maxima A, B and C are a good example for this. In the reflectance spectrum (Fig. 11b) the small peak A (half width ∿0.1 eV, reflectivity 40 %) is followed by a broad band (half width ∿0.4 eV, reflectivity 60 %), which is split into the two maxima Band C. In the ε_2 spectrum (Fig. 13b) however, peak A and B are almost identical whereas C has

shrunken to a small shoulder on the high energy side of B. The energy separation and the relative heights of the reflectance maxima B and C critically depend on the sample preparation. This is a strong indication that the splitting is connected to crystal growth problems and most probably is due to surface effects. On the basis of the existing experimental data it is impossible to decide whether the splitting is, for example, caused by the influence of surface roughness or by a deviation of the exciton energies in the planes close to the surface from the bulk exciton energies (Philpott, 1974). Due to the short wavelength limit of his source Baldini only found a broad maximum around 13.8 eV instead of the three maxima D, E and F.

3.4.3 Krypton

The energy positions of the maxima obtained for Kr are compiled in Table VI. The agreement between the results of reflectance and absorption measurements is good . The positions of the electron energy loss maxima reported by Schmidt (1972) are somewhat higher, but for an exact comparison the ε_2 spectrum should be calculated from the electron energy loss spectrum. Dressler's (1962) value for the position of the first exciton is too low. One of the most interesting aspects is the splitting of the n=1 members of the two exciton series into two peaks A, B and C, D respectively, observed in the reflectance measurements (Haensel et al. 1970c). This splitting has been well established for films evaporated at 20 K. It disappears for films evaporated at 8 K. The origin of the splitting is not clear. Its magnitude of about 100 meV seems to be too large to be caused by ordinary exciton phonon interaction. A possibly related effect has been observed in the reflectance spectra of the Cs-halides taken at low temperatures (Saile and Skibowski 1972) and has been ascribed to a Jahn-Teller effect by Sakoda and Toyozawa (1973). The strong influence of the substrate temperature makes an explanation in terms of surface effects very plausible.

3.4.4 Xenon

Table VII gives the energy positions of the maxima reported for solid Xe. The agreement between the results of different experiments is reasonable. The two maxima B and C at 8.76 eV and 8.926 eV detected by Steinberger et al. (1970) have not been confirmed by other experiments. The same holds for the structure of the 7.79 eV band found by Baldini (1962). In this context it should be mentioned that additional maxima have also shown up for example in the reflectance spectra of Ar below 15 eV (Harmsen et al. 1974). The appearance of these peaks critically depended on the way the samples has been prepared. The ability to characteristize the samples seems to be one of the keys to a full understanding of the spectra.

3.5 Interpretation and Discussion

Optical and electron energy loss experiments on RGS give information on the electron states and on the probability for photon induced transitions between the ground state and excited states. In the one-electron approximation the crystal electrons are considered to move independently in a periodic potential representing the interaction with the nuclei and the other electrons, and the energy of these electrons $E(\vec{k})$ form the band structure. For a discussion of the assumptions made in order to reduce the many particle problem to the one-electron band model the reader is referred to Rössler's review on band structure and excitons (chapter 8). A considerable number of band structure calculations have been performed on the RGS (Knox and Bassani (1961), Fowler (1963), Mattheis (1964), Reilly (1967), Rössler (1970), Ramirez and Falicov (1970), Lipari (1970, 1972), Lipari anf Fowler

(1970), Dagens and Perrot (1972), Kunz and Mickish (1973), Trickey et al. (1973), Euwema et al. (1974)). A detailed discussion of these calculations and a comparison of the different results is given by Rössler in Chapter 8. A schematic band structure representative of the energy bands calculated for the RGS is presented in Fig. 19.

A comparison of the experimental and theoretical results is best performed on the basis of the imaginary part ε_2 of the dielectric constant $\tilde{\varepsilon}$. From the energy bands $E_n(\vec{k})$ and the corresponding one electron wave functions $\psi_n(\vec{k})$, characterized by the band index n and the wave vector $\vec{k}$, ε_2 can be calculated by evaluating equation 3.11

$$\varepsilon_2(\omega) = C \cdot \frac{1}{\omega^2} \sum_{i,c} \int_{BZ} d^3\vec{k} |M_{ic}(\vec{k})|^2 \delta(E_c(\vec{k}) - E_i(\vec{k}) - \hbar\omega) \qquad (3.11)$$

The summation extends over all occupied bands $E_i(\vec{k})$ and empty conduction bands $E_c(\vec{k})$, the integration over the whole Brillouin zone. If the dipole matrix element given by

$$M_{ic}(\vec{k}) = \langle \psi_c(\vec{k}) | \vec{p} | \psi_i(\vec{k}) \rangle \qquad (3.12)$$

does not depend on the photon energy $\hbar\omega$ and the wave vector $\vec{k}$, the integral in equation (3.11) can be transformed in an integral over surfaces $S_{\vec{k}}$ of constant energy difference $\hbar\omega = E_c(\vec{k}) - E_i(\vec{k})$

$$\varepsilon_2 = C \cdot \frac{1}{\omega^2} \cdot |M_{ic}|^2 \sum_{i,c} \oint_{\hbar\omega} \frac{dS_{\vec{k}}}{|\nabla_k (E_c(\vec{k}) - E_i(\vec{k}))|} \qquad (3.13)$$

Under this assumption ε_2 is determined by the joint density of states

$$N(\omega) = \frac{1}{\Omega} \sum_{i,c} \oint_{\hbar\omega} \frac{dS_{\vec{k}}}{|\nabla (E_c(\vec{k}) - E_i(\vec{k}))|} \qquad (3.14)$$

where Ω is the volume of the Brillouin zone. For tightly bound core levels $\nabla_k E_i(\vec{k})$ vanishes and thus $N(\omega)$ is proportional to the density of states of the conduction bands.

In the spectra of all RGS sharp lines show up at the onset of electronic transitions, which cannot be understood in the framework of the one-electron band model. Baldini (1962) proposed to interprete these lines as members of Wannier type (see e.g. Knox, 1963) exciton series converging towards the conduction band minimum at point Γ of the Brillouin zone. This suggestion turned out to be very successful. Except for solid Ne, two series $\Gamma(3/2)$ and $\Gamma(1/2)$ originating from the spin-orbit split valence bands can be observed. In solid Xe the $\Gamma(1/2)$ series is hard to detect because of the overlapping continuum transitions of the $\Gamma(3/2)$ series. The energy E_n of the n^{th} member of a series is given by

$$E_n = E_G - \frac{E_B}{n^2} \qquad n=1,2,3... \qquad (3.15)$$

where E_G is the band gap. The binding energy E_B (in eV) can be computed from the effective reduced mass μ of the exciton (in units of free electron masses) and the dielectric constant ε.

$$E_B = 13.6 \frac{\mu}{\varepsilon^2} \qquad (3.16)$$

Using relation (3.15) the band gap E_G and the binding energy E_B have normally been determined from the energies of the n=2 and n=3 members of the series. (Baldini (1962), Bostanjolo and Schmidt (1966), Moorjani (1966), Steinberger and Schnepp (1967), Sinnock and Smith (1969), Haensel et al. (1969c, 1970c, 1970d), Steinberger et al. (1970), Boursey et al. (1970), Daniels and Krüger (1971), Schmidt (1972), Steinberger and Asaf (1973), Harmsen (1975), Pudewill (1975), Pudewill et al. (1976a)). The slightly different energies reported for the n=2 and n=3 excitons (Tables IV, V, VI, VII) result in different values for

E_G and E_B (see chapter 8, section 5.1). Representative values for E_B and E_G are given later in Table IX. Inserting E_B and the dielectric constants reported by Sinnock and Smith (1969) (Ar ε=1.66, Kr ε=1.86, Xe ε=2.18) into equation (31.6) yields the effective exciton masses μ listed in Table IX. For Ne a tentative value of the dielectric const (ε=1.24) was obtained from the density of solid Ne and the atomic polarizability by using the Lorentz-Lorenz formula (2.3). The experimental μ values are in good agreement with those determined from band calculations (chapter 8).

The first members of the exciton series, being too localized to be described in terms of the Wannier model, do not fit into the Rydberg series. This is already indicated by the similarity between the n=1 excitons and the corresponding absorption lines of the free atoms. Going from the gas to the solid the lines are shifted towards higher energies for Ne ($\sim$1 eV), Ar ($\sim$0.5 eV) and Kr ($\sim$0.2 eV) and slightly towards lower energies for Xe. The separation of the n=1 members of the $\Gamma(3/2)$ and $\Gamma(1/2)$ series is very close to the splitting of the $np^6 \rightarrow np^5(^2P_{3/2})(n+1)s$ and $np^6 \rightarrow np^5(^2P_{1/2})(n+1)s$ lines of the free rare gas atoms. This splitting is determined by the spin-orbit and the exchange energy (Condon and Shortley 1970). Onodera and Toyozawa (1967) have shown that from the energy splitting and the ratio of the oscillator strengths of the $\Gamma(3/2)$ and $\Gamma(1/2)$ excitons the exchange energy and the spin-orbit energy, giving detailed information on the coupling, can be obtained. There are some indications (see e.g. Harmsen et al. 1974) that in the solids the coupling is closer to jj-coupling than in the corresponding free atoms, where it is best described by Jl coupling (Moore, 1949, 1952, 1958). In regard of the considerable uncertainties involved in the determination of oscillator strengths results thus obtained can only be considered as preliminary.

The close correlation of the n=1 excitons and the atomic lines led to a tentative interpretation of these excitons as Frenkel excitons (Knox 1963) (see e.g. Baldini 1962). As has been discussed by Rössler (chapter 8) the problems encountered in describing the s-type final states by atomic wave function render the Frenkel exciton model not well suited to the RGS, and the best description of the n=1 excitons is given in terms of an intermediate exciton model (Knox (1962), Hermanson and Phillips (1966), Altarelli and Bassani (1971), Andreoni et al. (1975)). The binding energies $E_1\Gamma(3/2)$ of the $\Gamma(3/2)$ excitons calculated by Hermanson (1966), Rössler and Schütz (1973) and Andreoni et al. (1975) are presented in Table IX together with the experimental values. In agreement with the experimental results the calculations show that the central cell corrections, in comparison to the binding energies calculated from equations (3.15), (3.16), lead to a decrease of the binding energy for Ar and a slight increase for Xe. Starting from a four band model taking into account Coulomb and exchange interactions and the spin-orbit splitting of the valence bands Andreoni et al. (1975) achieved good agreement with the experimental results for the binding energies of the lowest $\Gamma(3/2)$ and $\Gamma(1/2)$ excitons of Ar. It is interesting to note, that the difference between the exciton binding energies determined by optical and by electron energy loss measurements is well described by the calculated separation of the transversal and longitudinal excitons.

For solid Ne even the higher series members can be correlated with atomic absorption lines. This indicates that these transitions mainly originate from the $2p^6 \rightarrow 2p^5ns$ ($n \geq 3$) transitions of atomic Ne. For solid Ar, Kr and Xe a similar correlation for the higher series members ($n \geq 2$) of the exciton series with transitions of the corresponding atoms cannot be found. There is some indication that maxima above the series limits of the exciton series can be ascribed to atomic like $p \rightarrow d$ transitions. The maximum showing up around 10.3 eV in the spectrum of solid Xe is an example for this (see chapter 8, section 5.1).

In comparing the results obtained by absorption, reflectance and electron energy loss measurements one has to take into account that corresponding maxima show up at slightly different energies due to the different relations between absorption, reflection and electron energy loss with the optical constants, the reflection and electron energy loss maxima are generally shifted towards higher energies with respect to the ε_2 maxima.

The energies also depend on the way the samples have been prepared and on the temperature of the samples. Considerable shifts of the excitons with temperature were detected by Steinberger and Asaf (1973) (see Fig. 9). As has been pointed out already these shifts are linear with temperature and density over the whole range from 6 K to 160 K. From this Steinberger and Asaf (1973) conclude that an interpretation in terms of exciton phonon interaction can be discarded because in that case the exciton energies should be temperature independent below the Debye temperature. Steinberger and Asaf proposed that the shift is caused by the change of the valence and conduction bands with lattice constant. The linear dependence of the observed shift on the density supports this explanation. The calculations of the dielectric constants led Doniach and Huggins (1965) to the same conclusion. Evaluating their data by means of equations (3.15) and (3.16) Steinberger and Asaf obtained a linear decrease of E_G and μ and linear increase of E_B with decreasing density. The different slopes of the curves E_G and E_B versus density result in the red shift of the exciton energies with decreasing density.

The interpretation of the broad structures found above the series limits of the exciton series is very difficult. Up to now there are no ε_2 spectra calculated from one electron energy bands available. There is little resemblance between the experimental results and the theoretical joint density of states of the valence and conduction bands. Kunz and Mickish

(1973) found some correspondence between the peak positions in the joint density of states and in the experimental spectra, but the relative heights are completely different. The joint density of states - see equation (3.14) - for Ne, Ar and Kr (Kunz and Mickish, 1973) are indicated in Figs. 12 and 13. The inclusion of the one electron matrix elements as in equation (3.13) will not improve the agreement. The spectra in this energy range are in fact dominated by excitonic effects, which greatly modify the strength of the valence band to conduction band transitions. Rössler and Schütz (1973) have demonstrated that the Coulomb interaction also gives rise to kinematic resonances above the band gap E_G, thus drastically changing the spectra. On account of these arguments any interpretation of the spectra in terms of critical points of the bands must be questionable.

Strong broad maxima have been found in the electron energy loss spectra around 19 eV in Ar, 17 eV in Kr and 15 eV in Xe. These maxima coincide with a strong decrease of the reflectivity in the reflectance spectra. This indicates that these maxima might be due to plasmon excitation of the outer p electrons as has been discussed for example by Keil (1968), Colliex and Jouffrey (1971), Schmidt (1972) and by Nuttall et al. (1975). The theoretical plasmon energy $\hbar\omega_{pe}$ is given by

$$\hbar\omega_{pe} = (E_G^2 + (\hbar\omega_p)^2)^{1/2} \qquad (3.17)$$

(Horie (1959), Miyakawa (1968), Cazaux (1972)) where $\hbar\omega_p$ is the free electron bulk plasmon energy (equation 1.17) and E_G the band gap. The plasmon energies calculated from equation (3.17) are 28.8 eV for Ne,

20.6 eV for Ar, 18.1 eV for Kr and 15.1 eV for Xe, and the correspondence with experimental values indicates that this explanation is undoubtedly correct in broad terms.

4. Optical spectra of RGS in the vacuum ultraviolet and the soft x-ray region

The first optical measurements on solidified rare gases in the soft x-ray region were performed by Soules and Shaw (1959). Using an x-ray source they determined the absorption of thin films of solid Ar and Kr near the K absorption edge. It took almost ten years until a group at DESY startet a thorough study of the optical properties of solid rare gases in this energy range using synchrotron radiation. Since then a lot of information has been obtained on the optical properties of solid Ne, Ar, Kr and Xe in the energy region of the Ne 2p,2s; Ar 3p,3s,2p; Kr 4p,3d,3p and Xe 5p,4d,4p,4s transitions (Haensel et al., 1969a,b, 1970a,b,1971, 1973; Schreiber, 1970; Keitel, 1970).

4.1 Experimental methods

As discussed in the previous section the optical constants of RGS have been determined near the onset of absorption by reflection, thin film absorption and electron energy loss measurements. For photon energies above 25 eV the normal incidence reflectivity of the solid rare gases is very small ($\lesssim$ 0.01 %), and long wavelength straylight, which is reflected with a much higher reflectivity, gives rise to considerable errors. Absolute values of the optical constants obtained by this method are, therefore, not very reliable. Only few electron energy loss measurements have been extended above 30 eV (Trebbia (1973), Farrell and Strongin (1972), Nuttall et al. (1975)). In what follows we will concentrate on thin film absorption measurements, since almost all available data have been obtained using this technique in the range above 30 eV.

A schematic representation of the experimental set up at DESY is given in Fig. 10. The spectrometer used in most of the measurements was a 1 m Rowland mounting with gratings of 2400 lines/mm and 3600 lines/mm. The resolution of the instrument was better than 0.1 Å in the entire spectral region. By choosing the appropriate angles of incidence onto the grating and by the use of a premirror in front of the entrance slit and of Al-, Mg- and Sb-filters, light of higher order reflections of the grating and stray light was essentially suppressed (for details see Samson, 1967).

Some absorption spectra have been obtained by a grazing incidence vacuum ultraviolet monochromator with fixed exit slit (not shown in Fig. 10) (Dietrich and Kunz, 1972). The parameters of this instrument are chosen to match the source characteristics at DESY. Scanning the spectrum from shorter towards longer wavelengths the angle of incidence of the incoming light onto the grating and a premirror is continuously decreased thus suppressing higher orders. Test measurements have shown that no higher order admixing occurs in the wavelength region from 40 Å to 350 Å. The instrument has a constant energy resolution of about 0.1 eV in the entire spectral region. The detector mounted behind the exit slit was an open Bendix multiplier for both instruments. The energy calibration of the spectrometer and the monochromator is based on the known energy positions of the absorption lines of atomic rare gases.

For the absorption measurements of the solid rare gases a He cryostat was mounted in front of the spectrometer or the monochromator respectively. The thin films of solid Ne, Ar, Kr and Xe were evaporated onto thin C, Al or Mg foils attached to the cryostat. The thickness of these substrates ranged from 200 Å to 1000 Å. The substrates were supported by a 75 µm copper mesh. They were cooled down to temperatures just below the sublimation point in vacuum at a pressure of 10^{-6} Torr (6 K for Ne, 15 K for Ar, 40 K for Kr, and 55 K for Xe). The temperature dependence of the spectrum of solid Ne has not been determined. Spectra of solid Ar, Kr and Xe evaporated at lower temperatures showed structures considerably broader than those of samples evaporated just below the sublimation point. Within the accuracy of the measurements no shift of the energy position of the maxima has been observed with temperature.

Under the above conditions the rare gases condense in the fcc phase forming polycrystalline samples, as has been proved in a separate experiment by the diffraction patternof 60 keV electrons. The sample preparation was exactly the same as for the optical experiments. The microstructure of samples such as these is discussed in chapter 10, § 5.1. To avoid contamination of the samples, the He cooled region was surrounded by a N_2 cooled shield with 40 cm long turbular extensions into both sides of the photon beam. The pressure in the vacuum system outside the cryostat was kept below 10^{-6} Torr. During the measurement of one sample (typical 1 h) no noticeable contamination of the sample was observed. The thickness of the solid rare gas films was not measured directly, but estimated by comparison with the absorption of the corresponding gas (see below). Samples of different thickness ranging from 1000 Å to 10000 Å were investigated.

As has been already mentioned above, Soules and Shaw (1959) used the continous Bremsstrahlung radiation emitted by an x-ray source to determine the K-absorption of solid Ar and Kr. The spectra were obtained with the help of a two crystal vacuum spectrometer. Ar and Kr were condensed on thin films of Be and Al respectively cooled to liquid He temperature. In this experiment the thickness of the films was determined by comparison with the known gas absorption coefficient at energies more than 100 eV from the absorption discontinuity.

4.2 Continuum absorption

4.2.1 Experimental results

The absorption spectra of solid Ne, Ar, Kr and Xe from the onset of absorption up to 500 eV are shown in Figs. 20 and 21. The absorption coefficients determined by reflection measurements (Skibowski (1971), Steinberger (1973), Saile (1974)) are included below 30 eV. The absorption cross sections of the corresponding free atoms are given for comparison.

As the thickness of the solid rare gas films has not been measured only the relative spectral dependence of the absorption coefficient could be determined experimentally. The determination of the absolute absorption cross section has been based on the assumption that the oscillator strength integrated over a large spectral region should be the same for both the gaseous and the solid phase. Thus the absolute values of the absorption cross section have been obtained by setting equal the oscillator strength of the solid and the gas integrated over the measured spectral region. This procedure is seen to be justified by the excellent agreement obtained between the absorption spectra of the gaseous and solid samples.

The absolute absorption coefficient has been calculated using the experimental values of the lattice constants; the estimated error of the absolute values is ±30 %. The relative accuracy is much better since differences in the absorption coefficient of the order of 1 % were clearly detectable if photon energies were not more than a few eV apart.

The real part n of the refractive index has been calculated by the Kramers-Kronig relation (1.10). The integration has been performed over the whole energy range shown in Figs. 20 and 21. For the extrapolation towards higher photon energies and for the interpolation in regions where there are no data for the solid rare gases the absorption cross section of the corresponding atoms have been used. The refractive indices deduced are given in Fig. 22. The errors estimated from the uncertainties in the absolute values of the absorption coefficient are indicated by error bars.

The number of effective electrons n_{eff} contributing to the absorption in the photon energy range from E_1 to E_2 is given by equation (1.19). From the experimentally determined values of the absorption coefficient and the real part of the refractive index the number of effective electrons contributing to the absorption of the solid rare gases from the onset of absorption up to 400 eV for Ne, 1000 eV for Ar and 500 eV for Kr and Xe has been calculated. As for the determination of n the absorption cross sections of the corresponding free atoms have been used for spectral regions where no data for the solid rare gases were available.

For Ne n_{eff} increases smoothly from the onset of absorption towards higher energies leveling off at about 400 eV where $n_{eff} \approx 8$. From the onset of absorption n_{eff} increases up to about 40 eV reaching a value of 5 for Ar, 9 for Kr and 7 for Xe. At higher energies n_{eff} increases very slowly. At 245 eV, the onset of the Ar 2p absorption $n_{eff} = 6.5$, at 90 eV, the onset of the Kr 3d absorption, $n_{eff} = 9$ and at 64 eV, the onset of the Xe 4d absorption, $n_{eff} = 7$. This means that the oscillator strength of the transitions from the outer shells (2p and 2s for Ne, 3p and 3s for Ar, 4p and 4s for Kr and 5p and 5s for Xe) is almost exhausted at the onset of the inner-shell transitions. Above the onset of these inner shell transitions we find a further increase of n_{eff} leading to $n_{eff} = 14.5$ at 1000 eV for Ar, $n_{eff} = 23$ at 500 eV for Kr and $n_{eff} = 22$ at 500 eV for Xe. This leads to the conclusion that most of the oscillator strength of the Ar 2p, Kr 3d and Xe 4d transitions is concentrated in this energy region. The n_{eff} values obtained for the solid rare gases are in agreement with the values given by Samson (1966) for the corresponding free atoms.

4.2.2 Discussion

As has been shown above, the absorption spectra of the solid rare gases at high energies are very similar to those of the corresponding free atoms. Solid state effects only show up prominently at the onset of transitions from inner shells and furthermore give rise to some weak structures superimposed on the smooth continuum absorption. Most of the gross features of the spectra, therefore, can be understood in terms of atomic theories.

The hydrogen-like model for photoionization has failed to describe the absorption of rare gases in the VUV adequately. This is primarily due to the departure of the effective electric field from the Coulomb law in the outer portions of the atoms where the main contribution to absorption in the VUV stems from. Single-electron models based on more realistic atomic potentials calculated by self-consistent methods, like those tabulated by Herman and Skillman (1963), give the gross features of the absorption spectra. The non-Coulomb attractive potential and its interplay with the repulsive centrifugal force can give rise to potential barriers causing a depression of the oscillator strength at the onset of transitions from tightly bound shells, quasiresonances above threshold and Cooper minima (Fano and Cooper, 1968). Since the transitions $\ell \rightarrow \ell+1$ dominate the transitions to continuum states, we will neglect the $\ell \rightarrow \ell-1$ transitions in our further discussion (see e.g. McGuire, 1968; Fano and Cooper, 1968).

In Ne the $2p \rightarrow \varepsilon d$ transitions are depressed at threshold. Towards higher energies the absorption due to these transitions increases, giving rise to the broad maximum at about 30 eV. For the Ar 3p, Kr 4p and Xe 5p absorption the depression at threshold is not easily disentangled from the effect of the resonance above threshold. The resonance causes the precipitous drop of the absorption coefficient with increasing photon energy in the energy range from 25 to 45 eV for Ar, from 20 to 80 eV for Kr and from 20 to 60 eV for Xe. The Cooper minimum, which is due to a zero of the matrix element of the $3p \rightarrow \varepsilon d$ transitions, is clearly to be seen at about 45 eV in Ar. Above this minimum the transition probability for these transitions increases slowly towards higher energies giving rise to the subsidiary maximum at 80 eV. In Kr and (Xe) the 3d (4d) absorption above 90 eV (64 eV) overlap the subsidiary maximum due to the $4p \rightarrow \varepsilon d$ ($5p \rightarrow \varepsilon d$) transitions. Above the onset the Ar 2p (at 245 eV) absorption almost shows a hydrogenic behaviour. The atomic potential for

the f symmetric continuum states in Kr is repulsive except for distances from the nucleus larger than 3 Å. The oscillator strength of the Kr $3d \rightarrow \varepsilon f$ transitions, therefore, is depressed at the onset and shifted towards higher energies. This explains the broad maximum found at about 100 eV above the threshold of these transitions at 90 eV. The two-valley atomic potential seen by the f-symmetric continuum states of Xe causes the resonant behaviour of the 4d absorption above threshold. The Xe 4d absorption is a very good example for this behaviour because the resonance maximum at 100 eV, the Cooper minimum at 200 eV and the subsidiary maximum at about 330 eV are not masked by overlapping transitions.

The absolute photoabsorption cross sections in the single particle approximation based on a local potential (in most of the calculations the potential tabulated by Herman ans Skillman (1963) is used) differs, considerably, sometimes by an order of magnitude, from the values given by experiment. These calculations give resonance maxima much narrower and at lower energies than found experimentally. Better agreement with the experimental results has been obtained by taking the intrachannel interaction (Fano and Cooper, 1968), which is part of the final state correlation effects, into account. This has been done by using the Hartree-Fock nonlocal potential (Kennedy and Manson, 1972) or by starting from a local central field and calculating the intrachannel effect by the reaction matrix method (Starace, 1970).

Using the apparatus of many-body theory, thereby taking into account many-electron correlations Amusia et al. (1971) and Amusia (1973, 1974) calculated the photoioni-

zation cross section of rare gases in the random phase approximation with exchange starting with essentially Hartree-Fock wave functions. The theoretical and the experimental cross sections coincide within the range of 10 %. Lin (1974) obtained similar results using a simplified random phase approximation based on the reaction matrix method including ground state correlation effects. The photoabsorption cross section for Ar calculated by means of a many-body perturbation theory (Kelly and Simons, 1973) is also in good agreement with the experimental results. The influence of many electron correlation and collective effects on atomic absorption have been subject of the work of Brandt et al. (1967) and of Wendin (1973, 1974).

We hope we have convinced the reader, that the gross features of the VUV spectra (above 25 eV for Ne and Ar, 15 eV for Kr and Xe) of the RGS can be understood in terms of atomic models alone. There are, as we discussed above, strong solid state effects up to 10 eV above the onset of the Ne 2p, Ar 3p, Kr 4p and Xe 5p absorption. Solid state effects also clearly manifest themselves, as we will see in section 4.3, for photon energies up to 15 eV above the Kr 3d and Xe 4d threshold and up to 30 eV above the Ar 1s,2p and Kr 1s threshold. Outside these regions the spectra of the RGS hardly deviate from the corresponding spectra of the free atoms. In the spectrum of solid Xe at 100 eV, for example, there are small maxima and minima not present in the spectrum of gaseous Xe. These oscillations of the absorption coefficient could be interpreted as extended x-ray absorption fine structure (EXAFS). The EXAFS has been studied for many years (see e.g. Azaroff, 1963, Sayers et al., 1970, 1971; Stern and Sayers, 1973; Schaich, 1973; Ritsko et al., 1974; Stern, 1974; Ashley and Doniach, 1975). The basic physical mechamism is inter-

ference between the outgoing photoelectron wave from the absorbing atom and the backscattered waves from the surrounding atoms. This mechanism may also be responsible for the broad maxima above the Ar 1s (3220 eV - 3250 eV), Ar 2p (255 eV - 280 eV), Kr 3d (95 eV - 120 eV), and Xe 4d (70 eV - 80 eV) threshold. Up to now no calculations of the EXAFS of the RGS are available. Due to the complex nature of the processes involved such calculations are by no means trivial (Fano, 1974). Most of the models proposed until now are relatively crude and therefore a lot of work remains to be done before a conclusive identification of the structures found in the RGS can be reached.

4.3 Fine structure at the onset of transitions from inner shells

The fine structure of the absorption spectra at the threshold of transitions from the Ne 2s, Ar 3s, Ar 2p, Ar 1s, Kr 3d, Kr 1s, and Xe 4d shell are shown in Figs. 23 to 26. For comparison the absorption spectra of the corresponding free atoms are included. The energy position of the absorption maxima are listed in Table VIII.

The interaction of the discrete final states with the underlying continuum gives rise to asymmetric lines for the 2s absorption of atomic Ne (Fig. 23a) and window type lines for the 3s absorption (Fig. 23b) of atomic Ar (Codling et al., 1967; Fano and Cooper, 1965,1968; Madden et al., 1969). In the spectra of the solids these lines are broadened and slightly shifted towards higher energies, due to the interaction with the neighbouring atoms. The characteristic line shapes are the same for both the solid and the gas. These leads to the suggestion that even in the solid these lines are due to atomic like excitations originating from the corresponding transitions in the gas. This inter-

pretation is supported by the results on rare gas alloys (Haensel et al.,1973). That we only see two members of the series is probably due to the broadening found in the solids that smears out structures caused by the higher members of the series. No indication of the onset of interband transitions could be detected in these spectra. This is in agreement with the relatively flat and featuresless joint density of states calculated by Kunz and Mickish (1973).

At the onset of the Ar 2p (Fig. 24), Kr 3d (Fig. 25a) and Xe 4d (Fig. 25b) absorption in the solids, a considerable number of discrete structures have been detected (Haensel et al., 1969a,b,1970a,1971; Keitel, 1970; Schreiber, 1970). These structures occur in pairs with the energy distances being equal to the spin orbit splitting of the core state (2.03 eV for Ar, 1.2 eV for Kr and 1.97 eV for Xe). The energy position of the absorption lines A, A' in Ar and B, B' in Kr and Xe is very close to the position of the corresponding absorption lines in the gas. The small shift towards higher energies is due to the interaction with the neighbouring atoms. Also the line shape and the width of the lines is comparable in both phases. Rössler (1971) and Kunz and Mickish (1973) showed that these lines cannot be explained by the density of states of the conduction band. All this leads to the interpretation of these lines as being due to atomic like excitations originating from the 2p→4s transition of atomic Ar, the 3d→5p transition of atomic Kr and the 4d→6p transition of atomic Xe. Again this explanation is supported by the results of the measurements on rare gas alloys (Haensel et al., 1973).

For Ar the oscillator strengths of these lines are similar in both the solid and the gaseous phase. As has been shown by Rössler (c.f. chapter 8) the final states in Ar lie below the s-symmetric conduction band minimum whereas in the case of Kr and Xe they lie above the conduction band minimum. The interaction of the discrete and fairly localized states with the overlapping band states might explain the smaller oscillator strengths found for the lines B,B' in solid Kr and Xe. Kunz and Mickish (1973) find the Ar lines sitting on a low density of band states whereas the density of overlapping band states in the case of Kr is much higher, thus the same argument holds. Whether excitonic effects are also responsible for the peaks B,B' in solid Ar and C,C' in solid Kr and Xe is not completely clear. Measurements on the rare gas alloys (Haensel et al., 1973) indicate some correlation between these maxima and the higher members of the series which show up in the gaseous spectra.

The interpretation of the lines A,A' and B,B' in the 2p spectrum of solid Ar as core excitons is supported by the theoretical results reported recently by Altarelli et al. (1974,1975). Altarelli et al. computed the binding energies of the lowest excitons of symmetry Γ_{15} using the 2p atomic wave functions, the Wannier functions of the conduction band, and the atomic spin-orbit splitting between the j=3/2 and j=1/2 states. According to their results peak A is the $\Gamma_{15}(3/2)$ exciton (binding energy 3.37 eV), peak A' the $\Gamma_{15}(1/2)$ exciton (binding energy 1.37 eV). The oscillator strength of the $\Gamma_{15}(3/2)$ exciton is twice that of the $\Gamma_{15}(1/2)$ exciton. Altarelli et al. place the onset of the interband transitions at ∿248.5 eV, close to the shoulder C. The peaks B and B' are tentatively ascribed to excitons due to higher conduction bands with d-like symmetry.

At higher energies the spectra can be interpreted in terms of interband transitions. Rössler (1971) and Kunz and Mickish (1973) found reasonable agreement between the calculated joint density of states and the experimental results for photon energies between 247 eV and 255 eV for Ar, 92 eV and 98 eV for Kr and 65 eV and 72 eV for Xe (see also chapter 8). This is in contrast to the situation above the onset of the valence band transitions discussed in section 3.4, where we found almost no correspondence between the experimental spectra and the calculated joint density of states, as excitonic effects completely dominate the valence band transitions in that spectral range. As we have seen above excitonic effects are also present right at threshold of the Ar 2p, Kr 3d and Xe 4d excitation giving rise to the lines A,A' and possibly B,B' in the spectrum of Ar and B,B' in the spectra of Kr and Xe. Except for these lines the excitonic effects seem to be less for the Ar 2p, Kr 3d and Xe 4d excitation than for the valence band transitions. This might be due to a reduction of the electron-hole interaction by the intervening closed Ar 3s,3p, Kr 4s,4p and Xe 5s,5p shells.

At the onset of the K absorption of solid Ar (Fig.26a) a broad somewhat asymmetric maximum has been found by Soules and Shaw (1959). At higher photon energies further broad structures have been detected. The width of the maxima found in the solid is much larger than the width of the 1s→4p and 1s-5p lines that are clearly resolved in the spectrum of atomic Ar. A broad maximum followed by broad structures towards higher energies also shows up in the K absorption spectrum of solid Kr (Fig.26b). The line structure in the spectrum of atomic Kr has not been resolved in these measurements.

5. Other measurements of electronic energy levels of RGS

5.1 Photoconductivity

No edge due to the onset of transitions from the uppermost valence band to the lowest conduction band has been detected either in the absorption or reflection spectra of the rare gas solids as the strong absorption due to excitons completely masks the onset of band to band transitions. The width of the band gap has normally been determined from the series limit of the Wannier excitons. As we have discussed already in section 3.5 the energy position of the n=1 exciton does not fit into the Rydberg series given by equation (3.15). In most measurements only the n=2 and n=3 members of the Wannier series could be resolved clearly. The series limit therefore has to be inferred from the energy positions of the n=2 and n=3 excitons alone. It is obvious that the application of a more direct method, such as the technique of photoconductivity for the determination of such a crucial parameter as the band gap is of great importance.

The first conductivity measurements on solid Xe were carried out by Asaf and Steinberger (1972). Later on Asaf and Steinberger (1974) investigated the photoconductivity of solid Xe at different temperatures and also expanded their studies to include liquid Xe. In these experiments research grade Xe was condensed within the cryostat in a closed cell having a LiF or a MgF front window. The gas inlet system and the cell previously had been pumped down to about 5.10^{-7} Torr by a sorption pump and an ion pump. The inner surface of the window was covered by gold electrodes in the shape of interlaced combs. The light from a Tanaka type Ar (Kr) lamp, monochromatized by a McPherson 1-m type 225 monochromator, reached the Xe condensed between the teeth of the combs after it passed through the window. D.C. voltages were applied and the currents measured by an electrometer amplifier.

Figure 27 represents the photocurrent of solid and liquid Xe as a function of photon energy. There is a striking similarity between the curves for solid and liquid Xe. Below 9.2 eV there is only a small photocurrent which might be due in part to direct ionization of impurities and to the creation of charge carriers at the surfaces. A weak maximum shows up at 8.6 eV close to the energy position of the n=1 $\Gamma(3/2)$ exciton. This indicates that conduction electrons created via energy transfer processes between excitons and impurities or the electrodes contribute to the conductivity below threshold. The onset of interband transitions corresponds to the steep increase of the photocurrent at about 9.27 eV. Table IX contains the photoconductivity thresholds determined by Asaf and Steinberger (1972, 1974). These values corroborate the value for the band gap inferred from the extrapolation of the Wannier exciton series included in Table IX. For a detailed comparison one has to take into account (i) the temperature dependence of the energy positions of the excitons and the corresponding series limit (ii) the possibility that higher order excitons $n \geq 3$ may dissociate thermally or create charge carriers by energy transfer processes at impurities or surfaces and thus give rise to a photoconductivity threshold somewhat lower than the band gap.

There is a marked dip in the photoconductivity curve at about 9.5 eV for solid and 9.45 eV for liquid Xe which, due to the low reflectivity (less than 20 %), can only partially be accounted for by the reflectivity maximum at the energy of the n=1 $\Gamma(1/2)$ exciton. The strong absorption due to the exciton considerably reduces the number of photons available for direct creation of conduction electrons. As we have already mentioned above the excitons may also contribute to the conductivity by the creation of conduction electrons via energy transfer processes. But due to the competing decay channels, for example luminescence, only a fraction of the excitons will result in conduction electrons.

For liquid Xe Asaf and Steinberger (1974) report 9.202 eV for the photoconductivity threshold and 9.22 eV for the series limit of the $\Gamma(3/2)$ exciton series. These values disagree with the band gap of 8.9 eV determined by photoconductivity measurements on liquid Xe performed by Roberts and Wilson (1973). The high concentration of impurities present in the liquid and complications due to photoemission from parts of the sample cell are possible explanation for the low value reported by Roberts and Wilson.

Recently Steinberger et al. (1974) employed a new electrode system, consisting of two interlaced phosphor bronze combs mounted without any substrate. Trading in the advantages of the closed cell, better crystal quality and wide temperature range, they gained the possibility to simultaneously determine the photoconductivity and the photoelectric yield of rare gas solids. We will come back to the photoelectric yield in section 5.2. At the moment we are only interested in the results of the photoconductivity measurements. No clear photoconductivity steps were observed for solid Ar and Kr. A small step detected at 14.25 eV for solid Ar might correspond to the photoconductivity threshold for transitions from the lower valence band (j=1/2) to the conduction band. The results for solid Xe are given in Table IX. Before leaving the subject of photoconductivity we want to mention the measurements by Spear and LeComber (see chapter 18). Their results are presented in Table IX. There is satisfactory agreement between these data and those published by Asaf and Steinberger (1972, 1974) and Steinberger et al. (1974).

5.2 Photoemission

5.2.1 Photoelectric yield

In the last decade photoemission has been proven to be an excellent technique to obtain detailed information on the structure of valence- and conduction bands

of solids (see e.g. Eastman 1974, Spicer 1974, Feibelman and Eastman 1974, Grobman 1975, Grobmann et al. 1975). For perfect insulators like the RGS photoemission studies are hampered by charging of the samples. These difficulties have been overcome for measurements of the photoelectric yield by applying voltages between sample and collector which are far above the saturation level of the photocurrent. O'Brien and Teegarden (1966) reported the first measurements of the photoelectric yield of thin films of Kr and Xe for photon energies below the LiF cut off. Thin Xe films condensed on a platinum substrate at 20 K (annealed at 55 K) showed a sharp increase of the photocurrent at 9.7 eV. This threshold corresponds to the onset of direct transitions to conduction band states above the vacuum level. Because of the limited energy range no threshold could be observed for solid Kr. For both, solid Kr and Xe the photoelectric yield spectra showed structure in the exciton region below threshold. In analogy to the interpretation of the photoemission of alkali halides containing colour centers O'Brien and Teegarden suggested that the photoemission in this region is due to the interaction of the excited states of the crystal with impurities or defect centers. O'Brien and Teegarden found marked differences between the yield spectra of annealed and unannealed films.

Schwentner et al. (1973) and Koch et al. (1974a) used the continuous spectrum of the synchrotron radiation to determine the photoelectric yield of solid Ne, Ar, Kr and Xe for photon energies between 10 eV and 32 eV. The experimental set-up, consisting of a normal-incidence spectrometer and an ultra-high vacuum system attached to it (base pressure 4.10^{-10} Torr) has already been described in section 3.2 in context with the reflection measurements. The films were condensed (at 5-8 K for Ne, at 10-30 K for Ar, Kr and Xe) on gold coated quartz crystals. Temperature effects and the influence of annealing were not studied systematically. A copper mesh in front of the sample served as a collector.

The current flowing to the isolated gold substrate was measured with an electrometer amplifier. The currents ranged from 10^{-10} A to 10^{-14} A. The results are presented in Fig. 28. For all RGS there is a small signal in the exciton region which can be explained by the following secondary mechanisms; emission of hot electron from the gold substrate, exciton induced emission from impurities or defect centers and a decay of excitons at the sample gold or sample vacuum boundary. The investigation of the dependence of the photoemission of doped rare gases in the exciton region on the nature of the impurities, the impurity concentration, the thickness and the preparation of the samples have provided exciting results on exciton dynamics (Koch et al. (1974a,1974b), Ophir et al. (1975), Pudewill et al. (1976b)).

Since we want to concentrate on the pure rare gas solids the reader is referred to an excellent review on this subject by Jortner (1974). At higher photon energies a steep increase of the photoelectric yield indicates the onset of transitions to conduction band states above the vacuum level. Above this threshold the yield increases with increasing film thickness till it saturates for films thick enough to totally absorb the incoming light above the onset of interband transitions (Schwentner et al. 1973, Koch et al. 1974a, 1974b). Table IX also includes the photoemission thresholds E_{Th} determined from yield spectra by Schwentner et al. (1974) and Koch et al. (1974a). It should be noted that since the threshold for Ne and Ar lies below the optically determined band gap, the value thus obtained can only form an upper limit for the energy position of the vacuum level.

For films thicker than the attenuation length of the incoming light, given by μ^{-1}, there is almost no similarity between the yield spectra and the optical spectra above threshold. This is consistent with the fact that for energies between E_G and E_G+E_X (E_X is the energy of the n=1 $\Gamma(3/2)$ exciton)

the escape depth L of the photoelectron is much larger than the attenuation length of the photons. (Schwentner et al. 1974). The dependence of the photoelectric yield Y per incoming photon on the reflectivity R, the absorption coefficient μ and the escape depth L can be approximated by

$$Y \propto (1-R)\ \frac{\mu}{\mu+1/L} \qquad (5.1)$$

(Spicer 1972)

Since $L \gg \mu^{-1}$ the yield Y does not depend on the absorption coefficient μ. For photon energies above E_{Th} the reflectivity R is less than 0.1 thus the factor 1-R only causes small variations of the yield.

At photon energies above E_G+E_X electron-electron scattering sets in. This leads to a decrease of the photoelectric yield for Kr and Xe since both electrons are scattered into states below the vacuum level and therefore don't contribute to photoemission. At even higher photon energies the energy of the scattered electrons may be sufficient for both electrons to escape into the vacuum and therefore the yield will begin to rise again. Electron-electron scattering is thus responsible for the minimum at 22 eV for solid Xe and at 24 eV for solid Kr. Since the vacuum level lies below the conduction band minimum there is no corresponding minimum in the yield spectra of solid Ne and Ar.

Evaporating only thin films on the phosphor bronze combs used as electrodes for the photoconductivity measurements (see section 5.1) Steinberger et al. (1974) determined the photoelectric yield of solid Ar, Kr and Xe for photon energies up to 15 eV. If no crystals bridge the gap between adjacent prongs the currents (of the order of 10^{-14} - 10^{-12} A) measured were due to electrons which left the sample covering the negative electrode and were collected at the positive

electrode. Table IX includes these photoemission thresholds. As in the measurements discussed above structures closely related to structures in the optical spectra could be detected below threshold.

Electron energy distribution

The energy distribution curves (EDC) for the photoelectrons emitted from the valence bands of solid Ne, Ar, Kr and Xe have been determined for the first time by Schwentner (1974), Schwentner et al. (1974,1975).
The experimental set-up has already been briefly discussed in context with the yield measurements. A commercial system (Aris) consisting of a retarding grid and a set of electrostatic lenses served as electron energy analyzer. An energy resolution of 0.2 eV was achieved. Thin films (thickness < 100 Å) were evaporated under ultra high vacuum conditions on to Au substrates in thermal contact with a He-flow cryostat. By using thin films Schwentner and coworkers succeeded in overcoming the difficulties due to charge building up in the samples under irradiation. For photoemission measurements on insulators charging of the sample forms a severe obstacle. It can give rise to an energy shift of the EDC but even more serious can result in a complete blurring of the EDC if an inhomogeneous charge distribution is formed. Varying the thickness of the films between 20 Å and 100 Å did not affect the characteristic features of the EDCs. The spectra, therefore, are considered as representative for the bulk. Since for all samples the reflectivity was determined simultaneously the EDCs could be normalized to the number of photons incident on the sample. At the same time the reflectivity spectra offered an easy but very sensitive check on the quality of the films.

The EDCs for solid Ne (at 5 - 8 K) and for solid Ar, Kr and Xe (at 10 - 30 K) for various photon energies below the onset of electron-electron scattering are presented in Fig. 29. The EDCs are plotted as a function of initial state binding energy. The zero binding energy corresponds to the top of the valence band. The curves for different photon energies have been displaced up wards by an amount proportional to the exciting photon energy. In this scheme constant initial states lie on top of each other whereas constant final states are diagonally shifted to the left with increasing photon energy. As an example the position of the vacuum level is marked for photon energies up to 2 eV above threshold. Locating the intersection of this line with the zero binding energy line provides a very precise method for the determination of the energy position of the vacuum level E_V. The results thus obtained are listed in Table IX. For Kr and Xe they agree with photoemission threshold E_{Th} determined by photoelectron yield measurements. From the values of E_V the electron affinities E_A ($E_A=E_V-E_G$) can be determined by subtracting the gap energies E_G determined by absorption or reflection measurements. The results are also compiled in Table IX. The data corroborate the trend from a negative electron affinity for Ne to a positive value for Xe predicted from estimates based on the relation

$$E_A = I + P^+ - E_G \qquad (5.2)$$

with I the ionization energy of the free atom (Raz and Jortner 1971). The values of the self energy of the hole P^+ (included in Table IX)were estimated by Fowler (1966) on the basis of the Mott-Littleton approximation.

The agreement between the experimental values for E_V and E_A and those obtained by band structure calculations forms, in addition to the gap energies E_G, a further criterion for the reliability of the calculated energy bands. For comparison the experimental and theoretical results for E_A, E_V and E_G are compiled in Table X.

Most of the values for the binding energy of the valence electrons at Γ_{15} obtained by band structure calculations are in reasonable agreement with the distance E_V between the top of the valence band and the vacuum level determined by the photoemission measurements. Especially those band calculations which include correlation reproduce the experimental data fairly well. In contrast there are considerable differences between the electron affinity E_A and the binding energy of the bottom of the conduction band at Γ_1. This clearly illustrates that the absolute energy of the tightly bound valence electrons can be calculated to a much higher accuracy than the energy of the conduction bands. The discrepancies found between the band gap determined experimentally (E_G) and theoretically ($\Gamma_1-\Gamma_{15}$) can to a large extend be blamed on the erroneous binding energy calculated for the bottom of the conduction band. In performing this comparison we tacitly ignored any complication due to surface effects, which seems to be consistent with the experimental results for RGS.

Above theshold the width of the EDC increases with increasing photon energy until the photon energy is sufficient to excite electrons from the bottom of the valence band (23 eV for Ne, 16.5 eV for Ar, 14.6 eV for Kr and 13.8 eV for Xe). In this region the width of the EDC corresponds to the width of the valence band and is independent of the energy of the exciting photons. Photoemission thus lends itself to a determination of the valence band width. The total valence band widths obtained by Schwentner (1974) and Schwentner et al. (1975) are presented in Table X together with the band widths predicted by calculations and the spin orbit splitting of the free atoms. The experimental band widths for all rare gases exceed the spin orbit splitting. This clearly proves that a description of the valence bands by two flat bands separated by the spin-orbit splitting considerably underestimates the influence of the crystal field which results in a marked dispersion of the bands.

It is obvious from the values compiled in Table X that most band calculations predict valence band widths smaller than found experimentally by this method.

For Ne even the largest width of 0.65 eV calculated by Euwema et al. (1974) is only half of the experimental width. Reasonable agreement with the experimental band width for Ar has been achieved by non relativistic band calculations by Ramirez and Falicov (1970) and by Kunz and Mickish (1973). The inclusion of the spin orbit interaction should affect the band widths only slightly.

The two relativistic band calculations by Rössler (1970) and Fowler (1963) available for Kr result in total band width considerably smaller than observed. The width of the non relativistic valence bands calculated by Lipari (1970) already exceeds the experimental width by 0.5 eV. Taking the spin orbit splitting of 0.7 eV into account should lead to an even larger discrepancy. Simply adding the spin orbit energy to the width of the nonrelativistic bands obtained by Kunz and Mickish (1973) leads to an excellent agreement between theory and experiment, but this approach might not stand a thorough scrutiny (Fowler, 1963). The valence bands of Xe obtained by Reilly (1967) and by Rössler (1970) are much smaller than the width inferred from the width of the EDCs.

Three maxima clearly can be distinguished in the EDCs of Xe for photon energies between 13 eV and 16 eV. Above 16 eV the two maxima with binding energies less than 2 eV coalesce into one broad band. Within the accuracy of the measurements the energy position of the three maxima are independent of the energy of the exciting photon. The maxima are therefore attributed to maxima of the density of states of the valence bands. At Γ, the center of the Brillouin zone there are two band $\Gamma(3/2)$ and $\Gamma(1/2)$ separated by the spin orbit splitting. Away from Γ the upper band is split into two bands by the crystal field. The main contribution

to the density of states stems from region close to the Brillouin zone boundaries. On the basis of this model we expect three maxima in agreement with the experimental result. The two maxima with binding energies less than 2 eV originate from transitions from the upper (j=3/2) valence bands. The third maximum is ascribed to transitions from the lowest (j=1/2) valence band. The separation of the peaks is determined by both the spin orbit splitting and the strong binding of the bands from the center of the zone towards the zone boundaries.

Going from Xe to Kr, Ar and Ne the spin orbit splitting and the dispersion of the bands decreases. This leads to a partial overlap of the three maxima, well separated in the EDCs of Xe. The EDCs of Kr and Ar only show two maxima for photon energies more than 3 eV above threshold. There is only one broad band for Ne. At 26.72 eV photon energy a small shoulder pops up. Transitions from the upper (j=3/2) valence bands give rise to the maxima at binding energies of 0.7 eV for Kr and 0.5 eV for Ar. The maxima at 2 eV for Kr and 1.4 eV for Ar originate from the lower (j=1/2) valence band. The separation of the peaks exceeds the spin orbit splitting (see Table X) and also the splitting of the bands at the Brillouin Zone boundaries predicted by most of the calculations. Since photoemission measurements on doped rare gases (Schwentner et al. 1975) confirmed that the spin orbit splitting is always close to the atomic value, theory and experiment can only be reconciled by postulating a k-dependence of the bands stronger than obtained in most calculations. When discussing the total widths of the bands we were already lead to the same conclusion.

Up till now we were mainly concerned with the energy positions of the maxima detected in the EDCs. A superficial inspection of the curves already shows that strong changes of shape and intensity occur as a function of the exciting photon energy. Neglecting matrix element effects and assuming direct transitions Schwentner et al. (1975) obtained estimates for the structure of the conduction

bands from these changes. They located the first maximum of the density of states, corresponding to flat regions of the lowest conduction band at 1.1 - 1.9 eV for Xe, 1.6 - 2.1 eV for Kr, 2.5 - 3.5 eV for Ar above the bottom of the conduction band.

For a more detailed comparison between theoretical and experimental results the structure of both the valence $E_V(\vec{k})$ and the conduction bands $E_C(\vec{k})$ and transition matrix elements have to be taken into account. The energy distribution $N(E,\hbar\omega)$ (E electron energy, $\hbar\omega$ photon energy) for direct transitions can be obtained from the results of band calculations by the relation

$$N(E,\hbar\omega) = C \sum_{V,C} \int_{BZ} d^3\vec{k} |M_{VC}|^2 \delta(E_C(\vec{k})-E_V(\vec{k})-\hbar\omega)\delta(E_C(\vec{k})-E). \qquad (5.3)$$

Where the integration extends over the whole Brillouin Zone, the summation over all valence and conduction bands. If the matrix element M_{VC} can be set constant equation (5.3) reduces to

$$N(E,h\omega) = C' \sum_{V,C} \int_{BZ} d^3\vec{k}\,\delta(E(\vec{k})-E_C(\vec{k})-\hbar\omega)\delta(E_C(\vec{k})-E) \qquad (5.4)$$

From the band structure obtained by the KKR method Rössler (1970) calculated the EDCs for solid Xe according to equation (5.4). Figure 30 presents Rössler's results together with the experimental EDCs. The theoretical EDCs reproduce the main features of the structure of the experimental curves fairly well. There are some differences in regard to the relative strength of the three maxima but this may be blamed on matrix element effects not included in the calculation. The most striking discrepancy lies in the much smaller width of the EDCs determined theoretically than found experimentally, but this is not a surprise after the above discussion.

Kunz et al. (1975) performed similar calculations for Kr, Ar and Ne. Since the Kr calculations are based on non-relativistic band structures and on a posteriori inclusion of the 0.7 eV spin orbit splitting, they have a somewhat speculative character, and we will only concentrate on the results for Ar. In this case the inclusion of the 0.2 eV spin orbit splitting should only modify the EDCs slightly. Figure 31 shows the theoretical and experimental EDCs. The total widths and the main features of both EDCs agree fairly well, though there are discrepancies in respect of the shape and the strengths of the maxima especially at 16.5 eV and 23.6 eV photon energy.

Acknowledgements

The author is indebted to the members of the synchrotron radiation group at the Deutsches Elektronen-Synchrotron for many helpful conversations. He especially would like to thank M. Skibowski, E.E. Koch, V. Saile, A. Harmsen and N. Schwentner who, by making available their results prior to publication and by many stimulating discussions made invaluable contributions. The benefit of many suggestions and comments by R. Haensel and J.A. Venables is gratefully acknowledged. The permission to reproduce figures from publications of a number of authors is greatly appreciated. The author is gratefully to Mrs. E. Thumann for her patience in carefully typing the manuscript. Thanks are also due to Mr. W. Knaut and Mrs. V. Budde for the skilful drafting and to Mr. J. Schmidt for the excellent photographic work.

References

Alexander, R.W. (1964), Bull. Am. Phys. Soc. 9, 626

Altarelli, M., and Bassani, F. (1971), J. Phys. C: Solid State Physics 4, L 328

Altarelli, M., and Bassani, F. (1972), in Proceedings of the 11th International Conference on the Physics of Semiconductors, 196 (Warsaw)

Altarelli, M., Dexter, D.L., Nussenzweig, H.M., and Smith, D.Y. (1972), Phys. Rev. B6, 4502

Altarelli, M., Andreoni, W., and Bassani, F. (1974), in Vacuum Ultraviolet Radiation Physics, ed. E.E. Koch, R. Haensel, and C. Kunz (Pergamon, New York)

Altarelli, M., Andreoni, W., and Bassani, F. (1975), Solid State Commun. 16, 143

Amey, R.L., and Cole, R.H. (1964), J. Chem. Phys. 40, 146

Amusia, M. Ya., Cherepkov, N.A., and Chernyshera, L.V. (1971), Sov. Phys.-JETP 33, 90

Amusia, M. Ya., (1973), in The Physics of Electronic and Atomic Collisions, Belgrade, Yugoslavia (1974), JETP 66, 1537

Amusia, M. Ya., (1974), in Vaccum Ultraviolet Radiation Physics, ed. E.E. Koch, R. Haensel, and C. Kunz (Pergamon, New York)

Andreoni, W., Altarelli, M., and Bassani, F. (1975), Phys. Rev. B11, 2352-2363

Asaf, U., and Steinberger, I.T. (1972), Phys. Letters 41A, 19-20

Asaf, U., and Steinberger, I.T., (1974), Phys. Rev. B10, 4464-4468

Ashley, C.A., and Doniach, S. (1975), Phys. Rev. B11, 1279

Azaroff, L.V. (1963), Rev. Mod. Phys. 35, 1012

Baldini, G. (1962), Phys. Rev. 128, 1562-1567

Baldini, G. (1965), Phys. Rev. 137, A508

Beaglehole, D. (1965), Phys. Rev. Letters 15, 551-553

Boersch, H., Bostanjoglo, O., and Schmidt, L. (1965), Tagung für Elektronenmikroskopie, Aachen (unpublished)

Born, M. (1965), Optik (Springer Verlag)

Bostanjoglo, O., and Schmidt, L. (1966), Phys. Letters 22, 130

Boursey, E., Roncin, J.-Y., and Damany, H. (1970), Phys. Rev. Letters 25, 1279-1280

Brandt, W., Eder, L., and Lundqvist, S. (1967), J. Quant. Spectros. Rad. Transf. 7, 185

Brown, F.C. (1974), Solid State Physics, 29, 1

Cairns, R.B., Harrison, H., and Schoen, R.I. (1970), Phil. Trans. Roy. Soc. A268, 163-167

Cazaux, J. (1972), Surface Sci. 29, 114-124

Codling, K., Madden, R.P., and Ederer, D.L. (1967), Phys. Rev. 155, 26

Codling, K., and Madden, R.P. (1972), J. Res. Natl. Bur. Std. (U.S.) At. Phys. Chem 76A, 1

Codling, K. (1973), Rep. Progr. Phys. 36, 541-624

Colliex, C., and Jouffrey, B. (1971), J. de Physique 32, 461-466

Comes, F.J., and Elzer, A. (1964), Z. Naturforsch. 19a, 721

Condon, E.U., and Shortley, G.H. (1970), The Theory of Atomic Spectra (Cambridge, University Press)

Cook, G.R., and Metzger, P. (1965), J. Opt. Soc. Am. 55, 516

Cuthbertson, Crp.(1911) Proc.Roy.Soc. A84, 13; (1927) Proc.Roy.Soc. A114, 650

Dagens, L., and Perrot, F. (1972), Phys. Rev. B5, 641-648

Daniels, J., v. Festenberg, C., Raether, H., and Zeppenfeld, K. (1970) in Springer Tracts in Modern Physics, (G. Höhler ed.) 54, (Springer-Verlag)

Daniels, J., and Krüger, P. (1971), Phys. Stat. Sol. (b) 43, 659

Dorgelo, H.B., and Abbink, J.H. (1926) Naturwiss. 14, 755;

(1927) Z. Phys. 44, 753

Dershem, E., and Schein, M. (1931), Phys. Rev. 37, 1238

Deslattes, R.D. (1968), Phys. Rev. Letters 20, 483

Deslattes, R.D. (1969), Phys. Rev. 186, 1

Dietrich, H., and Kunz, C. (1972), Rev. Sci, Instr. 43, 434

Doniach, S., and Huggins, R. (1965), Phil. Mag. 12, 393

Dressler, K. (1962), J. Quant, Spectrosc. Radiation Transfer 2, 683-688

Eastman, D.E. (1974), in Vacuum Ultraviolet Radiation Physics, ed. E.E. Koch, R. Haensel, and C. Kunz (Pergamon, New York)

Eatwell, A.J., and Jones, G.O. (1964), Phil. Mag. 10, 1059

Ederer, D.L., and Tomboulian, D.H. (1963), Phys. Rev. 133, A1525

Ederer, D.L. (1964), Phys. Rev. Letters 13, 760

Euwema, R.N., Wepfer, G.G., Surratt, G.T., and Whilhite, D.L. (1974), Phys. Rev. B9, 5249-5256

Fano, U. and Cooper J.W. (1965), Phys. Rev. 137, A1364

Fano, U. and Cooper, J.W. (1968), Rev. Mod. Phys. 40, 441

Fano, U. (1974), in Vacuum Ultraviolet Radiation Physics, ed. E.E. Koch, R. Haensel, and C. Kunz (Pergamon, New York)

Farrell, H.H., Strongin, M., and Dickey, J.M. (1972), Phys. Rev. B6, 4703-4710

Farrell, H.H., and Strongin, M. (1972), Phys.Rev. B6, 4711-4717

Feibelman, P.J. and Eastman, D.E. (1974), Phys.Rev. B10, 4932

Fowler, W.B. (1963), Phys.Rev. 132, 1591-1599

Fowler, W.B. (1966), Phys.Rev. 151, 657

Godwin, R.P. (1969), in "Springer Tracts in Modern Physics" (G. Höhler ed.) 51 (Springer Verlag)

Grobman, W.D. (1975), Comments on Solid State Physics 7, 27

Grobman, W.D., Eastman, D.E. and Freeouf, J.L. (1975), Phys.Rev. B12, 4405

Guertin, R.F. and Stern, F. (1964), Phys. Rev. 134, A 427

Haase, D., and Meyer, H. (1974), APS Bull. 19, 461

Haensel, R. and Kunz, C. (1967), Z. Angew. Phys. 23, 276-295

Haensel, R. Keitel, G. Schreiber, P., and Kunz, C. (1969a), Phys. Rev. Letters 22, 398

Haensel, R. Keitel, G., Schreiber, P., and Kunz, C. (1969b), Phys. Rev. 188, 1375

Haensel, R. Keitel, G., Koch, E.E., Skibowski, M., and Schreiber, P. (1969c), Phys. Rev. Letters 23, 1160-1163

Haensel, R. Keitel, G., Kunz, C., Schreiber, P., and Sonntag, B. (1970a), Mém. Soc. Roy. Sci, Lg. 5 série 20, 169

Haensel, R. Keitel, G., Kunz, C., and Schreiber, P. (1970b), Phys. Rev. Letters 25, 208

Haensel, R., Keitel, G., Koch, E.E., Skibowski, M., and Schreiber, P. (1970c), Opt. Comm. 2, 59-64

Haensel, R. Keitel, G., Koch, E.E., Kosuch, N., and Skibowski, M., (1970d), Phys. Rev. Letters 25, 1281-1283

Haensel, R., Keitel, G., Kosuch, N., Nielsen, U., and Schreiber, P. (1971), J. Phys. (France) 32, C4-236

Haensel, R. Kosuch, N., Nielsen, U., Sonntag, B., and Rössler, U. (1973), Phys. Rev. B7, 1577-1591

Harmsen, A., Koch, E.E., Saile, V. Schwentner, N., and Skibowski, M. (1974), in Vacuum Ultraviolet Radiation Physics, ed. E.E. Koch, R. Haensel, and C. Kunz (Pergamon, New York)

Harmsen, A. (1975), Diplomarbeit, Universität Hamburg (unpublished)

Hayes, W. (1972), Contemp. Phys. 13, 441

Henke, B.L., White, R., and Lundberg, B. (1957), J. Appl. Phys. 28, 98

Herman, F., and Skillman, S. (1963), "Atomic Structure Calculations", Prentice Hall, Englewood Cliffs, N.J.

Hermanson, J., and Phillips, J.C. (1966), Phys. Rev. 150, 652-660

Hermanson, J. (1966), Phys. Rev. 150, 660-669

Hertz, G. and Abbink, J.H. (1926) Naturwiss. 14, 648

Heybey, O.W., and Lee, D.M. (1967), Phys. Rev. Letters 19, 106-108

Hörl, E.M., and Suddeth, J.A. (1961), J. Appl. Phys. 32, 2521-2525

Horie, C. (1959), Prog. Theor. Phys. 21, 103

Hubbel, J.A. (1971), Atomic Data 3, 241

Hudson, R.D., and Kiefer, L.S. (1971), Atomic Data 2, 205

Huffmann, R.E., Tanaka, Y., and Larrabee, J.C. (1963), Appl. Opt. 2, 947

Jones, G.O., and Smith, B.L. (1960), Phil. Mag. 5, 355

Jortner, J. (1974), in Vacuum Ultraviolet Radiation Physics, ed. E.E. Koch, R. Haensel, and C. Kunz (Pergamon, New York)

Keil, P. (1966), Z. Naturf. 21a, 503

Keil, P. (1968), Z. Phys. 214, 251-265

Keil, T.H. (1967), J. Chem. Phys. 46, 4404

Keitel, G. (1970), Thesis, University Hamburg (unpublished), Internal Report DESY F41-70/7 (1970)

Kelly, H.P., and Simmons, R.L. (1973), Phys. Rev. Letters 30, 529-532

Kennedy, D. J., and Manson, S.T. (1972), Phys. Rev. A5, 227

Klucker, R., and Nielsen, U. (1973), Computer Phys. Commun. 6, 187

Knox, R.S., and Bassani, F. (1961), Phys. Rev. 124, 652-657

Knox, R.S. (1963), Theory of Excitons, Solid State Physics, Supplement 5, ed. F. Seitz, and D. Turnball (Academic Press, New York)

Koch, E.E., Saile, V., Schwentner, N., and Skibowski, M. (1974), Chem. Phys. LeHers 27, 562-564

Koch, E.E., Saile, V., Schwentner, N., Skibowski, M., Steinmann, W., and Raz, B. (1974b),Jap. Journal.Appl. Phys. Suppl. 2, 775-778

Koch, E.E. and Otto, A. (1976), Int. J. Radiat.Phys.Chem. 8, 113

Koch, E.E., Kunz, C. and Weiner, E.W. (1976), Optik 44 (to be published)

Krause, M.O. (1969), Phys. Rev. 177, 151

Krause, M.O. (1970), Oak Ridge National Lab. ORNL-TM-2943

Krüger, P. (1970), Diplomarbeit, Universität Hamburg (unpublished)

Kruger, J. and Ames, W.J. (1959), J. Opt. Soc. Am. 49, 1195

Kunz, A.B., and Mickish, D.J. (1973), Phys. Rev. B8, 779

Kunz, A.B., Mickish, D.J., Mirmira, S.K.V., Shima, T., Himpsel, F.J., Saile, V., Schwentner, N., and Koch, E.E. (1975), Solid State Commun. 17, 761

Kunz, C. (1976), in Optical Properties of Solids - New Developments, ed. B.O. Seraphin (North-Holland, Amsterdam)

Lefkowitz, I., Kramer, K., Shields, M.A., and Pollack, G.L. (1967), J. Appl. Phys. 38, 4867

Lin, C.D. (1974), Phys. Rev. A9, 171

Lipari, N.O. (1970), Phys. Stat. Sol. 40, 691

Lipari, N.O. (1972), Phys. Rev. B6, 4o71-4o72

Lipari, N.O., and Fowler, W.B. (1970), Phys. Rev. B2, 3354-3370

Lukirskii, A. P., and Zimkina, T.M. (1963), Bull. Acad. Sci. USSR Phys. Ser. 27, 8o8

Lukirskii, A.P., Brytoy, I.A., and Zimkina, T.M. (1964), Opt. Spectroscop. 17, 234

Lyman, T. and Saunders, F.A. (1925) Nature 116, 358

Madden, R.P., Ederer, D.L., and Codling, K. (1969), Phys.Rev. 177, 136

Madden, R.P. (1974), in X-Ray Spectroscopy, ed. L.V. Azâroff (McGraw-Hill, New York)

Marcoux, J.E. (1969), J.Opt.Soc.Am. 59, 998

Marcoux, J.E. (1970a), Can.J.Phys. 48, 244

Marcoux, J.E. (197ob), Can. J. Phys. 48, 1947

Mattheiss, L.F. (1964), Phys. Rev. 133, A 1399-14o3

Mazo, R.M. (1964), J. Am. Chem. Soc. 86, 347o

McGuire, E.I. (1968), Phys. Rev. 175, 20

MeLennan, J.C. and Shrum, G.M. (1929), Proc.Roy.Soc. A106, 32

Meyer, H. (1975), private communication

Molgaard, H.V.D. (1971), DPhil Thesis, University of Sussex

Moorjani, K. (1966), Phys. Letters 23, 652-653

Miyakawa, T. (1968), J. Phys. Soc. Japan 24, 768-786

Moore, Ch. (1949), NBS Circular 467, Vol. I, U.S. Government Printing Office and Vol. II (1952), as well as Circular 467, Vol. III (1958)

Nelson, J.R., and Hartmann, P.L. (1959), Bull. Am. Phys. Soc. 4, 371

Nielsen, U. (1974), DESY internal report F41-74/3

Nuttall, J.D., and Gallon, T.E. (1974), Solid St. Commun. 15, 329-332

Nuttall, J.D., Gallon, T.E., Devey, M.G., and Mathew, J.A.D. (1975), J. Phys. C: Solid State Phys. 8, 445-458

O'Brien, J.F., and Teegarden, K.J. (1966), Phys. Rev. Letters 17, 919-921

Onodera, Y., and Toyozawa, Y. (1967), J. Phys. Soc. Japan 22, 833-844

Ophir, Z., Raz, B., Jortner, J., Saile, V., Schwentner, N., Koch, E.E., Skibowski, M., and Steinmann, W. (1975), J. Chem. Phys. 62, 65o-665

Philpott, M.R. (1974), J. Chem. Phys. 60, 1410-1419

Po Lee, and Weissler, G.L. (1955), Phys. Rev. 99, 54o

Pudewill, D. (1975), Diplomarbeit, Universität Hamburg (unpublished)

Pudewill, D., Himpsel, F.J., Saile, V., Schwentner, N., Skibowski, M. and Koch, E.E. (1976a), phys.stat.sol. (b) (to be published)

Pudewill, D., Himpsel, F.J., Saile, V., Schwentner, N., Skibowski, M., Koch, E.E. and Jortner, J. (1976b), J.Chem.Phys. (to be published)

Ramirez, R., and Falicov, L.M. (1970), Phys. Rev. B1, 3464

Raz, B., and Jortner, J. (1971), Chem. Phys. Letters 9, 222

Reilly, M.H. (1967), J. Phys. Chem. Solids 28, 2o67-2o85

Ritsko, J.J., Schnatterly, S.E., and Gibbons, P.C. (1974), Phys. Rev. Letters 32, 671

Roberts, I., and Wilson, E.G. (1973), J. Phys. C: Solid State Phys. 6,2169-2183

Roncin, J.-Y., Chandrasekharan, V., and Damany, N. (1964), Compt. Rend. 258, 2513-2516

Roncin, J.-Y., and Moorjani, K. (1967), Phys. Stat. Sol. 23, K1

Roessler, D.M., and Walker, W.C. (1967), Phys. Rev. 159, 711

Roessler, D.M., and Walker, W.C. (1968), Phys. Rev. 166, 599

Rössler, U. (1970), Phys. Stat. Sol. 42, 345-356

Rössler, U. (1971), Phys. Stat. Sol. (b), 45, 483

Rössler, U., and Schütz, O. (1973), Phys. Stat. Sol. 56, 483-494

Rössler, U., Himpsel, F.J., Saile, V., Schwentner, N., Skibowski, M., and Koch, E.E. (1976) (to be published)

Rustgi, O.P., Fischer, E.T., and Fuller, C.H. (1964), J. Opt. Soc. Am. 54, 745

Saile, V., and Skibowski, M. (1972), Phys. Stat. Sol. (b), 50,661-672

Saile, V. (1974), private communiation

Saile, V., Gürtler, P., Koch, E.E., Kozevnikov, A., Skibowski, M. and Steinmann, W. (1976a), (to be published)

Saile, V., Gürtler, P., Koch, E.E., Kozevnikov, A., Skibowski, M. and Steinmann, W. (1976b) Applied Optics, to be published

Sakoda, S., and Toyozawa, Y. (1973), J. Phys. Soc. Japan 35, 172

Samson, J.A.R. (1963), Phys. Rev. 132, 2122

Samson, J.A.R. (1964a), J. Opt. Soc. Am. 54, 42o and (1964b), J. Opt. Soc. Am. 54, 842

Samson, J.A.R. (1965), J. Opt. Soc. Am. 55, 935

Samson, J.A.R. (1966), Adv. At. Mol. Phys. 2, 178

Samson, J.A.R. (1967), "Techniques of Vacuum Ultraviolet Spectroscopy", John Wiley & Sons, Incs., New York

Saunders, F.A. (1925), Proc.Nat.Acad.Sci. (Washington) 12, 566; (1927) ibid. 13, 596

Sayers, D.E., Lyttle, F.W., and Stern, E.A. (1970), Adv. X-ray Anal. 13,248

Sayers, D.E., Lyttle, F.W., and Stern, E.A. (1971), Phys. Rev. Letters 27, 12o4

Schaich, W.L. (1973), Phys. Rev. B8, 4o28

Scharber, Jr., S.R., and Webber (1971), J. Chem. Phys. 55, 3985-3993

Schnepp, O., and Dressler, K. (1960), J. Chem. Phys. 33, 49

Schmidt, L. (1971), Phys.Letters 36A, 87-88

Schmidt, L. (1972), Thesis, Technische Universität Berlin (unpublished)

Schreiber, P. (1970), Thesis, University Hamburg (unpublished); Internal Report DESY F41-70/5

Schwentner, N. Skibowski, M., and Steinmann, W. (1973), Phys. Rev. B8,2965-68

Schwentner, N. (1974), Thesis, University München (unpublished)

Schwentner, N., Himpsel, F.J., Koch, E.E., Saile, V., and Skibowski, M. (1974), in Vacuum Ultraviolet Radiation Physics, ed. E.E. Koch, R. Haensel, and C. Kunz (Pergmanon, New York)

Schwentner, N., Himpsel, F.J., Saile, V., Skibowski, M., Steinmann, W., and Koch, E.E. (1975), Phys. Rev. Letters 34,528-31

Sinnock, A.C., and Smith, B.L. (1967), Phys. Letters 24A, 387

Sinnock, A.C., and Smith, B.L. (1968), Phys. Letters 28A, 22

Sinnock, A.C., and Smith, B.L. (1969), Phys. Rev. 181, 1297

Skibowski, M., and Steinmann, W. (1967), J. Opt. Soc. Am. 57, 112

Skibowski, M. (1971), III. Intern. Conference on Vacuum Ultraviolet Radiation Phys, Tokyo (unpublished)

Smith, B.L. (1963), Rev. Sci, Instr. 34, 19

Smith, B.L. and Pings, C.J. (1963), Physica 28, 555

Smith, B.L. and Pings, C.J. (1968), J. Chem. Phys. 48, 2387

Smith, B.L. (1974), Experimental Thermodynamics Vol. 2, Chapter 12 (published by IUPAC)

Soules, J.A. and Shaw, C.H. (1959), Phys. Rev. 113, 470

Spicer, W.E. (1972), in The Optical Properties of Solids, ed. F. Abelès (North-Holland, Amsterdam)

Spicer, W.E. (1974), in Vacuum Ultraviolet Radiation Physics, ed. E.E. Koch, R. Haensel, and C. Kunz (Pergamon, New York)

Starace, A.F. (1970), Phys. Rev. A2, 118

Steinberger, I.T., and Schnepp, O. (1967), Sol. State Comm. 5, 417-18

Steinberger, I.T., Atluri, C., and Schnepp, O. (1970), J. Chem. Phys. 52, 2723

Steinberger, I.T., and Asaf, U. (1973), Phys. Rev. B8, 914-18

Steinberger, I.T. (1973), J. Appl. Opt. 12, 614

Steinberger, I.T., Munro, I.H., Pantos, E., and Asat, U. (1974), in Vacuum Ultraviolet Radiation Physics, ed. by E.E. Koch, R. Haensel, and C. Kunz (Pergamon, New York); see also 47A, (1974) 299

Stern, E.A., and Sayers, D.E. (1973), Phys. Rev. Letters 30, 174

Stern, E.A. (1974), Phys. Rev. B10, 3027

Surko, C.M., Dick, G.I., Reif, F., and Walker, W.C. (1969), Phys. Rev. Letters 23, 842

Tanaka, Y. (1955), J. Opt. Soc. Am. 45, 710

Trebbia, P. (1973), Dissertation, Université de Paris-Sud (unpublished)

Trickey, S.B., Green, F.R., and Averill, F.W. (1973), Phys. Rev. B8, 4822-4832

Vegard, L. (1930) Annal. der Phys. 6, 487; (1934) Proc.Acad.Sci. Amsterdam 37, 780

Vos, Y.E., Veenengakingma, R., Van der Gaag, F.J., and Blaisse, B.S. (1967), Phys. Letters, 24A, 738; see also Physica 37 (1967) 51

Watson, W.S., and Morgan, F.J. (1969), J. Phys. B2, 277

Webber, S., Rice, S.A., and Jortner, J. (1964), J. Chem. Phys. 41, 2911

Wendin, G. (1973), J. Phys. B6, 42-61

Wendin, G. (1974), in Vacuum Ultraviolet Radiation Physics, ed. E.E. Koch, R. Haensel, and C. Kunz (Pergamon, New York)

Wolter, H. (1956), in Handbuch der Physik, ed. S. Flügge 24, 461-554 (Springer Verlag)

Wuilleumier, F., and Combet Farnoux, F. (1969), Compt. Rend. serie B269, 968

Wuilleumier, F. (1970), Compt. Rend. serie B, 270,272

Wuilleumier, F., and Bonnelle Ch. (1970), Compt. Rend. serie B, 270,1o29

Wuilleurmier, F., and Krause, M.O. (1971), in Photoelectron Spectroscopy, ed. D.A. Shirley (North-Holland Publ. Comp., Amsterdam, London, 1972),p.259

Table I Binding energies of the occupied levels of the rare gas atoms in eV. (Krause,1970). The $1s^2S_{1/2}$, $np^5\ ^2P_{3/2}$ and $np^5\ ^2P_{1/2}$ series limits as given by Moore (1949,1952,1958) are included.

	He	Ne	Ar	Kr	Xe
K	24.6	870.2	3206.0	14329	34566
L_I		48.5	326.3	1925.3	5453.2
L_{II}		21.56	250.6	1731.5	5107.2
L_{III}			248.4	1679.0	4787.2
M_I			29.24	292.6	1148.7
M_{II}				222.2	1002.1
M_{III}			15.76	214.5	940.6
M_{IV}				95.04	689.5
M_V				93.82	676.7
N_I				27.52	213.1
N_{II}				14.67	155
N_{III}				14.00	145.5
N_{IV}					69.52
N_V					67.55
O_I					23.49
$O_{II,III}$					12.13
$1s\ ^2S_{1/2}$	24.580				
$np^5\ ^2P_{3/2}$		21.559	15.755	13.996	12.127
$np^5\ ^2P_{1/2}$		21.656	11.933	14.662	13.433

Table II Low frequency dielectric onstants ε of solid Ar, Kr and Xe

Material	Temperature	a	b	c	d
Ar	mp	1.56±0.01	1.599		1.6078
	77 K			1.586±0.032	
Kr	mp	1.78±0.01	1.784		
Xe	mp	1.98±0.01	2.033		

a Marcoux, 1970a; b Amey and Cole, 1964; Lefkowitz et al., 1967;
d Smith and Pings, 1963

Table III Smoothed values of the refractive index, density, and F_{LL} for solid Ar, Kr and Xe as a function of wavelength (Å) (Sinnock and Smith 1969)

	T °K	Wavelength (Å) 6439	5780	5461	5086	4753	4358	4063[b]	3650[b]	3612[b]	ρ^* (10^{-2} mole/cm³)	LL (cm³/mole)
Ar	Solid											
	20	1.2895	1.2903	1.2910	1.2918	1.2926	1.2938	1.2950	1.2972	1.2975	4.416	4.117
	30	1.2879	1.2887	1.2894	1.2901	1.2909	1.2921	1.2934	1.2956	1.2959	4.385	4.124
	40	1.2854	1.2862	1.2869	1.2876	1.2885	1.2896	1.2909	1.2931	1.2934	4.343	4.132
	50	1.2822	1.2831	1.2838	1.2845	1.2853	1.2865	1.2878	1.2900	1.2903	4.293	4.138
	60	1.2786	1.2795	1.2801	1.2809	1.2817	1.2829	1.2841	1.2863	1.2866	4.235	4.144
	70	1.2742	1.2751	1.2757	1.2765	1.2773	1.2785	1.2797	1.2820	1.2822	4.170	4.148
	80	1.2693	1.2702	1.2708	1.2716	1.2724	1.2736	1.2748	1.2771	1.2773	4.093	4.156
	83.81	1.2673	1.2681	1.2688	1.2695	1.2704	1.2716	1.2728	1.2750	1.2753	4.061	4.160

	T °K	Wavelength (Å) 6439	5780	5461	5086	4753	4358	4063[b]	3631[b]	ρ^* (10^{-2} mole/cm³)	LL cm³/mole
Kr	Solid										
	67	1.3648	1.3664	1.3674	1.3688	1.3704	1.3727	1.3749	1.3787	3.542[b]	6.344
	75	1.3622	1.3638	1.3648	1.3662	1.3678	1.3701	1.3723	1.3761	3.511[b]	6.360
	85	1.3587	1.3602	1.3612	1.3627	1.3642	1.3666	1.3688	1.3726	3.471[d]	6.377
	95	1.3547	1.3562	1.3572	1.3587	1.3603	1.3626	1.3648	1.3686	3.429	6.392
	105	1.3498	1.3514	1.3524	1.3538	1.3554	1.3578	1.3600	1.3638	3.383	6.400
	115.95	1.3436	1.3451	1.3462	1.3476	1.3492	1.3515	1.3537	1.3576	3.330	6.398

	T °K	Wavelength (Å) 6439	5780	5461	5086	4806	4700	4358	4063[b]	3650[b]	3612[b]	ρ^* (10^{-2} mole/cm³)	LL cm³/mole
Xe	Solid												
	80	1.4808	1.4833	1.4854	1.4882	1.4906	1.4917	1.4954	1.4995	1.5080	1.5091	2.771	10.350
	90	1.4775	1.4800	1.4821	1.4848	1.4873	1.4884	1.4921	1.4962	1.5047	1.5058	2.750	10.365
	100	1.4740	1.4765	1.4786	1.4814	1.4838	1.4849	1.4886	1.4927	1.5012	1.5024	2.730	10.380
	110	1.4701	1.4727	1.4748	1.4775	1.4800	1.4811	1.4848	1.4889	1.4974	1.4986	2.709	10.388
	120	1.4660	1.4686	1.4706	1.4734	1.4759	1.4770	1.4807	1.4848	1.4934	1.4945	2.687	10.396
	130	1.4616	1.4641	1.4662	1.4690	1.4715	1.4726	1.4763	1.4804	1.4890	1.4901	2.664	10.399
	140	1.4569	1.4594	1.4616	1.4643	1.4668	1.4679	1.4716	1.4757	1.4843	1.4855	2.640	10.403
	150	1.4520	1.4545	1.4566	1.4594	1.4619	1.4629	1.4667	1.4708	1.4794	1.4805	2.615	10.407
	161.35	1.4461	1.4486	1.4507	1.4535	1.4560	1.4571	1.4608	1.4650	1.4736	1.4747	2.585	10.411

Table IV Energy positions (eV) of the maxima detected in the spectra of solid Ne

reference		n	a	b	c	d	e	f	g	h	i
A	Γ(3/2,1/2)	1	17.83	17.49	17.74	17.75	17.2	17.4	17.48	16.67	16.84
B	Γ(3/2,1/2)	2	20.38	20.24	20.36	20.3	20.2	20.4	20.22	19.68	19.78
C	Γ(3/2,1/2)	3	21.09	20.87	21.2	20.98		21.1	20.9	20.57	20.66
D	Γ(3/2,1/2)	4	21.38	21.30		21.25		21.5		20.94	21.04
E	Γ(3/2,1/2)	5	21.5								
F								22.5			
G								24.0			
H								25.1			
I					26.5	26.0	26.6	25.9			
J					29.6	29.1	29.5	29.0			
K								30.7			
L					32.9	32.0	32.6	32.4			
M						35.5	35.6	34.0			
N							37.0	36.1			
O								40.0			
P							42.0	42.0			
Q								44.5			
R	2s→p							46.9			
S	2s→p							48.0			

References: a reflectance (Haensel et al. 1970d, Pudewill 1975); b ε_2 (Skibowski 1971); electron energy loss, c (Daniels and Krieger 1971); d (Schmidt 1972); e (Farell and Strongin 1972); absorption, f (Haensel et al. 1970d, Keitel 1970); g (Boursey et al. 1970). For comparison the energies of the atomic transitions $2p^6 \rightarrow 2p^5(^2P_{3/2})ns$ and $2p^6 \rightarrow 2p^5(^2P_{1/2})ns$ are given in column h and i (Moore 1949). The second column gives the identification of the exciton peaks.

Table V Energy positions (eV) of the maxima detected in the spectra of solid Ar

reference		n	a	b	c	d	e	f	g	h	i	j
A	Γ(3/2)	1	12.07	12.09	12.04	12.08		12.2	12.2	12.06		12.0
B	Γ(1/2)	1	12.28	12.33	12.45	12.50	12.6		12.5		12.3	12.3
C			12.51	12.36								
D	Γ(3/2)	2	13.57	13.58	13.52	13.55			13.4			
E	Γ(1/2)	2	13.74	13.76	13.72	13.76						13.8
F	Γ(3/2)	3	13.89	13.91	14.12	13.92						
G	Γ(3/2)	4	14.00	14.09								
H	Γ(1/2)	3	14.06						14.4			
I			16.05			16.5		15.0	16.5			
J			16.90		17.3	17.3	16.9		17.2			
K			19.40		20.2	19.7	19.8		19.2			
L									20.8			
M							26.2	25.4	26.4			
N	3s→p		27.52			27.4		28.2	28.2			
O	3s→p		28.02									
P									33.4			
Q									45			

References: a reflectance (Haensel et al. 1969c, Harmsen 1975); b ε_2 (Skibowski 1971); electron energy loss, c (Krieger 1970); d (Schmidt 1972); e (Colliex and Jouffrey 1971); f (Farell and Strongin 1972); g (Nuttall et al. 1975); absorption, h (Dressler 1962); i (Nelson and Hartmann 1959); j (Baldini 1962). The energies of the atomic transitions $3p^6 \rightarrow 3p^5(^2P_{3/2})4s$ and $3p^6 \rightarrow 3p^5(^2P_{1/2})4s$ are 11.62 eV and 11.82 eV (Moore 1949). The second column gives the identification of the exciton peaks.

Table VI Energy positions (eV) of the maxima detected in the spectra of solid Kr

reference		n	a	b	c	d	e	f	g	h	i
A	Γ(3/2)	1	10.25	10.23		10.55	10.3	10.1	10.19	10.16	10.2
B			10.37	10.3							
C	Γ(1/2)	1	10.89	10.87	10.8	11.20		10.8	10.88		10.88
D			10.97	10.93							
E	Γ(3/2)	2	11.28	11.27		11.50		11.3	11.24		11.2
F	Γ(3/2)	3	11.47	11.44		11.80			11.48		
G	Γ(3/2)	4				11.93					
H	Γ(1/2)	2	11.95	11.95		12.25			11.95		
I	Γ(1/2)	3	12.22	12.22		12.32					
J			12.8			12.9		12.6	12.8		
K			13.3				13.1				
L			14.2								
M			14.45		14.9	15.1	14.5	14.6			
N			15.6				16.1	15.5			
O			16.9			17.7		16.8			
P					17.8	18.5		17.9			
Q							21.3	21.4			
R							23.8	24.0			
S	4s→np				24.3	25	26	25.9			
T							32	31.3			
U							39	41			
V							45				
W							59				
X							66				

References: a reflectance (Haensel et al. 1970c); b ε_2 (Skibowski 1971); electron energy loss, c (Colliex and Jouffrey 1971); d (Schmidt 1971 ,1972); e (Farell and Strongin 1972); f (Nuttall et al. 1975); absorption, g (Baldini 1962); h (Dressler 1962); i (Roncin et al. 1964). The energies of the atomic transitions $4p^6 \rightarrow 4p^5(^2P_{3/2})5s$ and $4p^6 \rightarrow 4p^5(^2P_{1/2})5s$ are 10.03 eV and 10.56 eV (Moore 1952). The second column gives the identification of the exciton peaks.

Table VII Energy positions (eV) of maxima detected in the spectra of solid Xe

reference		n	a	b	c	d	e	f	g	h	i	j	k	l	m
A	Γ(3/2)	1	8.45	8.40	8.378	8.53	8.4	8.2	8.5	8.6	8.2	8.35	8.36	8.35	8.36
B					8.76										
C					8.926										
D	Γ(3/2)	2	9.12	9.10	9.029	9.10			9.1			9.12	9.06	9.11	9.07
E	Γ(3/2)	3	9.23	9.21	9.146				9.23				9.21		9.19
F	Γ(3/2)	4			9.235				9.3				9.27		9.28
G	Γ(1/2)	1	9.56	9.47	9.462	9.8			9.75		9.4	9.5		9.5	9.53
H	Γ(1/2)	2	9.85	9.80	9.79			10.0	10.0						
I			10.33		10.23	10.55			10.55	10.0	10.3	10.33			10.0
J			11.01			11.3			11.35						11.1
K			11.61												11.5
L			11.86												
M			12.1						12.4	12.2	12.4				12.2
N			12.6						12.75						12.9
O			13.0								13.1				13.4
P			13.4												
Q			13.9						13.7						
R			15.0			15.2		15.0	14.95		14.6				
S									15.6		16.9				
T											17.4				
U			19.1						19.2		19.8				
V	5s→p		20.6					20.3	20.5		20.9				21.5
W										25	24.6				
X										29	28.3				
Y										34	35				
Z										37					
A'										39					
B'										47					
C'										53					
D'										56					

References: a) reflectance, (Haensel et al. 1970c); b) ε_2 (Skibowski 1971)reflectance, c) (Steinberger et al., 1970); electron energy loss, d (Keil, 1968). e) (Hörl and Suddeth, 1961); f) (Colliex and Jouffrey, 1971); g) (Schmidt 1972); h) (Farrell and Strongin, 1972); i) (Nuttal et al., 1975); absorption, j) (Roncin et al., 1964); k) (Steinberger and Schnepp 1967; l) (Schnepp and Dressler, 1960); m) (Baldini, 1962). The energies of the atomic transitions $5p^6 \rightarrow 5p^5(^2P_{3/2})6s$ and $5p^6 \rightarrow 5p^5(^2P_{1/2})6s$ are 8.43 eV and 9.57 eV (Moore,1958). The second column gives the interpretation of the exciton peaks.

Table VIII Energy positions (eV) of the maxima detected in the spectra of solid Ar, Kr and Xe near the onset of Ar2p, Kr3d and Xe4d transitions (Haensel et al.,1969b and 1971).

peak	Ar 2p	Kr 3d	Xe 4d
A	245.2 ±0.07	90.28±0.08	64.36±0.08
A'	247.36±0.1		
B	247.85±0.07	91.61±0.04	65.28±0.04
B'	250.25±0.07	92.90±0.04	67.24±0.04
C	248.4 ±0.1	91.99±0.04	65.48±0.05
C'		93.22±0.04	67.53±0.1
D	250.25±0.07	92.13±0.05	65.87±0.08
D'	252.27±0.1		67.87±0.05
E	251.5 ±0.07	94.19±0.05	66.60±0.08
E'	254.4±0.1	95.34±0.08	
F	256.3 ±0.1	94.62±0.08	66.79±0.05
F'			68.68±0.05
G	257.37±0.2	94.96±0.05	69.98±0.05
G'		96.28±0.1	
H	259.0 ±0.2	95.82±0.06	72.17±0.07
H'		96.97±0.06	74.19±0.07
I		98.18±0.06	
I'		99.47±0.06	
J	261.8 ±0.2	98.75±0.06	
J'	264.4 ±0.2		
K	269.7 ±0.3	101.05±0.06	
K'		102.33±0.06	

Table IX Band gap E_G, effective exciton mass μ (in units of free electron masses), photoconductivity threshold E_{pc}, binding energy of the first exciton $E_1\Gamma(3/2)$, photoemission threshold E_{Th}, vacuum level E_V, electron affinity E_A, self-energy of the hole P^+, ionization energy of the free atoms I. All energies are given in eV.

	Ref.	Ne	Ar	Kr	Xe
E_G	a	21.69 (∿6 K)	14.15 (∿20 K)	11.6 (∿40 K)	9.3 (∿40 K)
E_G	b				9.295 (40 K)
					9.278 (130 K)
E_B	a	5.24	2.32	1.4	0.8
μ	a	0.6	0.44	0.36	0.28
μ	c	0.78	0.45	0.36	
μ	d		0.44	0.35	0.30
E_{pc}	e				9.25 (60 K)
E_{pc}	f				9.265 (130 K)
$E_1\Gamma(3/2)$	a	3.86	2.08	1.35	0.9
$E_1\Gamma(3/2)$	g		1.97	1.41	0.89
$E_1\Gamma(3/2)$	h			1.47	0.94
$E_1\Gamma(3/2)$	i		2.12		
E_{Th}	j	21.4 (∿6 K)	13.9 (∿10 K)	11.9 (∿10 K)	9.7 (∿10 K)
E_{Th}	k			≥11.7 (20 K)	9.7 (20 K)
E_{Th}	l		14.1 (17 K)	12.0	9.84 (60 K)
E_V	m	20.3 (∿6 K)	13.8 (∿10 K)	11.9 (∿10 K)	9.8 (∿10 K)
E_A	m	-1.4	-0.4	0.3	0.5
E_A	n	-0.6	-0.3	0.62	0.39
P^+		-1.26	-1.96	-2.1	-2.33
P^+	o	-0.68	-1.1	-1.2	-1.32
I	p	21.559	15.755	13.996	12.127

References
a) Haensel et al. (1969c, 1970c, 1970d); Harmsen et al. (1974); Harmsen (1975); Pudewill (1975); Pudewill et al. (1976a
b) Asaf and Steinberger (1973); Steinberger et al. (1970)
c) Kunz and Mickish (1973)
d) Rössler (1970)
e) Asaf and Steinberger (1974)
f) Spear and Le Comber (chapter 18)
g) Rössler and Schütz (1973)
h) Hermanson (1966)
i) Andreoni et al. (1975)
j) Koch et al. (1974); Schwentner et al. (1973), Schwentner (1974)
k) O'Brien and Teegarden (1966)
l) Steinberger et al. (1974)
m) Schwentner et al. (1975); Schwentner (1974)
n) Raz and Jortner (1969)
o) Fowler (1966)

Table X Parameters of the band structure of RGS as obtained by experiment (exp.) and calculation (calc.). All energies in eV. Band gap E_G, vacuum level E_V, electron affinity E_A, total width of the valence bands W_V, spin-orbit splitting E_{so}

	Ref.		E_G	E_V	E_A	W_V	E_{so}
Ne	exp.	a	21.69	20.3	-1.4	1.3	<0.1
	calc.	b	22.16	21.8	-0.36	0.4	
		c	22.46	20.48	-1.98	0.5	
		d				0.4	
		e				0.65	
	atom						0.10
Ar	exp.	a	14.15	13.8	-0.4	1.7	0.2
	calc.	b	15.22	14.1	-1.12	1.3	
		c	15.99	13.76	-2.23	1.2	
		d				1.0	0.18
		f	13.7	13.64	-0.06	2.3	
		g	16.37	13.97	-2.4	2.6	
		g	16.2	13.95	-2.25	2.6	
		h	13.3	17.04	3.73	0.6	
		i	12.4	20.5	8.1	0.6	
		j				2.0	
	atom						0.18
Kr	exp.	a	11.6	11.9	0.3	2.3	0.64
	calc.	b	13.57	12.3	-1.27	1.6	
		d				1.6	0.7
		k	15.12	12.91	-2.21	2.8	
		l	11.3	15.5	4.2	1.5	
	atom						0.67
Xe	exp.	a	9.8	9.3	0.5	3.0	1.3
	calc.	d				1.8	1.37
		m	7.8	11.5	3.7	1.7	
	atom						1.31

References: a) Haensel et al. (1969c,1970c,1970d); Harmsen et al. (1974); Harmsen (1975); Pudewill (1975); Schwentner et al. (1975); b) Kunz and Mickish (1973); c) Dagens and Perrot (1972); d) Rössler (1970); e) Euwema et al. (1974); f) Lipari and Fowler (1970); g) Lipari (1972); h) Mattheis (1964); i) Knox and Bassani (1961); j) Ramirez and Falicov (1970); k) Lipari (1970); l) Fowler (1963); m) Reilly (1967)

Figure Captions

Fig. 1(a) Refractive indices of liquid and solid Ar. The continuous lines correspond to equation 2.6 with values ω_o = 11.725 eV, ω_p^2 = 31.69 eV^2, V_o(TP) = 7.99 eV^2 and χ_1 = 0.2811 (Sinnock and Smith 1969).

Fig. 1 (b) Refractive indices of liquid and solid Kr. The continuous lines correspond to equation 2.6 with values ω_o = 10.03 eV, ω_p^2 = 29.10 eV^2, V_o(TP) = 7.55 eV^2 and χ_1 = 0.3578 (Sinnock and Smith 1969).

Fig. 1(c) Refractive indices of liquid and solid Xe. The continuous lines correspond to equation 2.6 with values ω_o = 8.43 eV, ω_p^2 = 23.145 eV^2, V_o(TP) = 3.35 eV^2 and χ_1 = 0.47425 (Sinnock and Smith 1969).

Fig. 2 Variation of F_{LL} with density for solid Ar at 5461 Å. The theoretical curve is based on the tight-binding calculation by Keil(1967) (Sinnock and Smith 1969).

Fig. 3 Schematic representation of the film holder used by Baldini (1962)

Fig. 4 Absorption spectrum of solid Ar at 20 K (bandpass 2 Å). The two short vertical lines show the energy of the resonance doublet in the free atom (Baldini,1962)

Fig. 5 Absorption spectrum of solid Kr at 20 K (annealed at 44 K), solid line, and at 40 K, dashed line (bandpass 2 Å). The two short vertical lines show the energy of the resonance doublet in the free atom (Baldini,1962)

Fig. 6 Absorption spectrum of solid Xe (annealed at 53 K) at 21 K (bandpass 1 Å). The two short vertical lines show the energy of the resonance doublet in the free atom (Baldini,1962)

Fig. 7 Absorption spectrum of clean solid Xe (dotted line). A surface layer of Ar quenches the maximum at 8.21 eV (solid line). Gently heating the sample, and thus removing the Ar surface layer, restores the spectrum of clean Xe (dashed line). (Saile et al. 1976a).

Fig. 8a Reflectivity vs photon energy for annealed solid Xe. Dots = data calculated directly from experiment; curve = calculated at the last step of the approximation procedure (Steinberger et al.,1970)

(b) The imaginary part of the dielectric constant $\varepsilon_2 = 2nk$ (dots) as a function of photon energy for annealed solid Xe. The drawn curves represent the resolution into damped harmonic oscillator absorption bands.

(c) The real part of the dielectric constant $\varepsilon_1 = n^2-k^2$ as a function of photon energy for annealed solid Xe (Steinberger et al.,1970)

Fig. 9 Exciton peak positions in condensed Xe as a function of temperature (o Steinberger and Asaf,1973; + Baldini,1962; Δ Steinberger et al.,1970)

Fig. 10 Schematic representation of the experimental set up at the Deutsches Elektronen-Synchrotron DESY. The Wadsworth monochromator was used for photon energies below 40 eV, the Rowland spectrometer for photon energies above 30 eV. (E electron orbit, V valve, S beam shutter, RS rotating shutter, MO monitor, M1, M2, M3 photomultiplier, S1, S2 slits, G1, G2 gratings, F filter, M concave mirror, RA rotating arm).

Fig. 11(a) Reflectance spectrum of solid Ne (Haensel et al., 1970d; Skibowski, 1971)

(b) Reflectance spectrum of solid Ar (Haensel et al., 1969c; Skibowski, 1971)

Fig. 12(a) Reflectance spectrum of solid Kr (b) Reflectance spectrum of solid Xe (Haensel et al., 1970c; Skibowski, 1971).

Fig. 13 Dielectric constants of (a) solid Ne (Skibowski,1971) and (b) solid Ar (Saile, 1974). ε_1 dashed line, ε_2 solid line. On (a) and (b) the joint density of states (dotted line) as calculated by Kunz and Mickish (1973) and on (b) ε_1 (open circles) and ε_2 (crosses) determined by Harmsen et al. (1974) have been included.

Fig. 14 Dielectric constants of (a) solid Kr and (b) solid Xe (Skibowski, 1971). ε_1 dashed line, ε_2 solid line. On (a) the joint density of states as calculated by Kunz and Mickish (1973) has been included.

Fig. 15 The absorption (in arbitrary units) and reflection spectra of (a) Kr films and (b) Xe films at 20.4 K. The atomic resonance lines are indicated by vertical lines (Scharber and Webber, 1971).

Fig. 16 The spectrum of ε_1 and ε_2 for (a) solid Kr and (b) solid Xe. The half-height widths (in eV) of the $\Gamma(3/2)$ and $\Gamma(1/2)$ resonances in ε_2 are indicated (Scharber and Webber, 1971). On (b) the real part ε_1 and the imaginary part ε_2 of the dielectric constant as determined by Steinberger (1973) from the reflectance spectrum reported by Scharber and Webber have been included (dashed line).

Fig. 17 Schematic representation of (a) the experimental set-up for electron energy loss measurements and (b) the cooling unit (Schmidt, 1972).

Fig. 18 Electron energy loss spectrum of (a) solid Ne, (b) solid Ar (Schmidt, 1971) and (c) solid Kr (Schmidt, 1972) and (d) solid Xe (Schmidt 1972).

Fig. 19 Schematic energy band scheme for RGS. For simplicity only the lowest conduction band and one core level are shown. Double group notation and notation used in the text (in parenthesis) of energy levels are given. The vacuum level and exciton states are indicated. The arrows show the energies discussed in the text: E_G band gap, E_V vacuum level, E_A electron affinity, E_X excitation energy of the n=1 $\Gamma(3/2)$ exciton, E_B exciton binding energy.

Fig. 20(a) Absorption coefficient of solid (solid line) and gaseous (dashed line) Ne determined by reflectance (Haensel et al.,1970d; Skibowski,1971) and absorption measurements (Haensel et al.,1971) (+ Samson,1965; □ Comes and Elzer,1964; ○ Ederer and Tomboulian,1963; ⊕ Dershem and Schein,1931; △ Henke et al.,1957)

(b) Absorption coefficient of solid (solid line) and gaseous (dashed line) Ar determined by reflectance (Haensel et al.,1969c, Harmsen et al.1974; Saile, 1974) and absorption measurements (Haensel et al., 1971) (+ Lukirskii and Zimkina,1963; ▲ Dershem and Schein,1931; △ Henke et al.,1957; □ Comes and Elzer,1964; ○ Deslattes,1969; ⊕ Samson,1964a; ⊞ Polee and Weissler,1955; ● Madden et al.,1969; ■ Alexander,1964)

Fig. 21(a) Absorption coefficient of solid (solid line) and gaseous (dashed line) Kr determined by reflectance (Haensel et al.,1970c; Skibowski,1971) and absorption measurements (Haensel et al.,1969b) (···· Samson,1963; ○ Rustgi et al.,1964; ■ Lukirskii et al.,1964; -·-·- Cook and Metzger,1965; ---- (between 15 and 20 eV) Huffmann et al.,1963)

Fig. 21(b) Absorption coefficient of solid (solid line) and gaseous (dashed line) Xe determined by reflectance (Haensel et al., 1970c; Steinberger, 1970) absorption measurements (-·-·- Baldini, 1962; Haensel) et al.,1969b) (○ Samson,1964b; ◊ Cairns et al.,1970; △ Ederer,1964; ● Lukirskii et al.,1964).

Fig. 22 Refractive indices of solid Ne, Ar, Kr, and Xe for photon energies above 30 eV. (Schreiber,1970; Keitel,1970)

Fig. 23 Absorption spectrum of solid (solid line) (Haensel et al., 1970b) and atomic (dashed line) (Madden et al., 1969) (a) Ne near the onset of 2s transitions. The joint density of states (dot-dashed line) as calculated by Kunz and Mickish (1973) is included. (b) Ar near the onset of 3s transitions.

Fig. 24 Absorption spectrum of solid and gaseous Ar near the onset of 2p transitions (Haensel et al.,1971). Spin orbit partners are denoted by primed and unprimed letters.

Fig. 25 Absorption coefficient of solid and gaseous (a) Kr near the onset of 3d transitions and (b) Xe near the onset of 4d transitions (Haensel et al.,1969b). Spin orbit partners are denoted by primed and unprimed letters.

Fig. 26 Mass absorption coefficient of solid (solid line) and gaseous (dashed line). (a) Ar and (b) Kr near the onset of 1s transitions (Soules and Shaw, 1959).

Fig. 27 Photocurrent, normalized to equal number of incident photons, as a function of photon energy. For clarity, the plots are staggered vertically. The 110 and 140 K plots refer to the solid. (Asaf and Steinberger, 1974).

Fig. 28 Relative photoyield per incident photon for solid Ne, Ar, Kr and Xe. The arrows mark the positions of the band gap E_G, $2E_G$, and the sum of the band gap and the energy of the first exciton $E_1 = E_G + E_X$. E_{Th} marks the onset of the steep increase of the yield. The maximum yields are estimated as 0.5 to 1 electron per incident photon. The dots indicate the results of O'Brien and Teegarden (1966) for an annealed Xe film at 55 K, normalized at 12 eV (Schwentner et al., 1973).

Fig. 29 EDC's for solid Ne, Ar, Kr and Xe for various photon energies below the onset of electron-electron scattering. Maximum counting rates have been normalized except near threshold. The zero-count line for each individual curve is shifted upwards proportional to the exciting photon energy (Schwentner et al.,1975).

Fig. 30 Experimental (left side) (Schwentner et al.,1975) and calculated (right side) (Rössler et al. 1975) EDC's for Xe for various photon energies.

Fig. 31 Experimental (dashed line) (Schwentner et al., 1975) and calculated (solid line) (Kunz et al., 1975) EDC's for solid Ar for various photon energies.

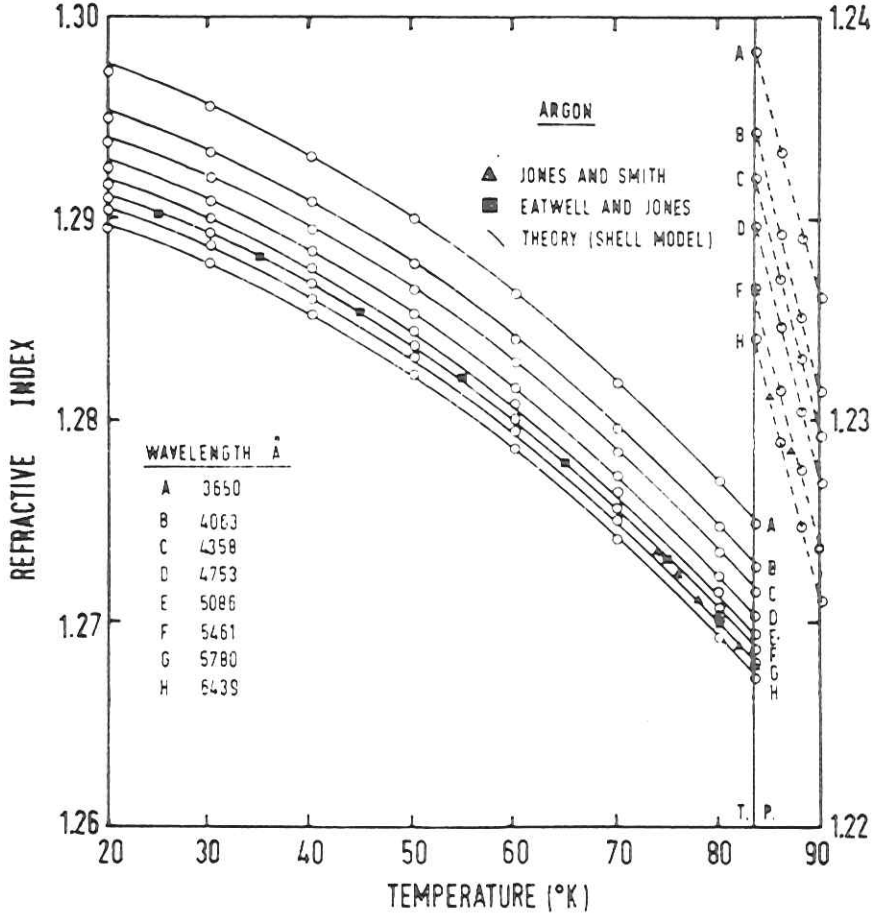
ARGON
JONES AND SMITH
EATWELL AND JONES
THEORY (SHELL MODEL)
WAVELENGTH Å
A 3650
B 4063
C 4358
D 4753
E 5086
F 5461
G 5780
H 6439
REFRACTIVE INDEX
TEMPERATURE (°K)
T. P.

Fig. 1a

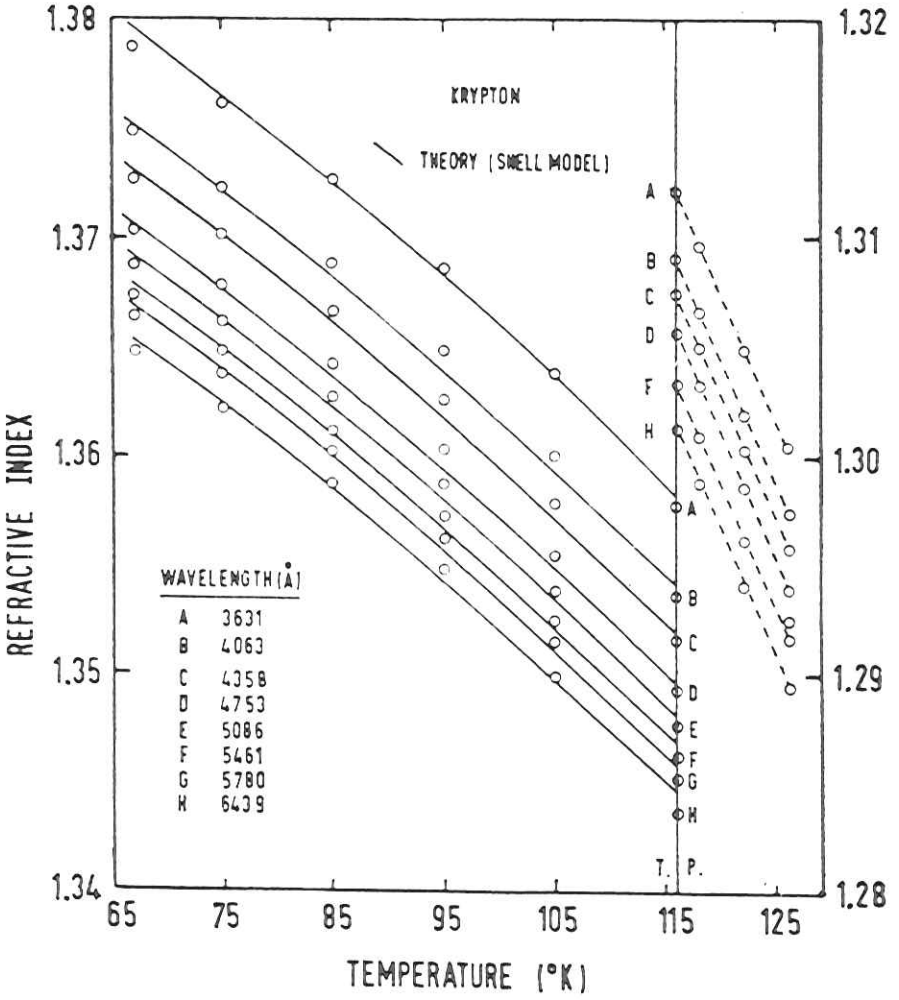
KRYPTON
THEORY (SHELL MODEL)
WAVELENGTH (Å)
A 3631
B 4063
C 4358
D 4753
E 5086
F 5461
G 5780
H 6439
REFRACTIVE INDEX
TEMPERATURE (°K)
T. P.

Fig. 1b

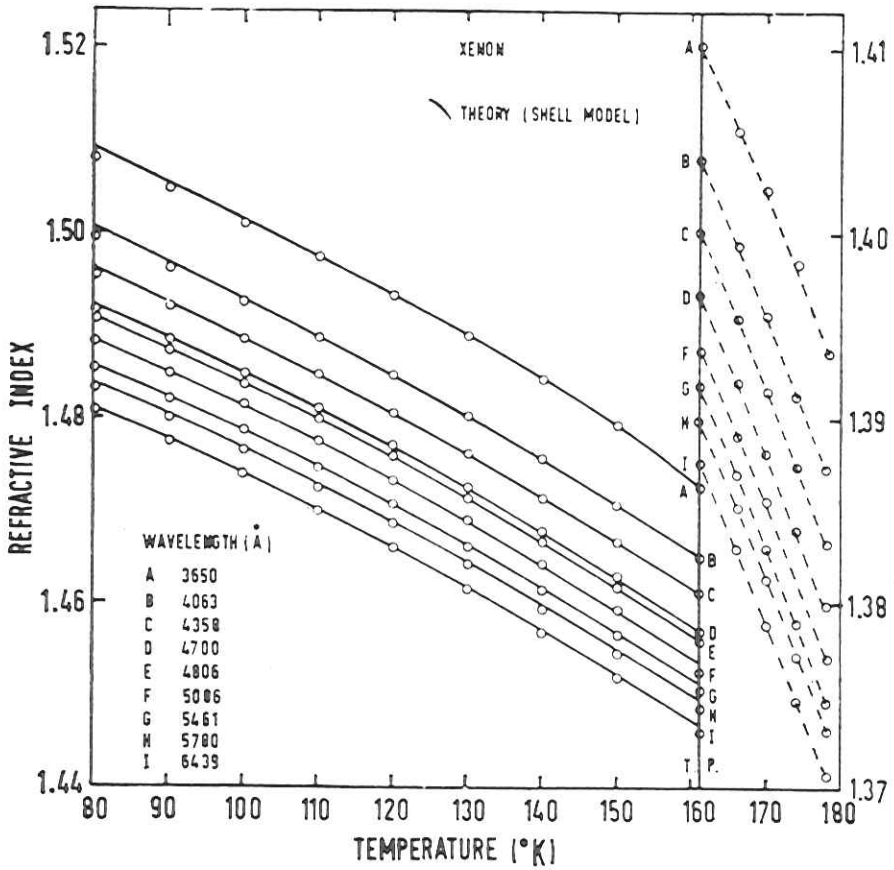
XENON
THEORY (SHELL MODEL)
WAVELENGTH (Å)
A 3650
B 4063
C 4358
D 4700
E 4806
F 5086
G 5461
H 5780
I 6439
REFRACTIVE INDEX
TEMPERATURE (°K)
1.52
1.50
1.48
1.46
1.44
1.41
1.40
1.39
1.38
1.37
80
90
100
110
120
130
140
150
160
170
180
T
P.

Fig. 1c

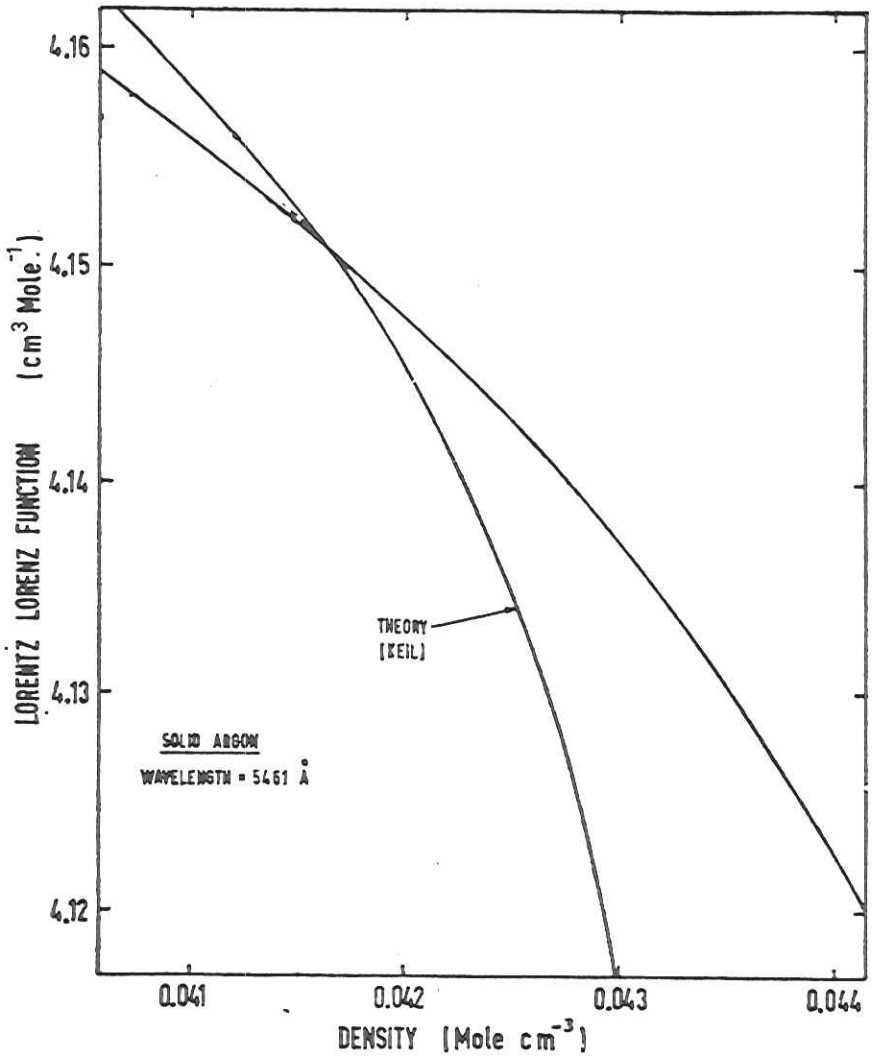
LORENTZ LORENZ FUNCTION (cm³ Mole⁻¹)
DENSITY (Mole cm⁻³)
4.16
4.15
4.14
4.13
4.12
0.041
0.042
0.043
0.044
THEORY
(KEIL)
SOLID ARGON
WAVELENGTH = 5461 Å

Fig. 2

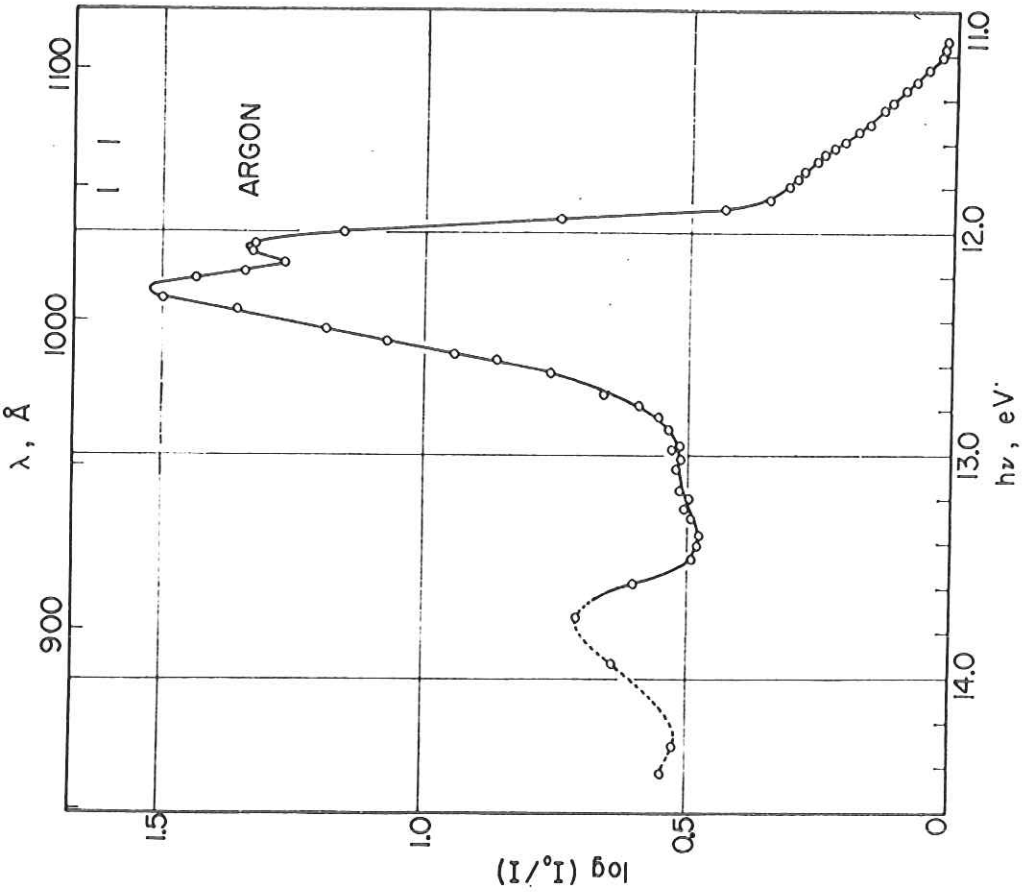
ARGON
λ, Å
hν, eV
log (I°/I)
1100
1000
900
11.0
12.0
13.0
14.0
1.5
1.0
0.5
0

Fig. 4

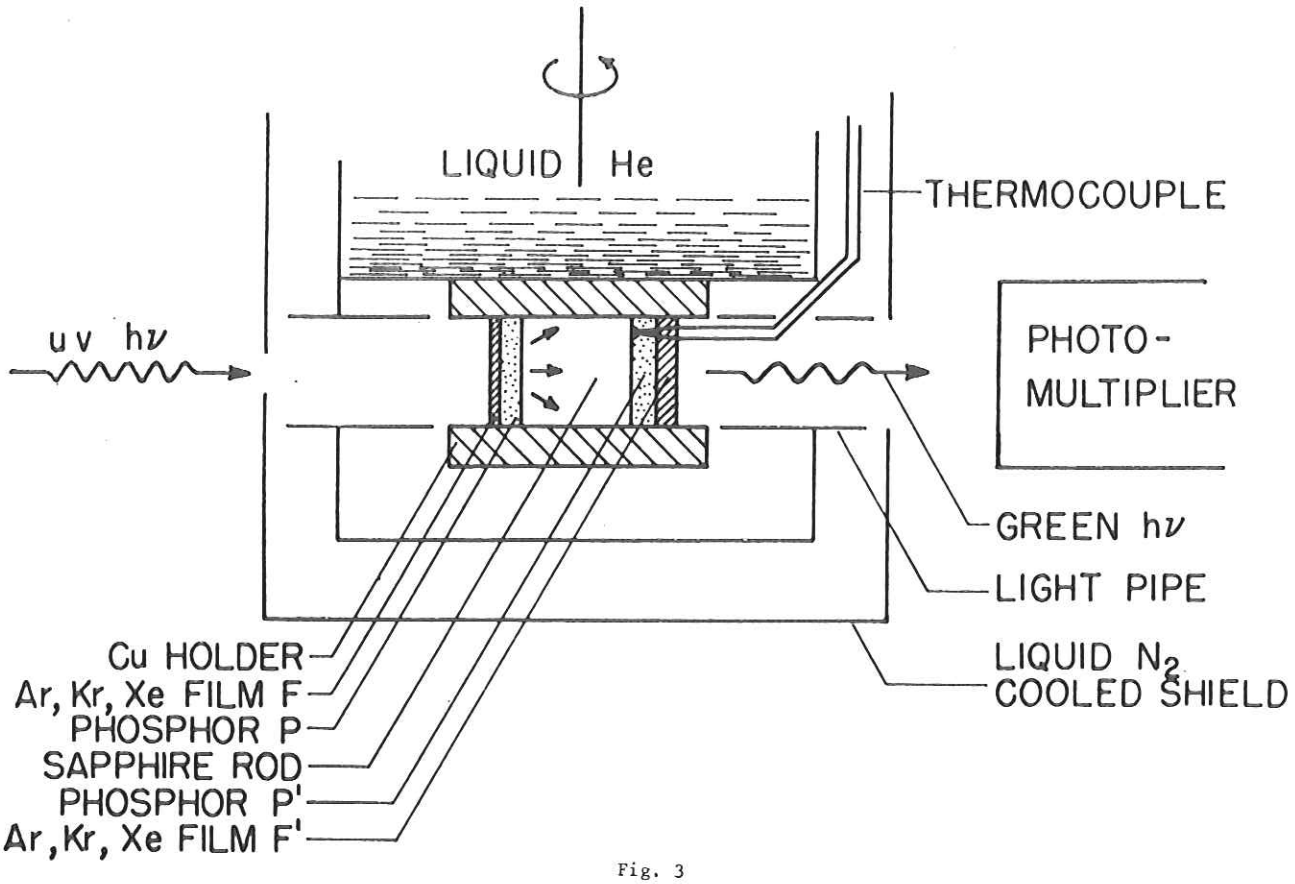
LIQUID He
THERMOCOUPLE
uv hν
PHOTO-
MULTIPLIER
GREEN hν
LIGHT PIPE
LIQUID N2
COOLED SHIELD
Cu HOLDER
Ar, Kr, Xe FILM F
PHOSPHOR P
SAPPHIRE ROD
PHOSPHOR P'
Ar, Kr, Xe FILM F'

Fig. 3

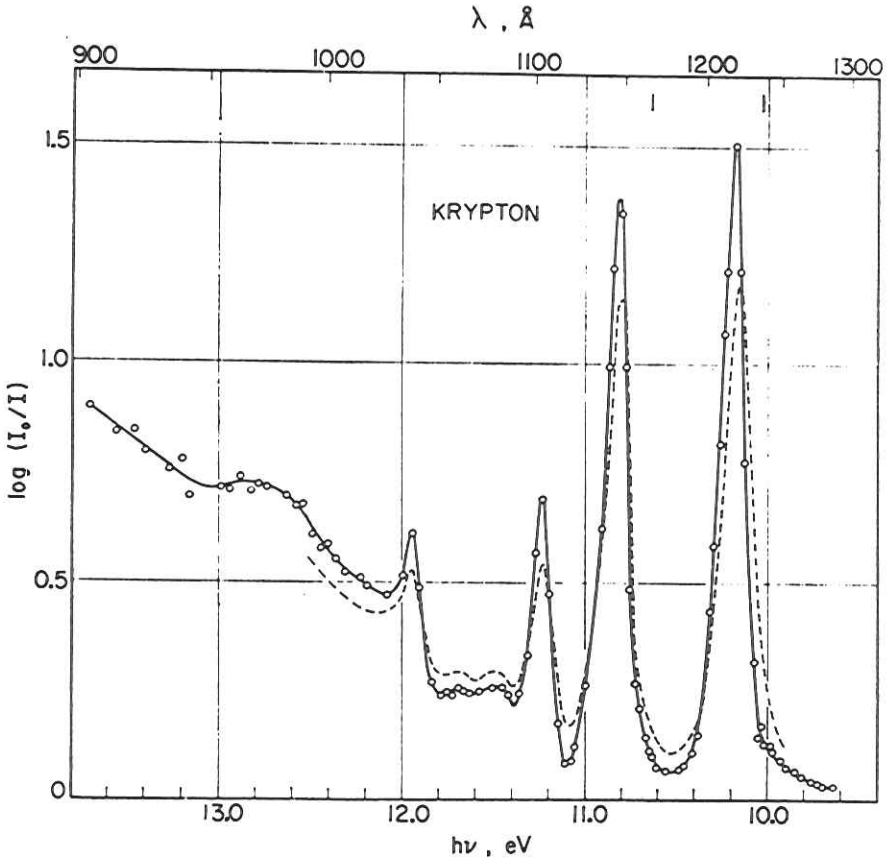
λ , Å
900
1000
1100
1200
1300
KRYPTON
log (I₀/I)
1.5
1.0
0.5
0
13.0
12.0
11.0
10.0
hν , eV

Fig. 5

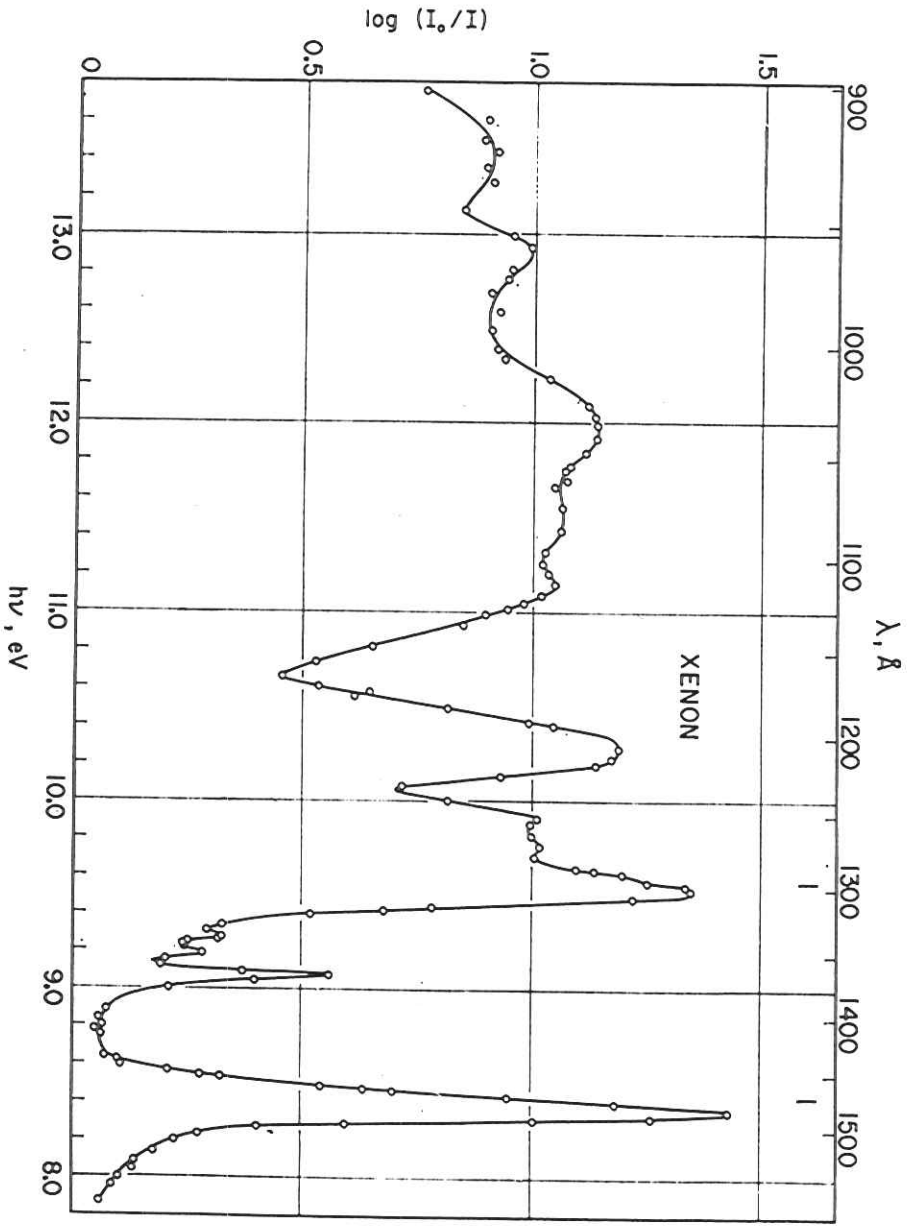
log (I₀/I)
0
0.5
1.0
1.5
XENON
hν , eV
13.0
12.0
11.0
10.0
9.0
8.0
λ, Å
900
1000
1100
1200
1300
1400
1500

Fig. 6

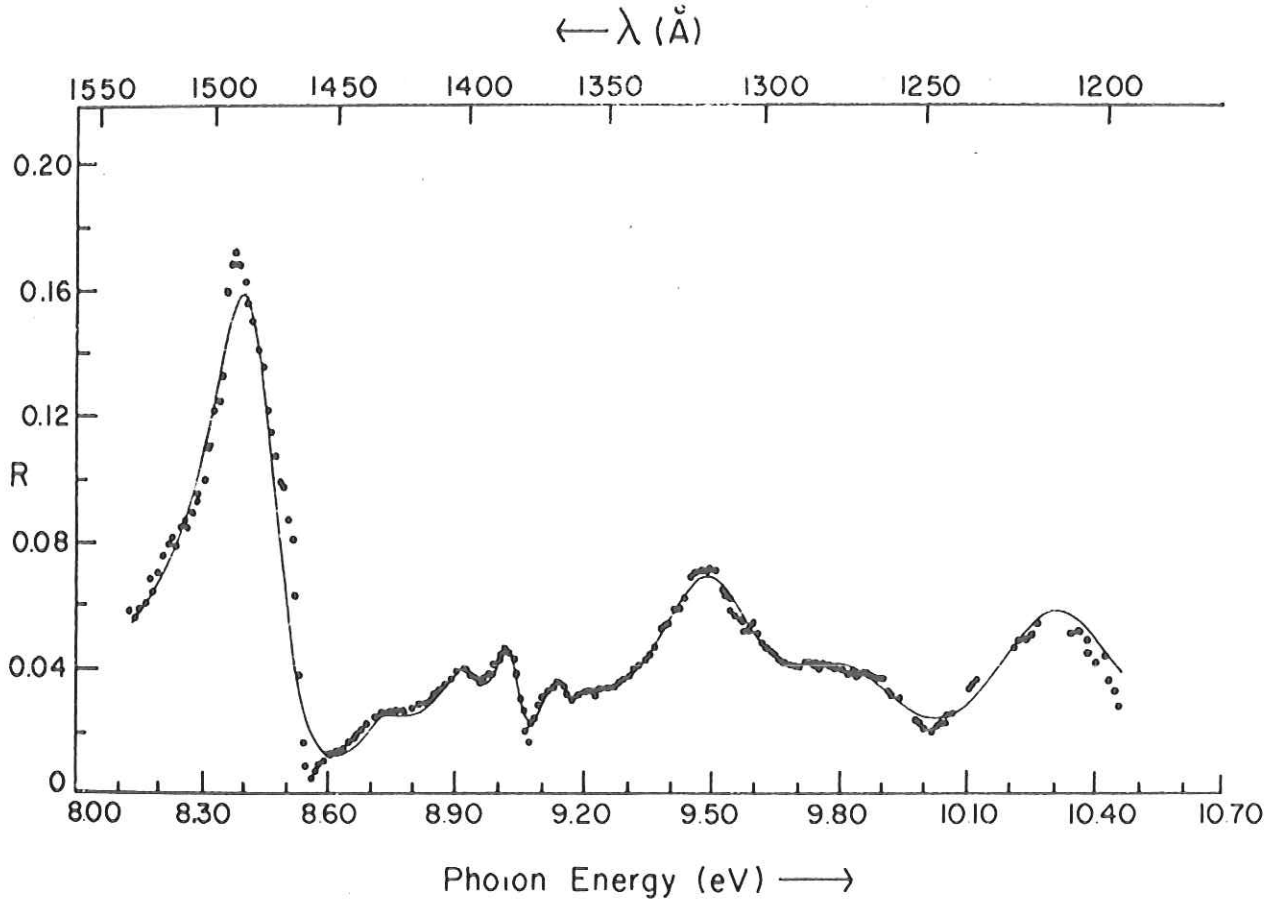
←λ (Å)
1550
1500
1450
1400
1350
1300
1250
1200
0.20
0.16
0.12
R
0.08
0.04
0
8.00
8.30
8.60
8.90
9.20
9.50
9.80
10.10
10.40
10.70
Photon Energy (eV) ⟶

Fig. 8a

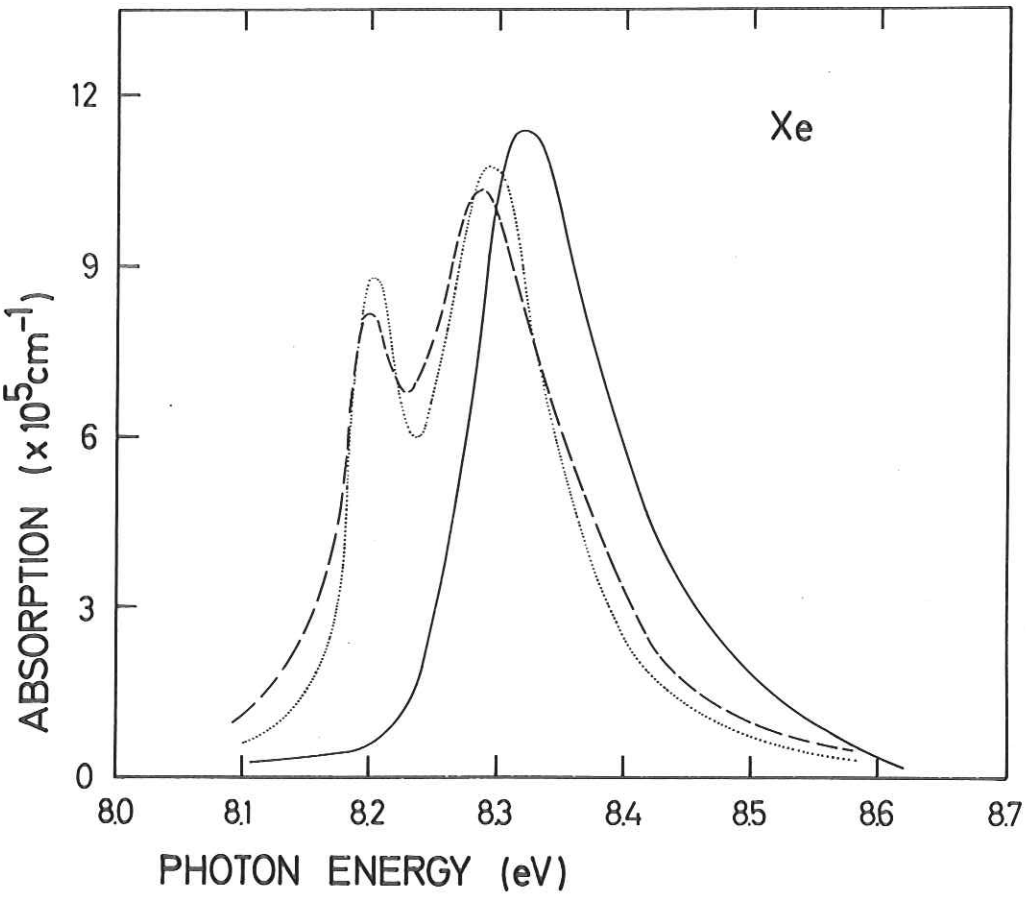
Xe
ABSORPTION (x 10^5 cm^-1)
12
9
6
3
0
8.0
8.1
8.2
8.3
8.4
8.5
8.6
8.7
PHOTON ENERGY (eV)

Fig. 7

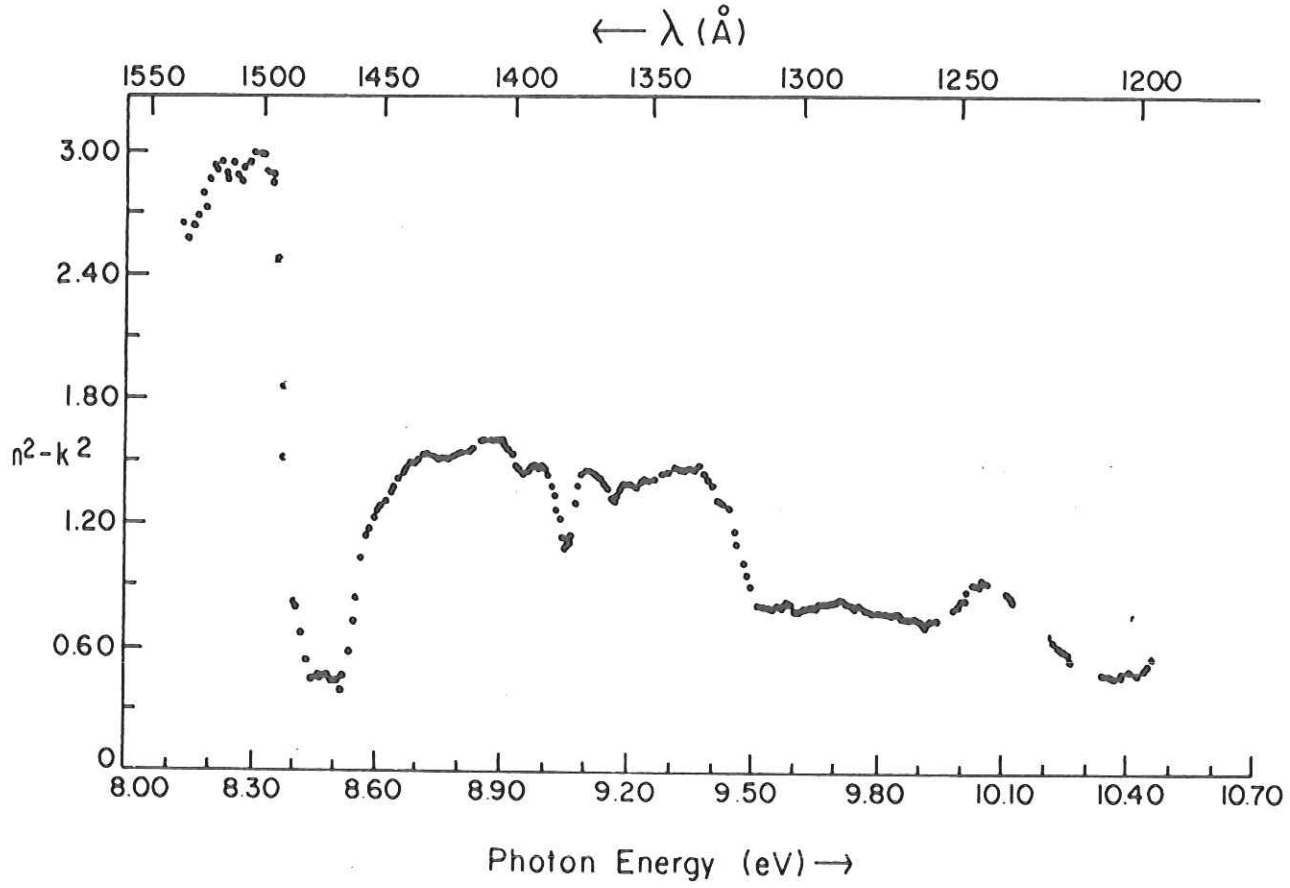
← λ (Å)
1550 1500 1450 1400 1350 1300 1250 1200
3.00
2.40
1.80
n²-k²
1.20
0.60
0
8.00 8.30 8.60 8.90 9.20 9.50 9.80 10.10 10.40 10.70
Photon Energy (eV) →

Fig. 8c

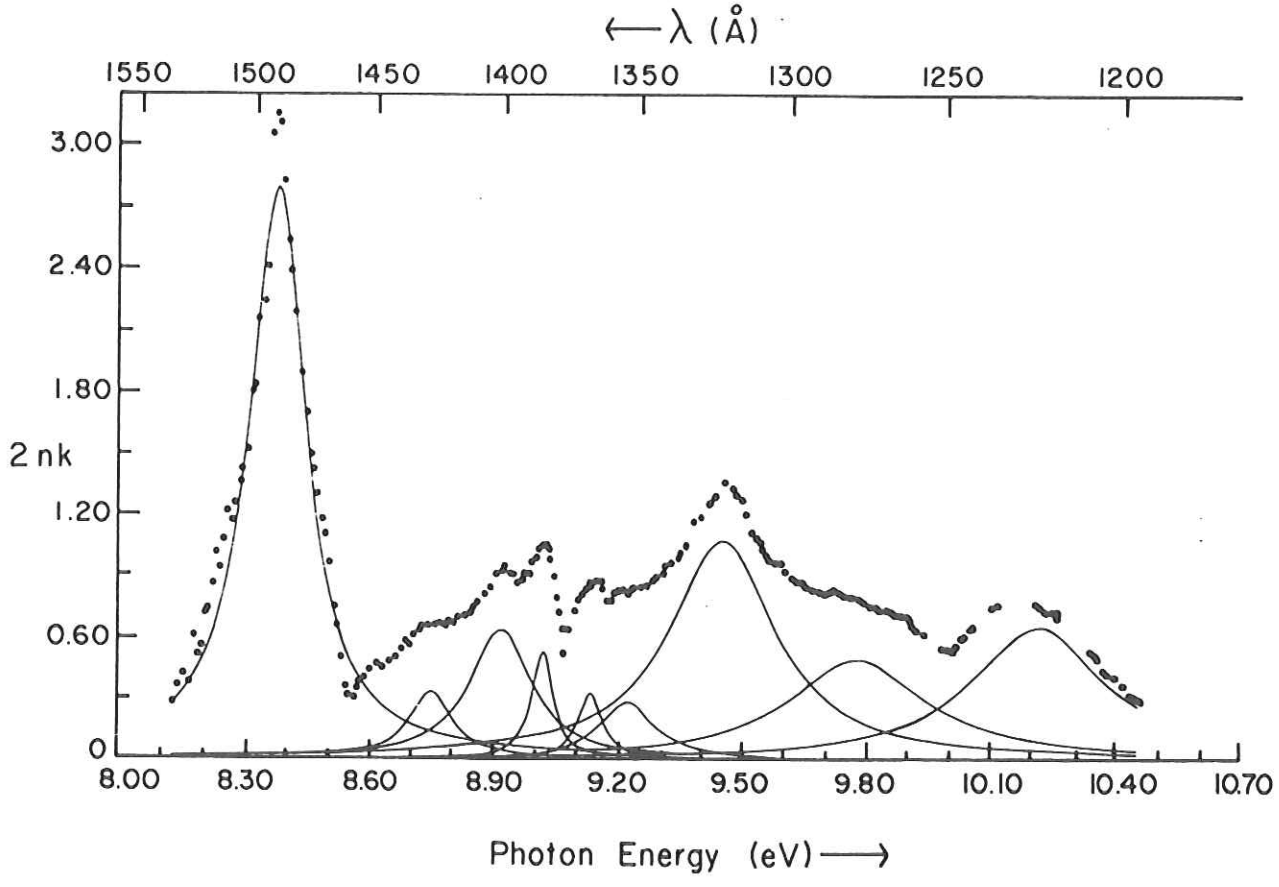
← λ (Å)
1550 1500 1450 1400 1350 1300 1250 1200
3.00
2.40
1.80
2 nk
1.20
0.60
0
8.00 8.30 8.60 8.90 9.20 9.50 9.80 10.10 10.40 10.70
Photon Energy (eV) ⟶

Fig. 8b

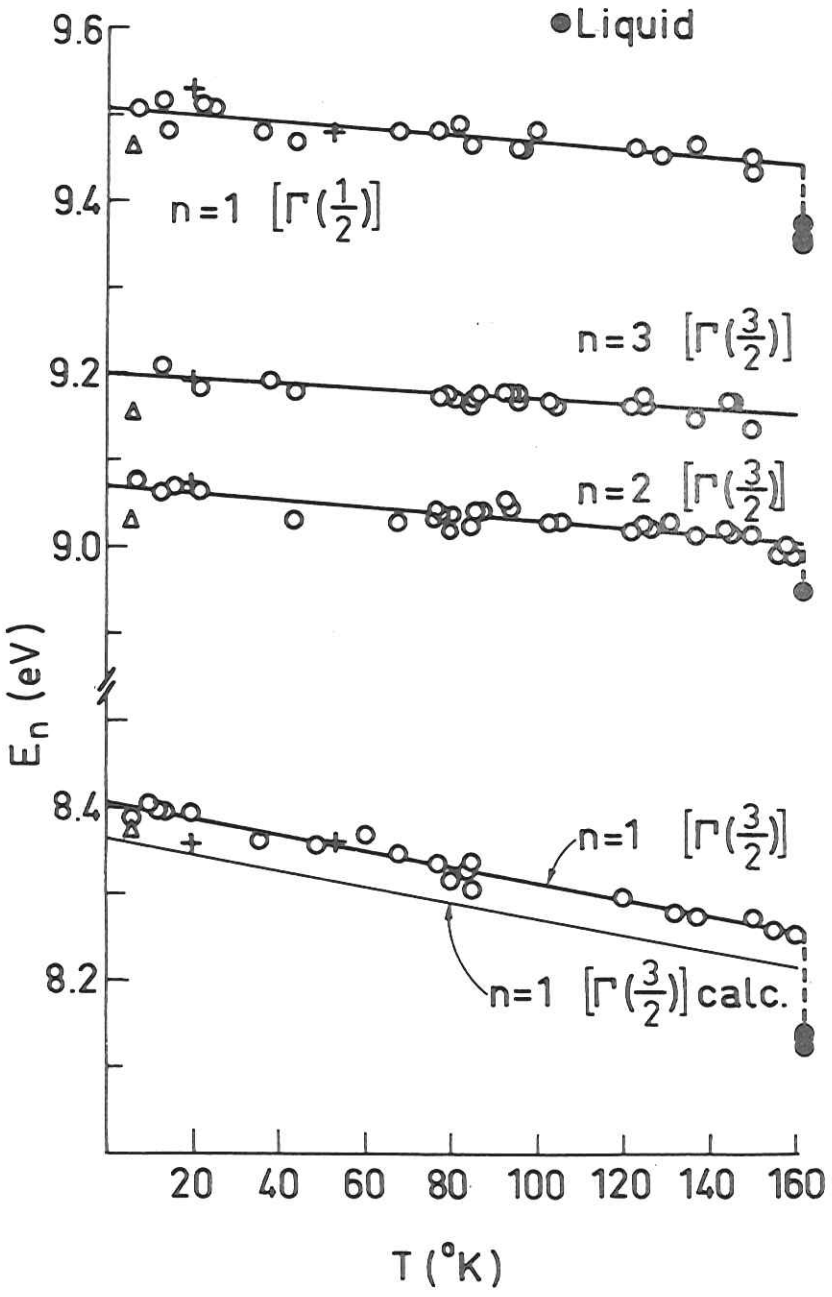
Liquid
9.6
9.4
9.2
9.0
8.4
8.2
n=1 [Γ(1/2)]
n=3 [Γ(3/2)]
n=2 [Γ(3/2)]
n=1 [Γ(3/2)]
n=1 [Γ(3/2)] calc.
Ξn (eV)
20 40 60 80 100 120 140 160
T (°K)

Fig. 9

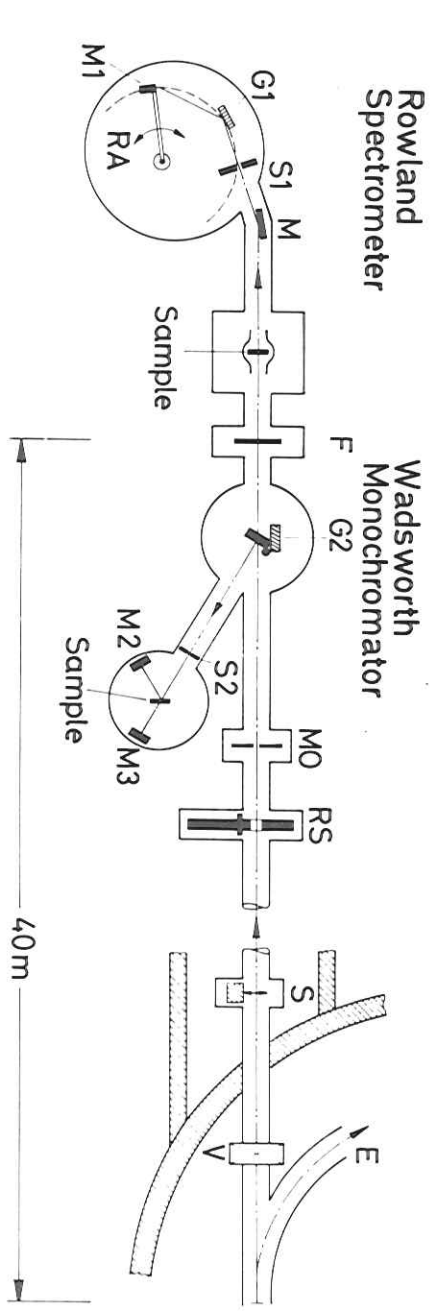
Rowland Spectrometer
Wadsworth Monochromator
M1
G1
RA
S1
M
Sample
F
G2
M2
S2
Sample
M3
M0
RS
40m
S
V
E

Fig. 10

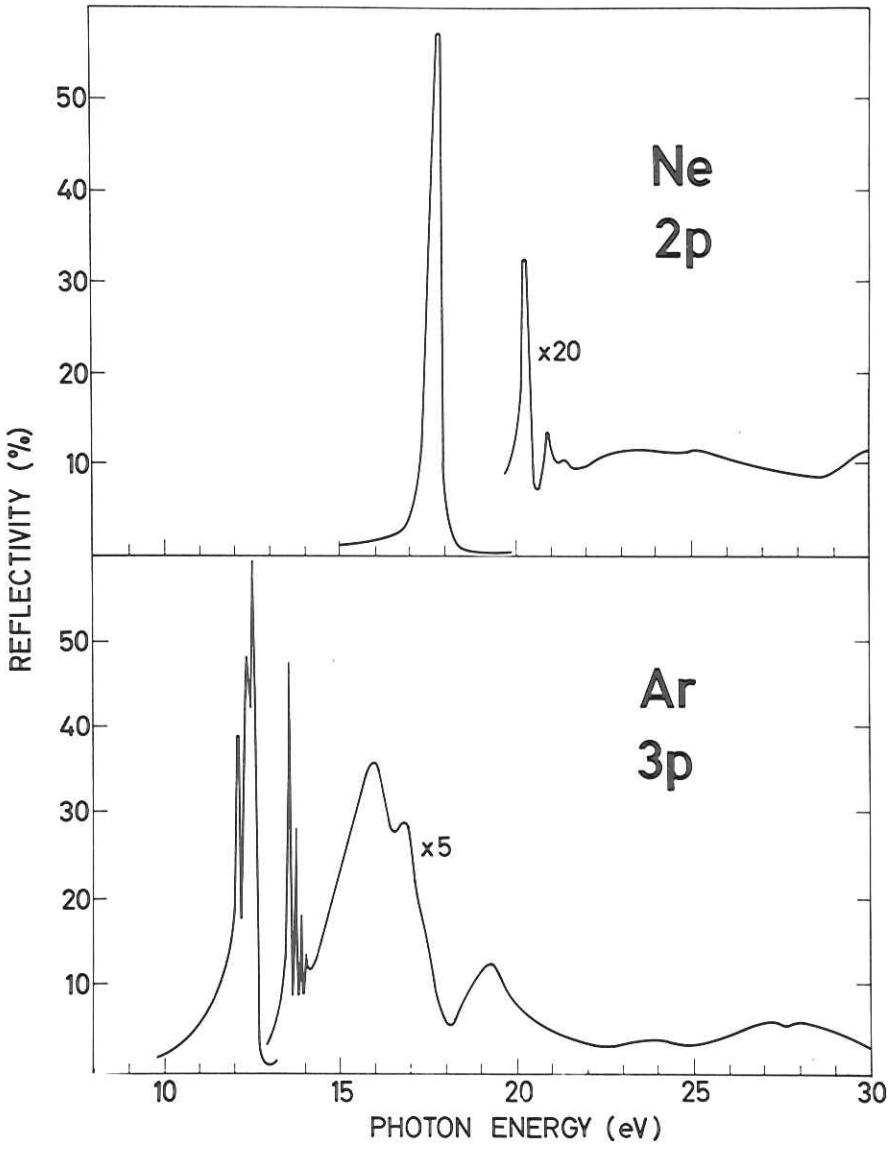

Fig. 11a

Fig. 11b

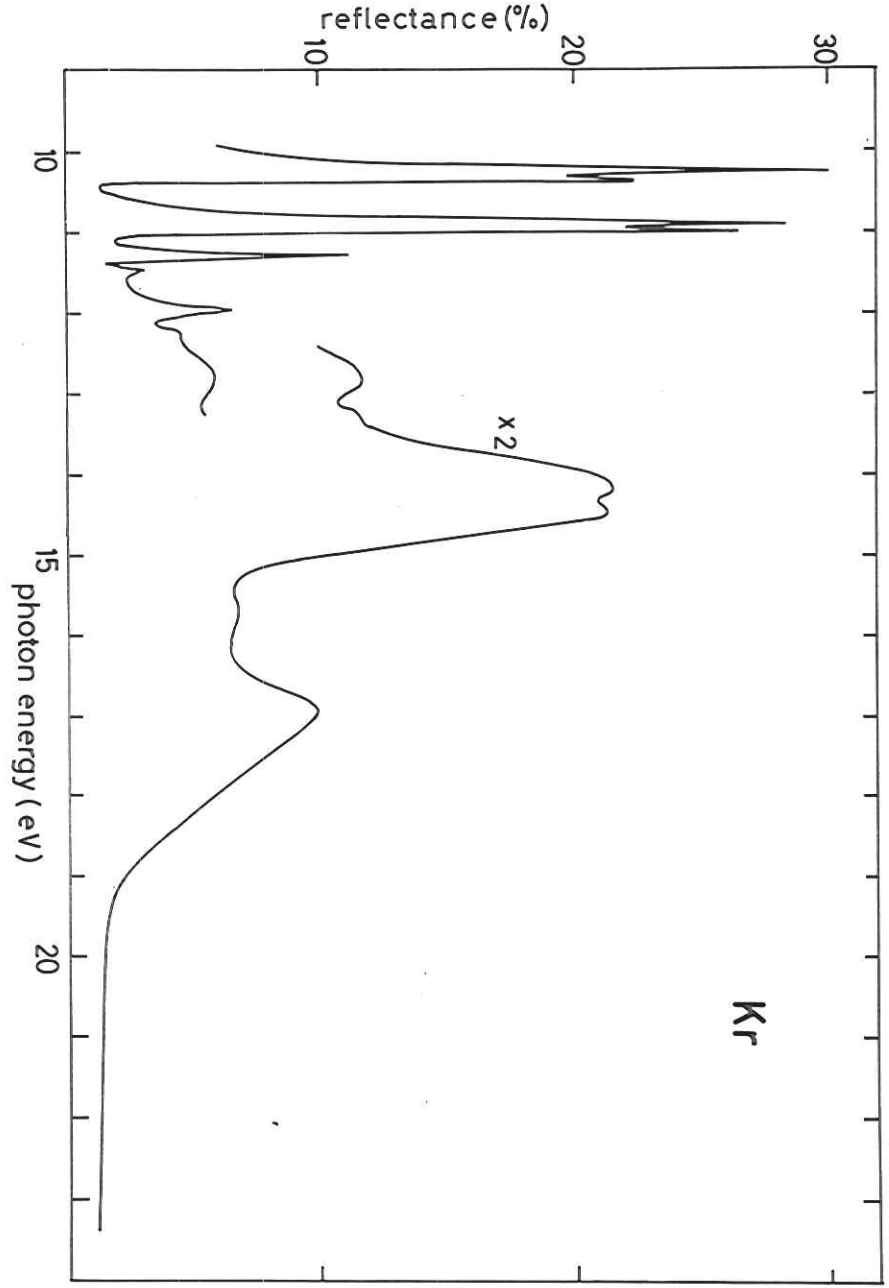

Fig. 12a

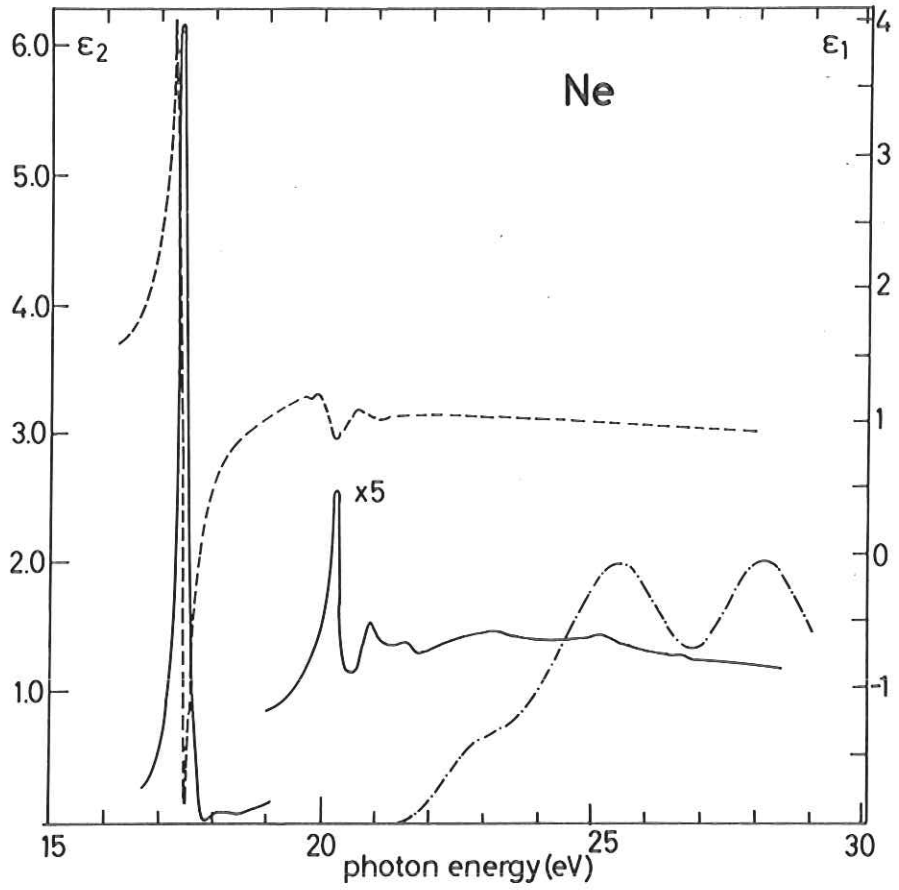

Fig. 13a

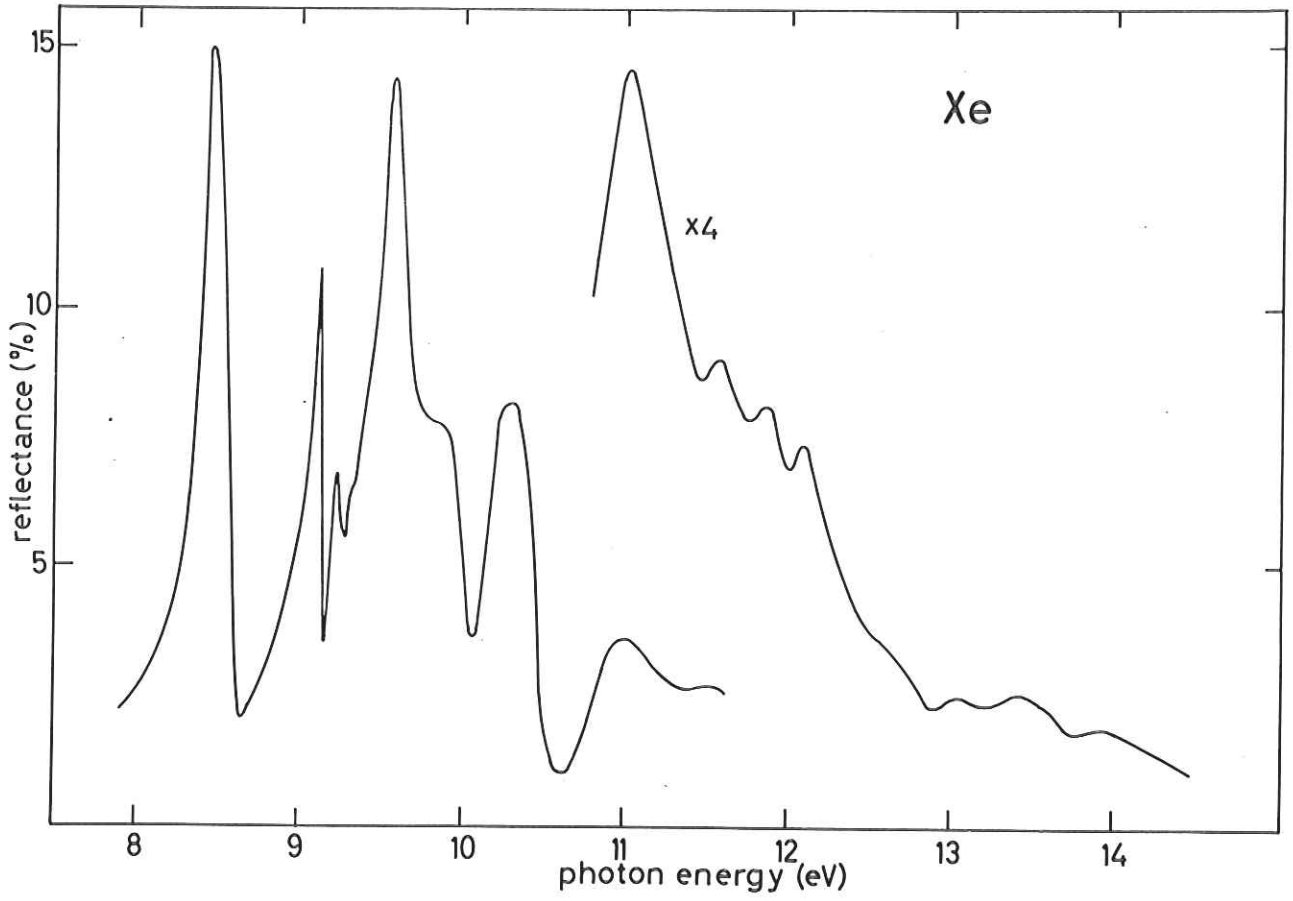

Fig. 12b

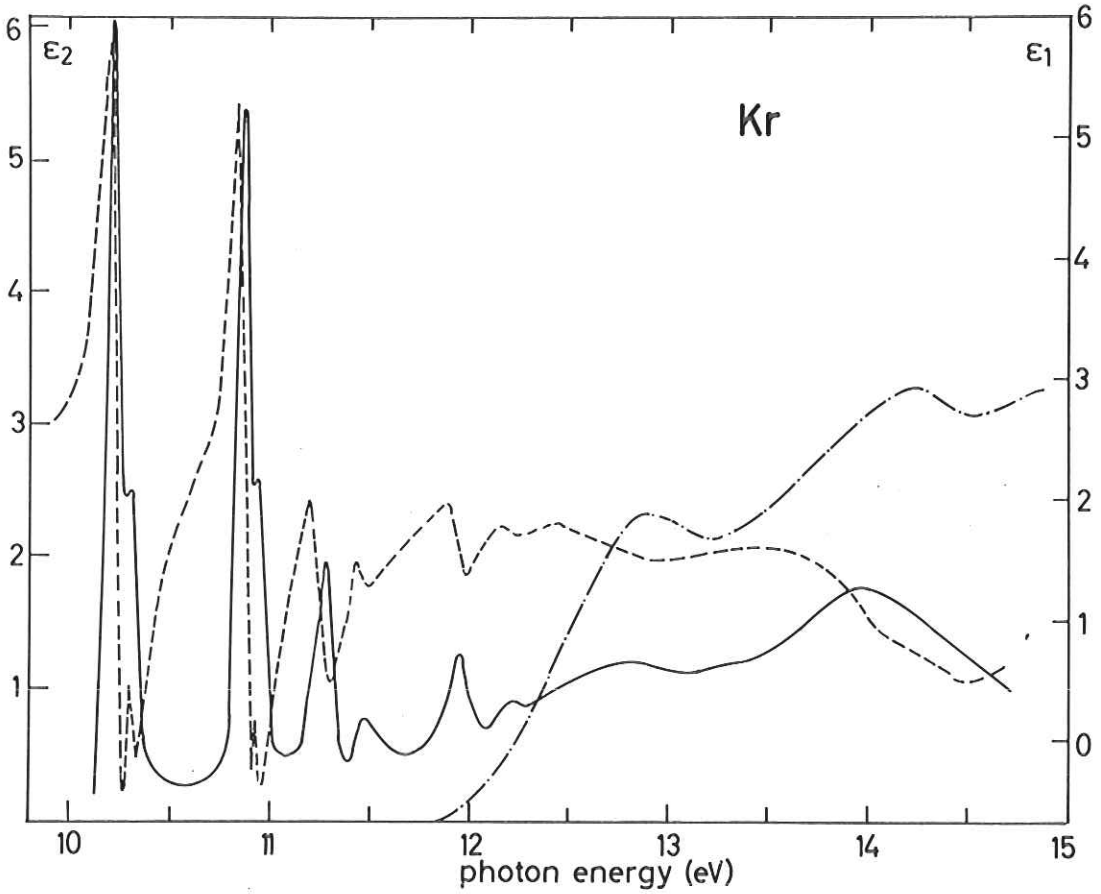

Fig. 14a

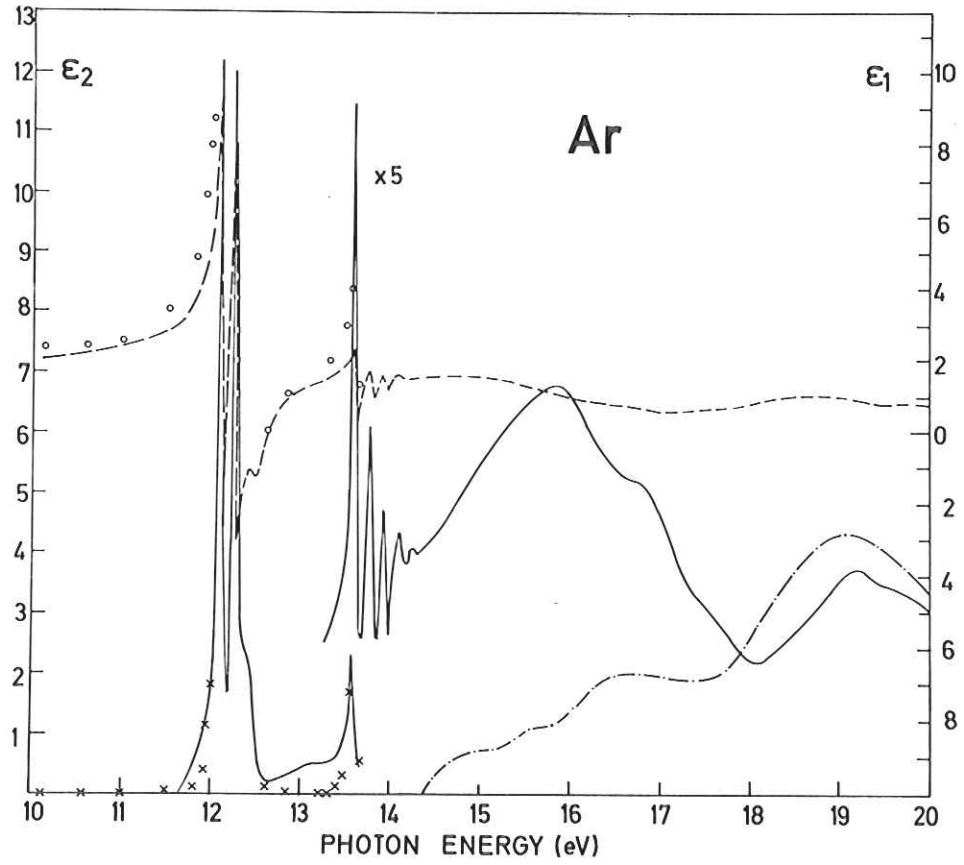

Fig. 13b

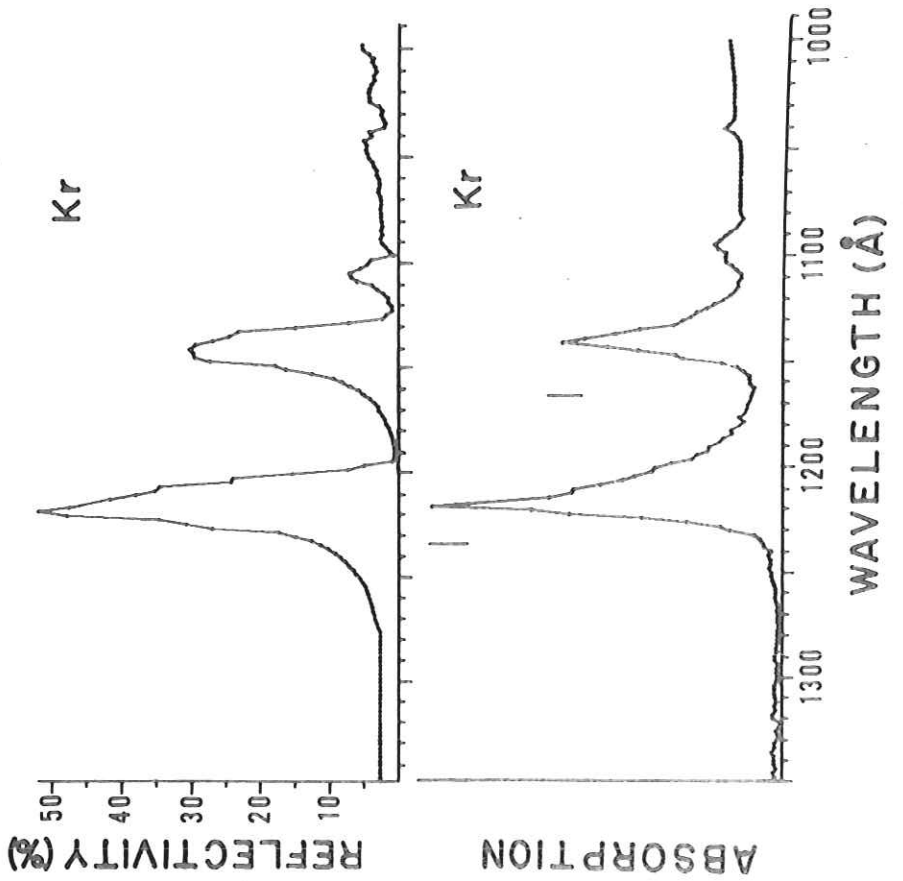

Fig. 15a

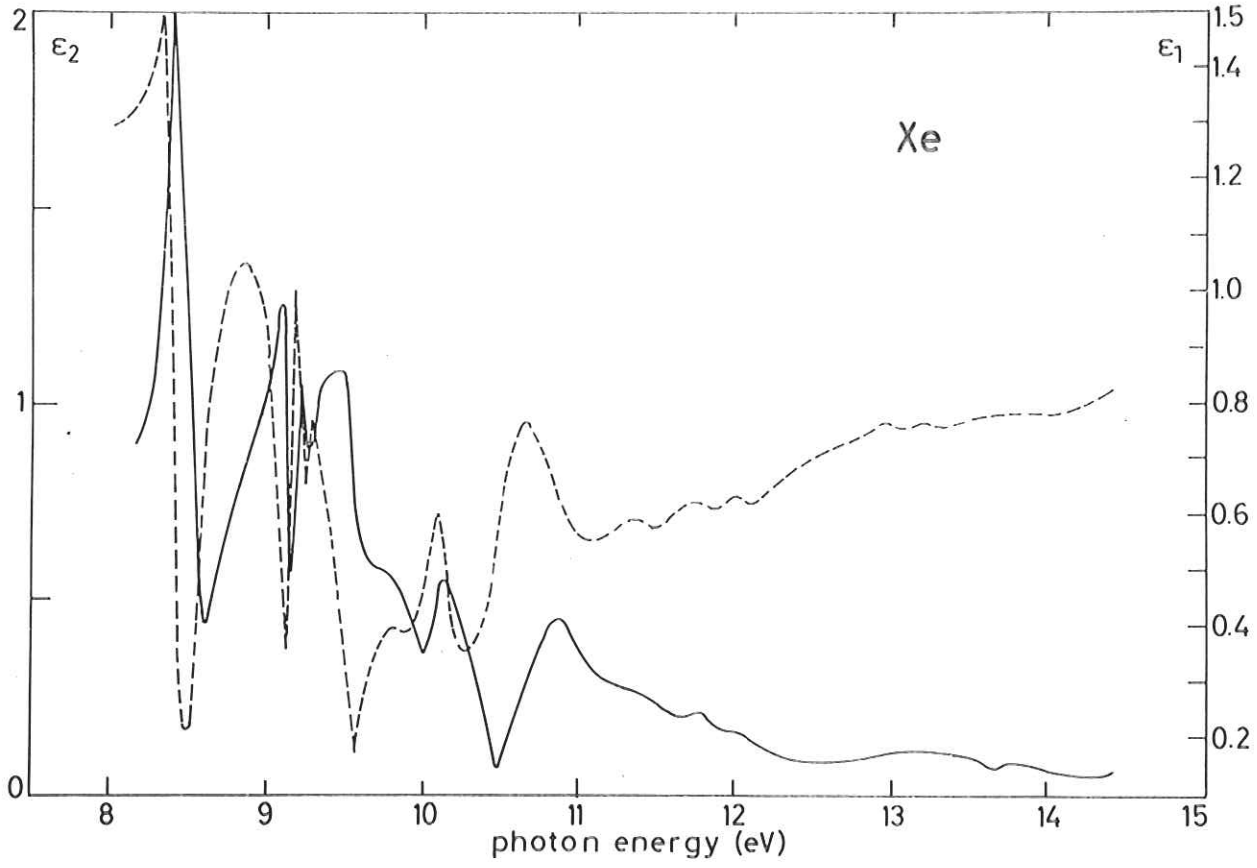

Fig. 14b

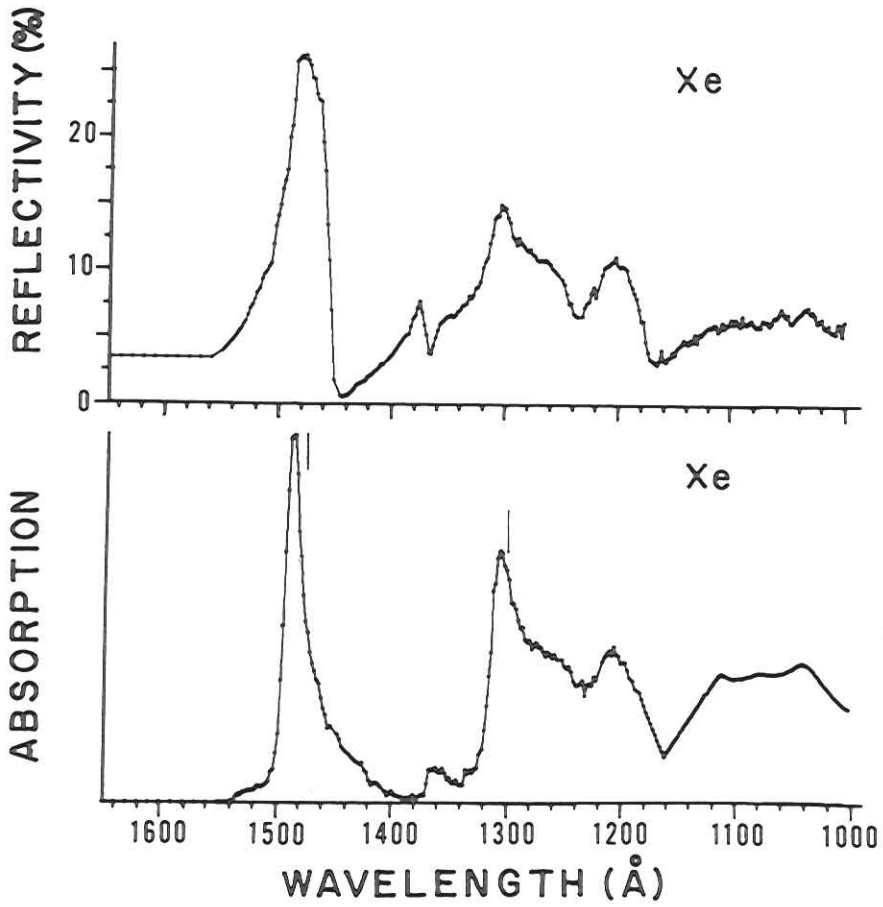

Fig. 15b

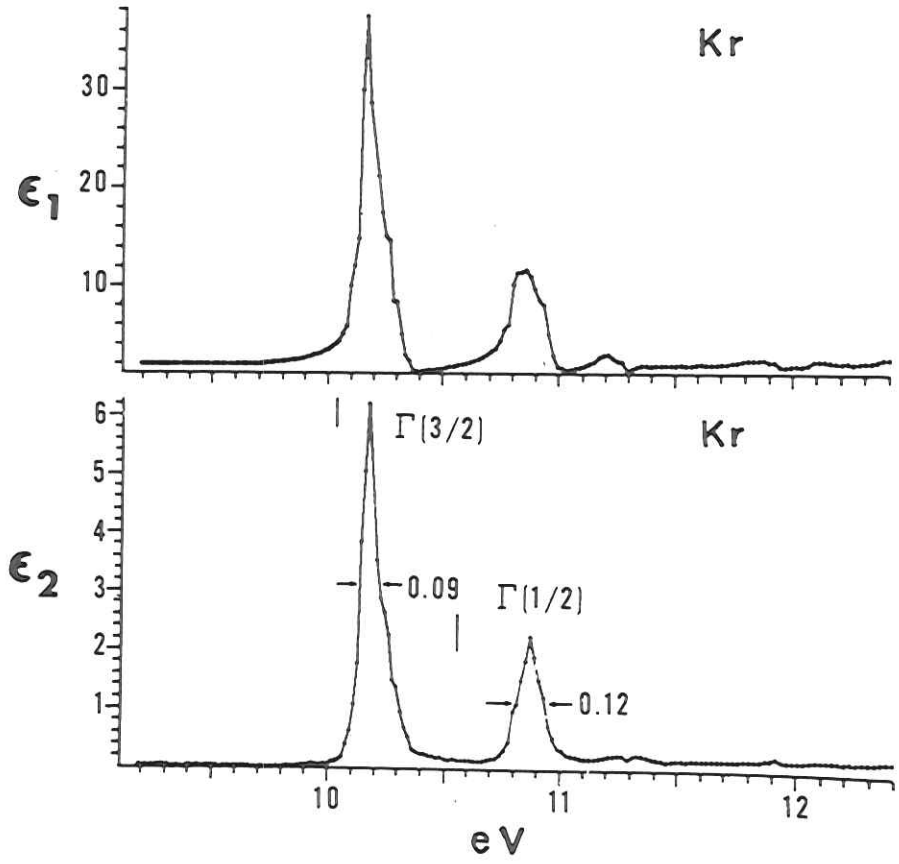

Fig. 16a

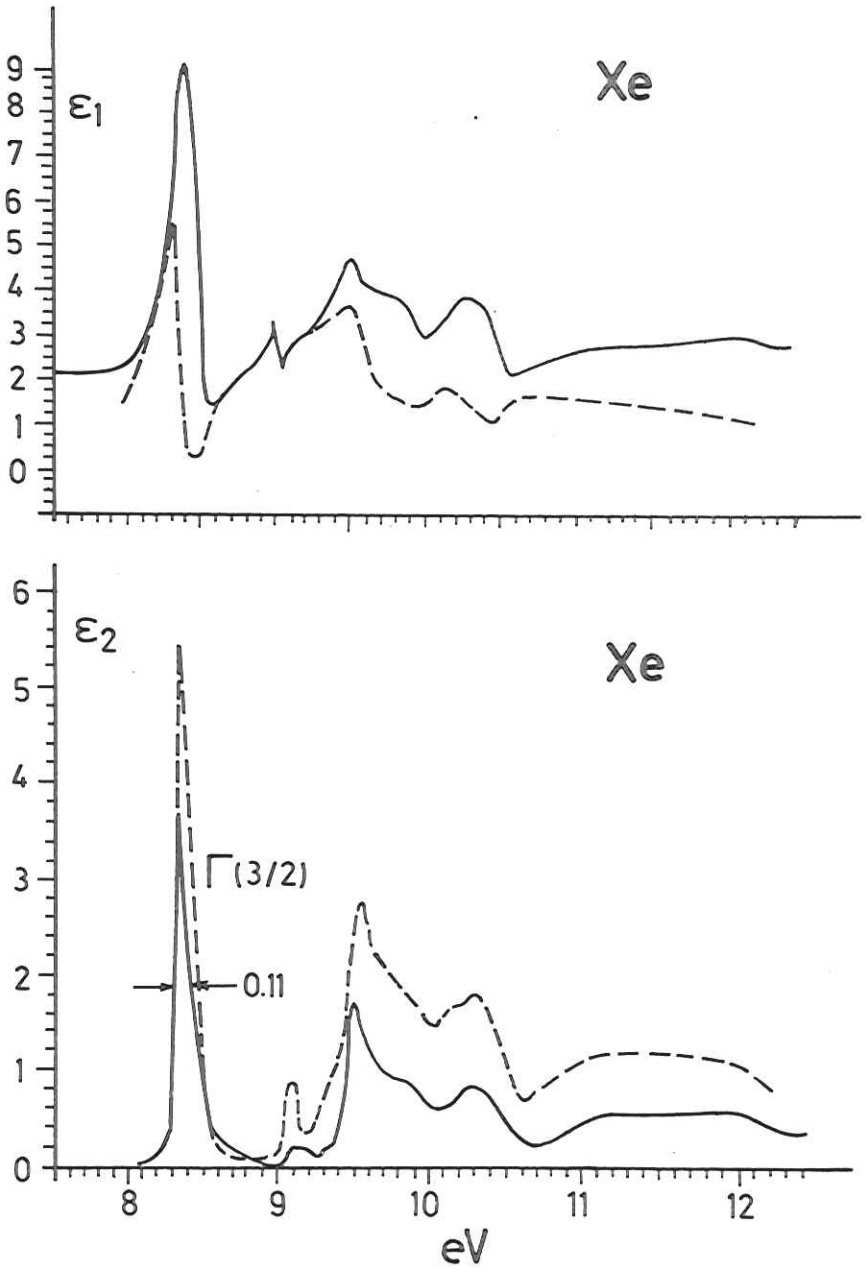

Fig. 16b

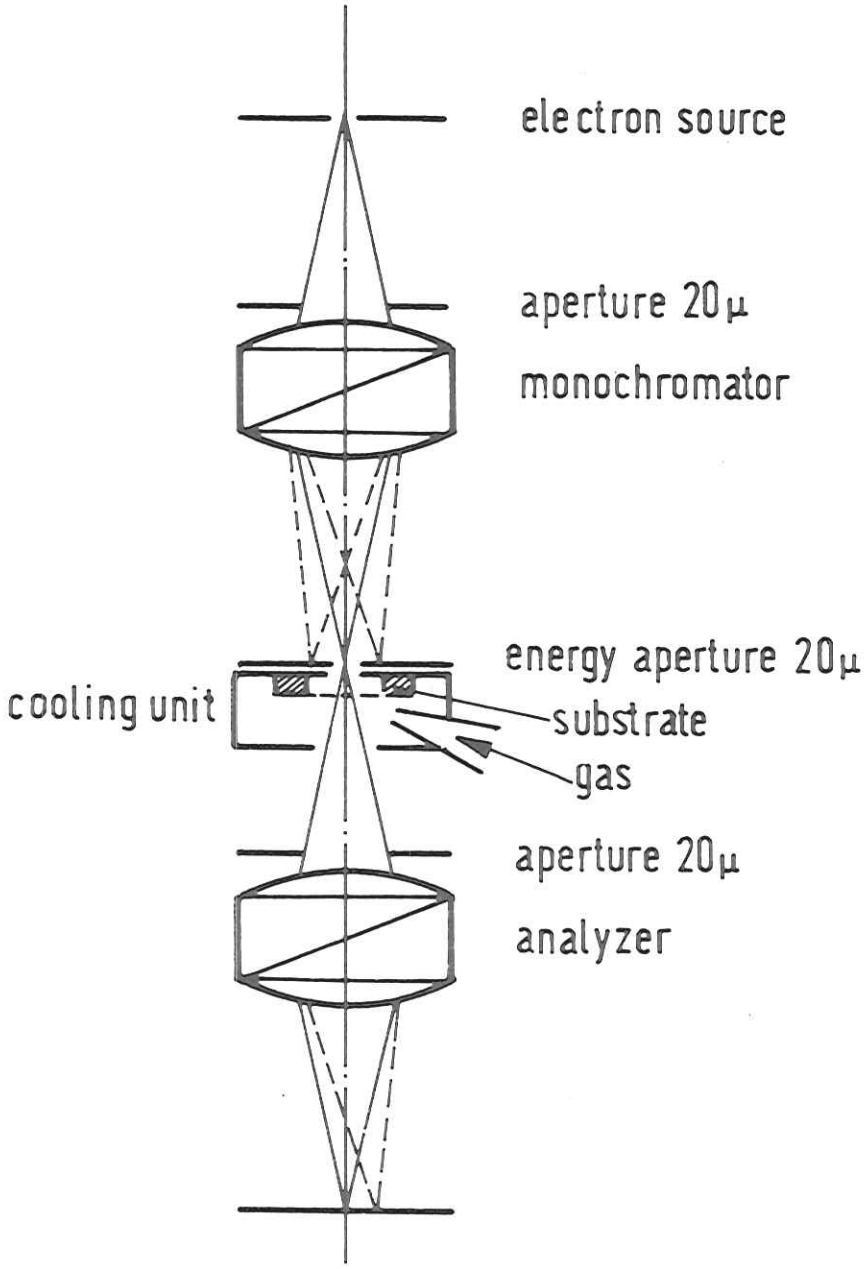

Fig. 17a

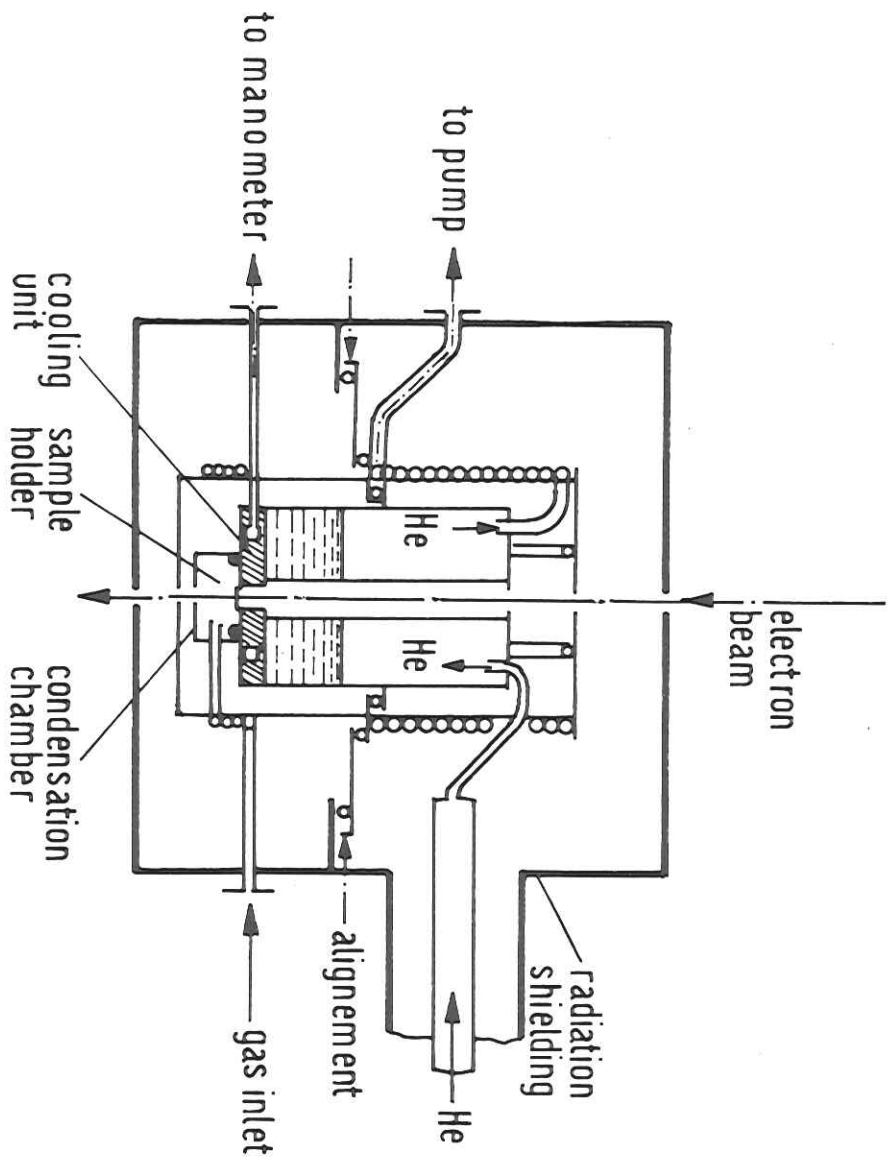

Fig. 17b

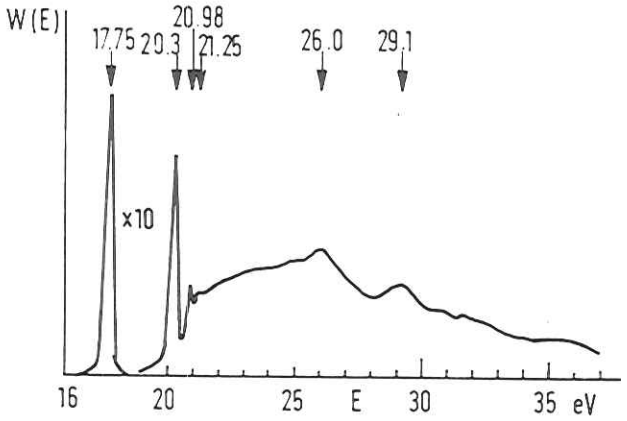

Fig. 18a

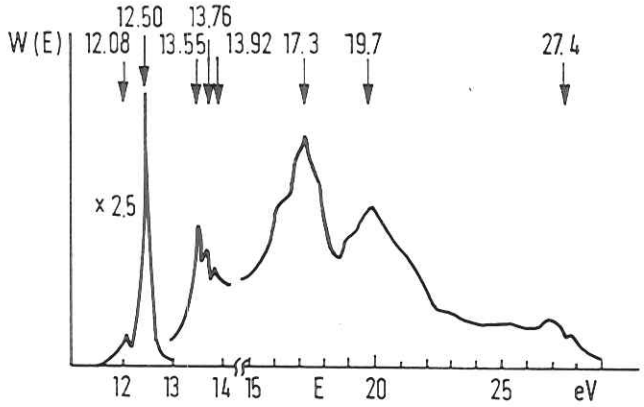

Fig. 18b

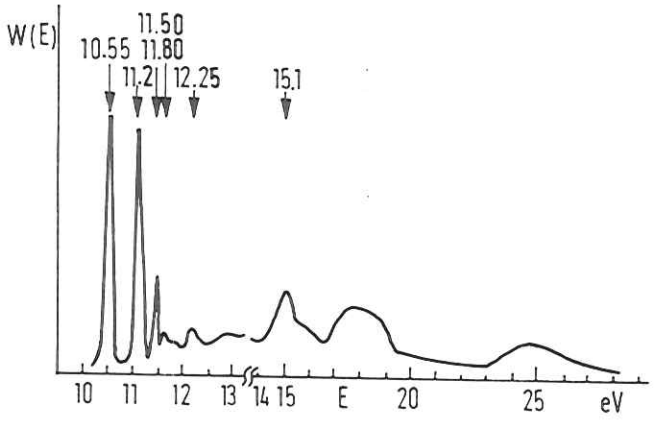

Fig. 18c

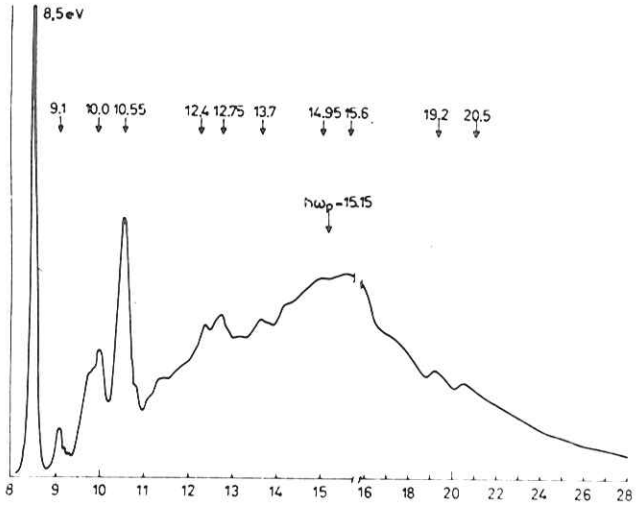

Fig. 18d

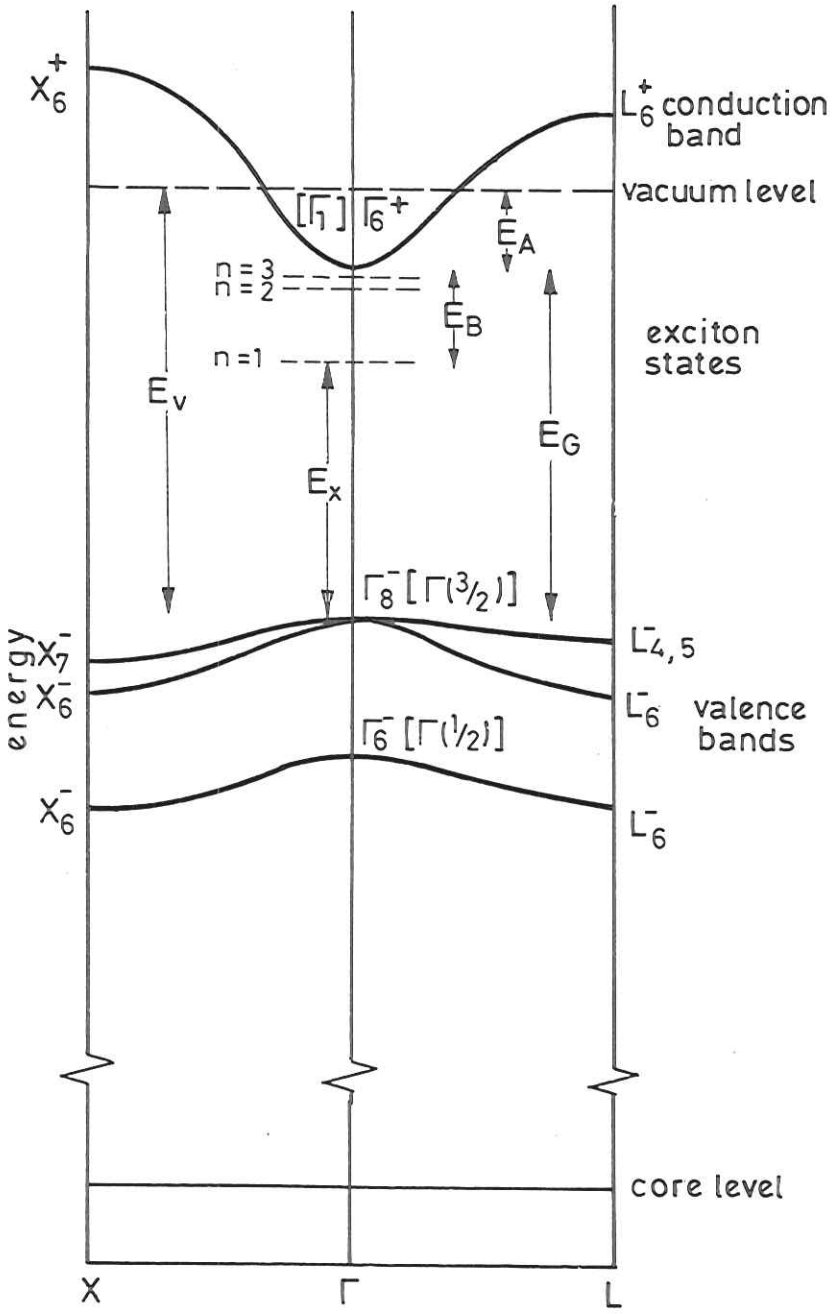

Fig. 19

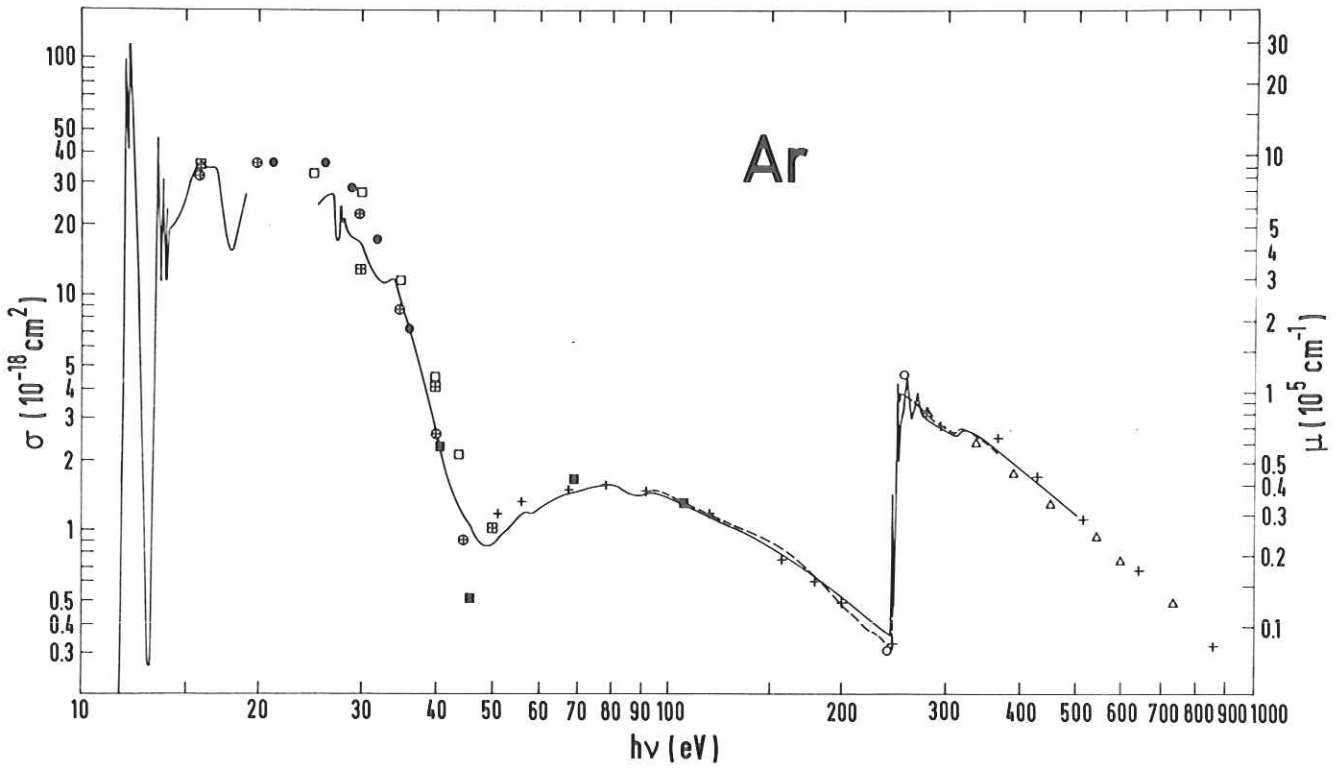

Fig. 20b

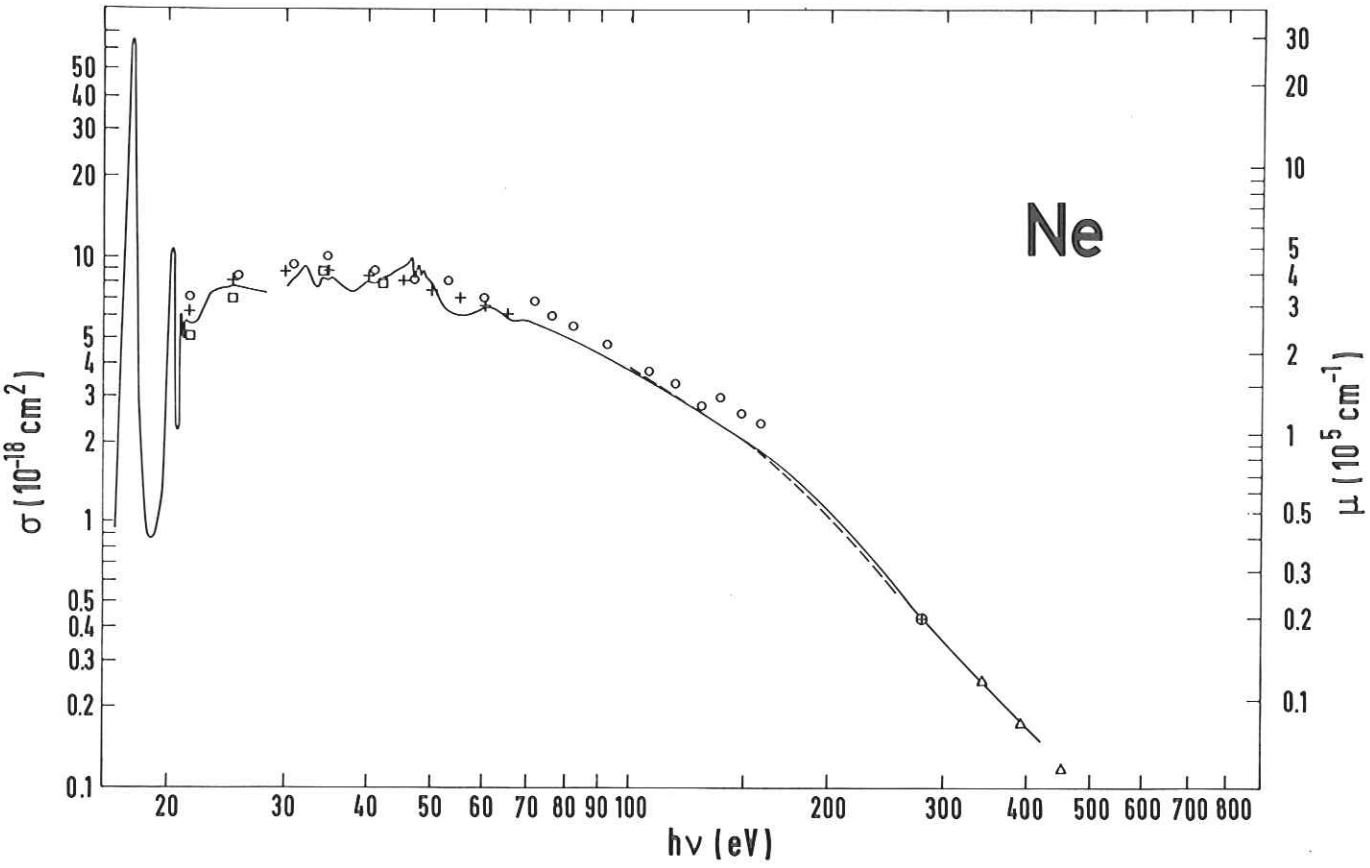

Fig. 20a

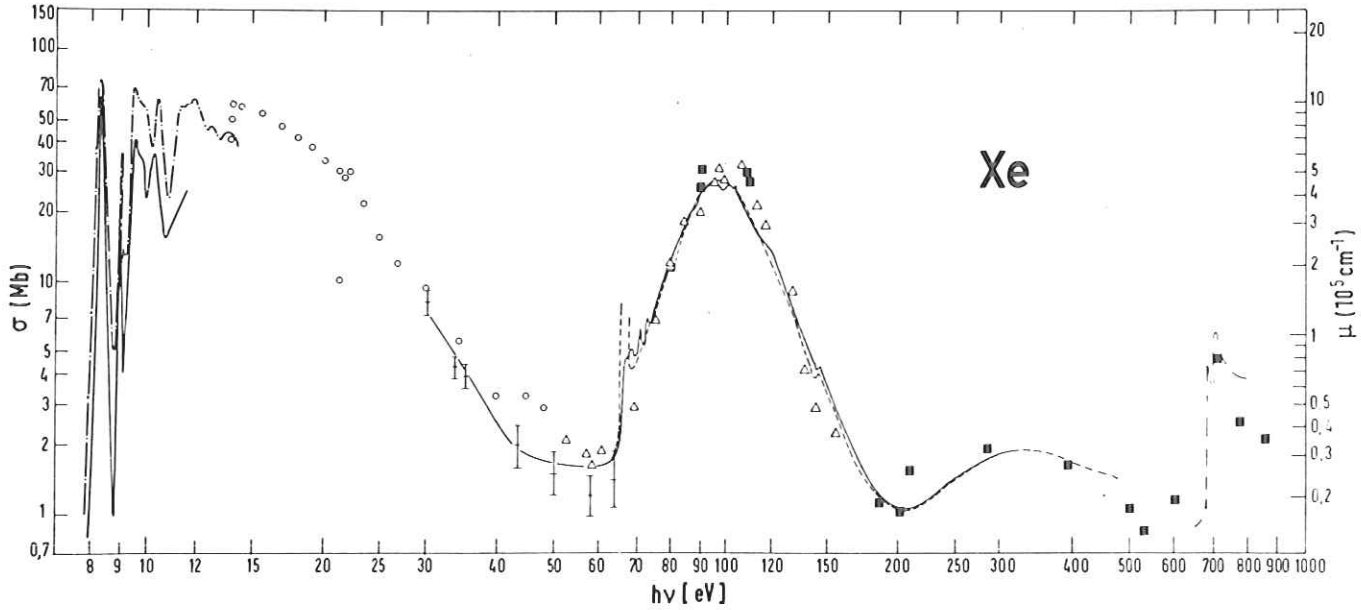

Fig. 21b

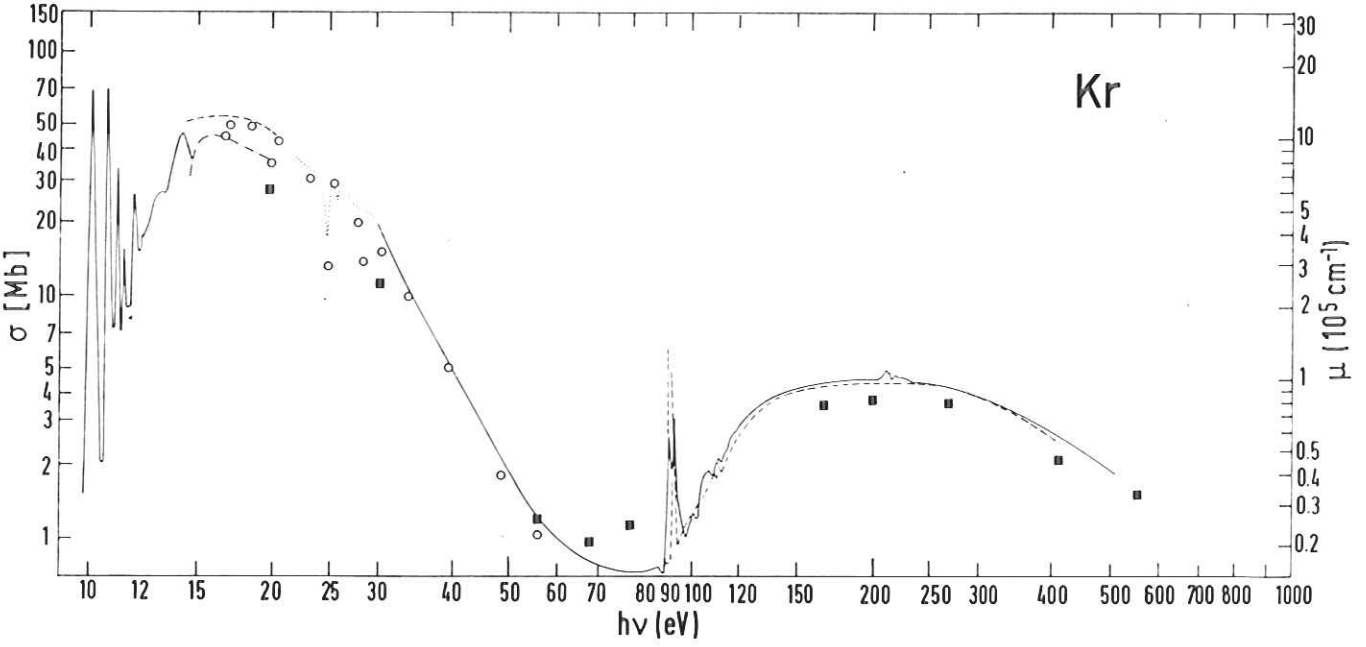

Fig. 21a

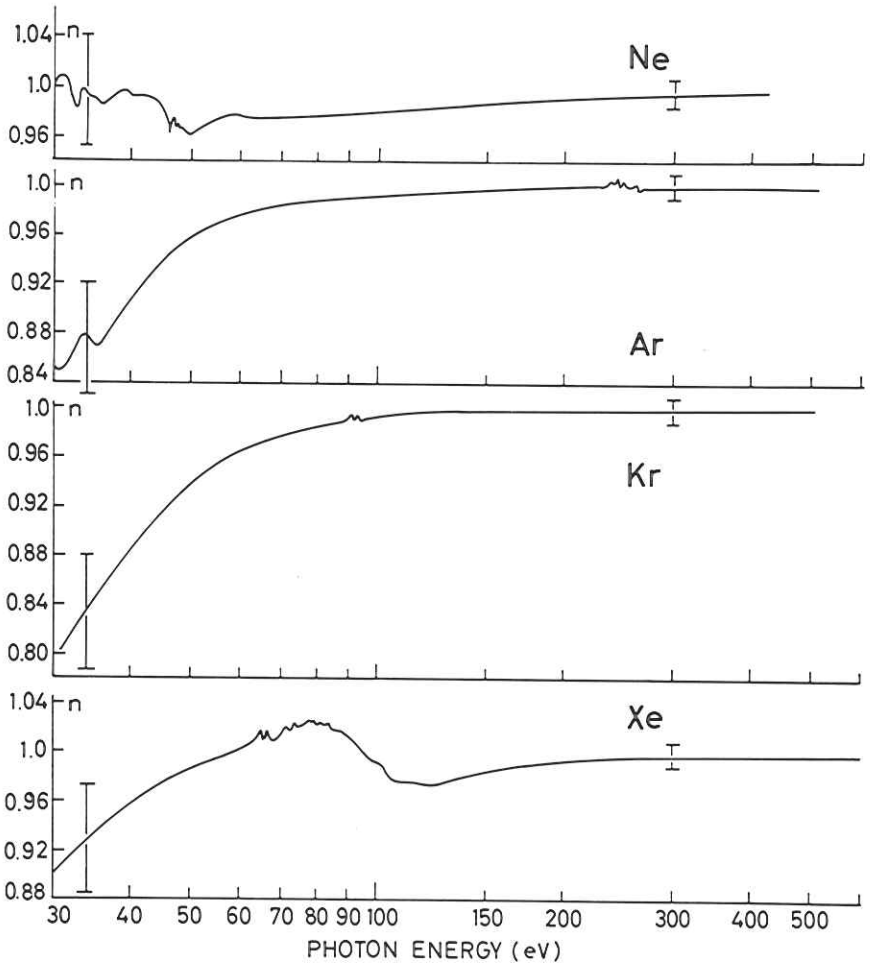

Fig. 22

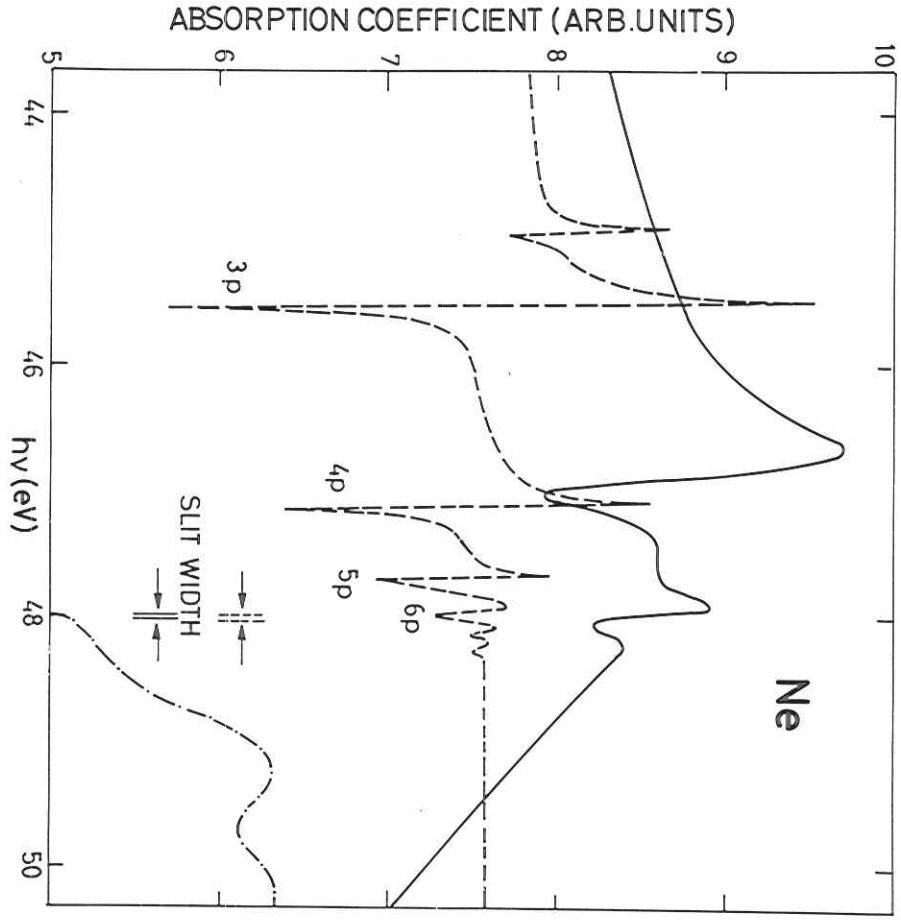

Fig. 23a

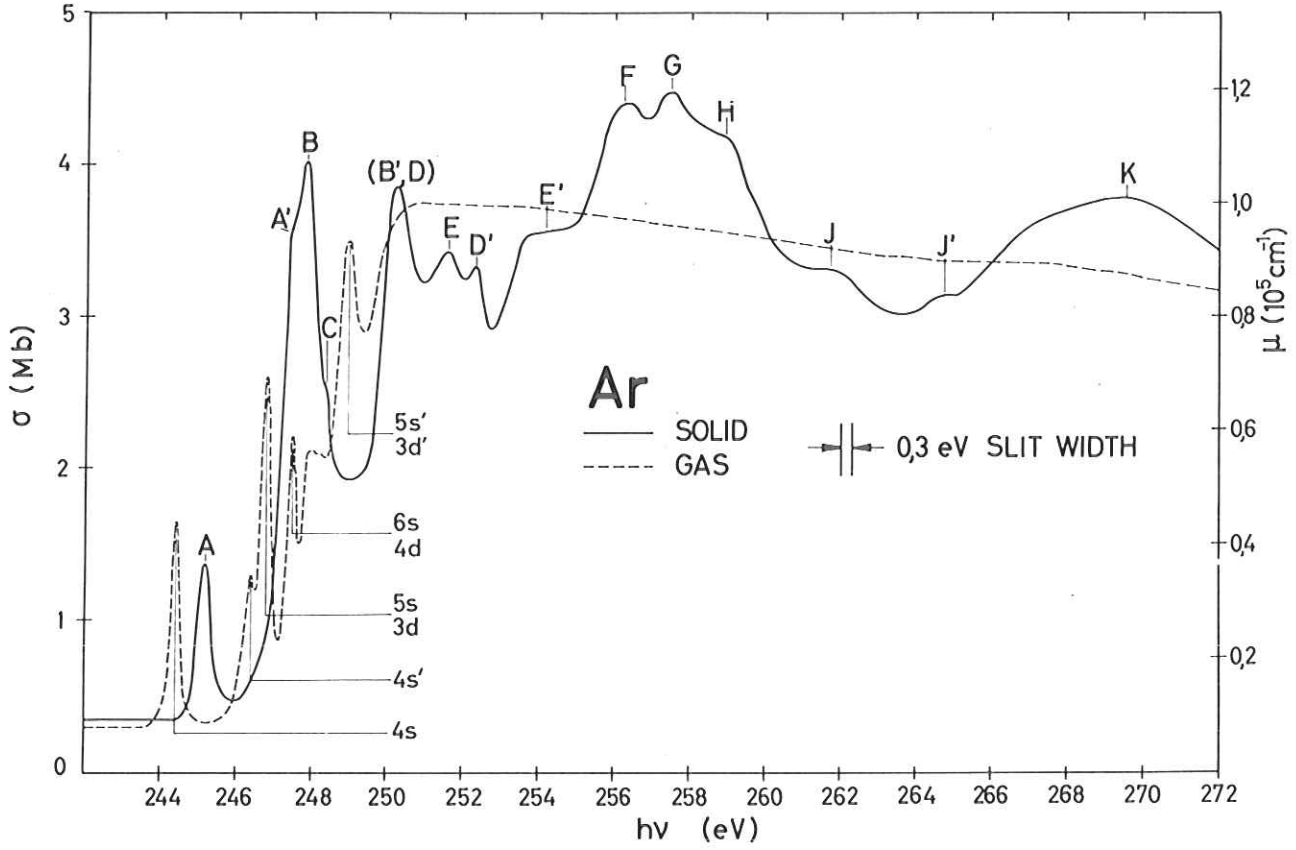

Fig. 24

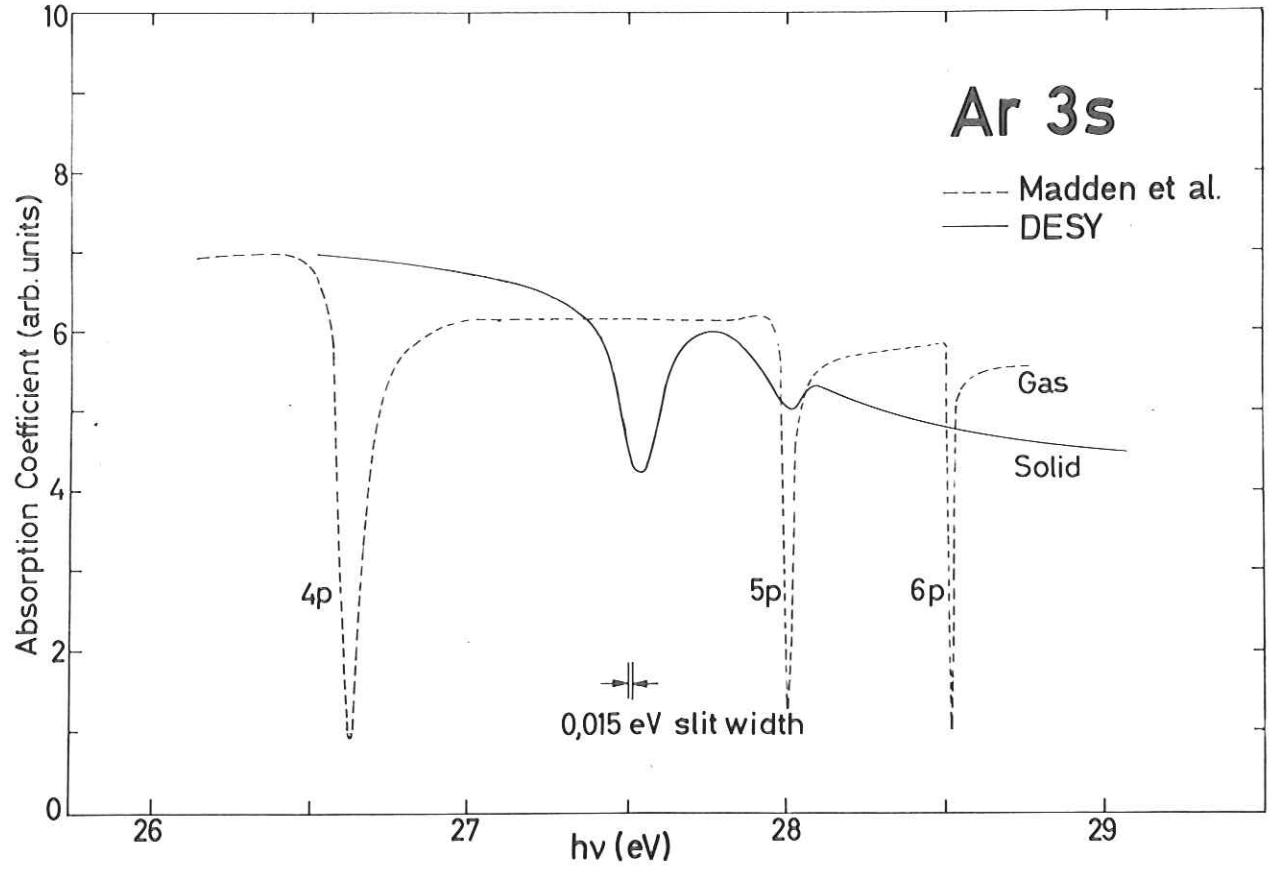

Fig. 23b

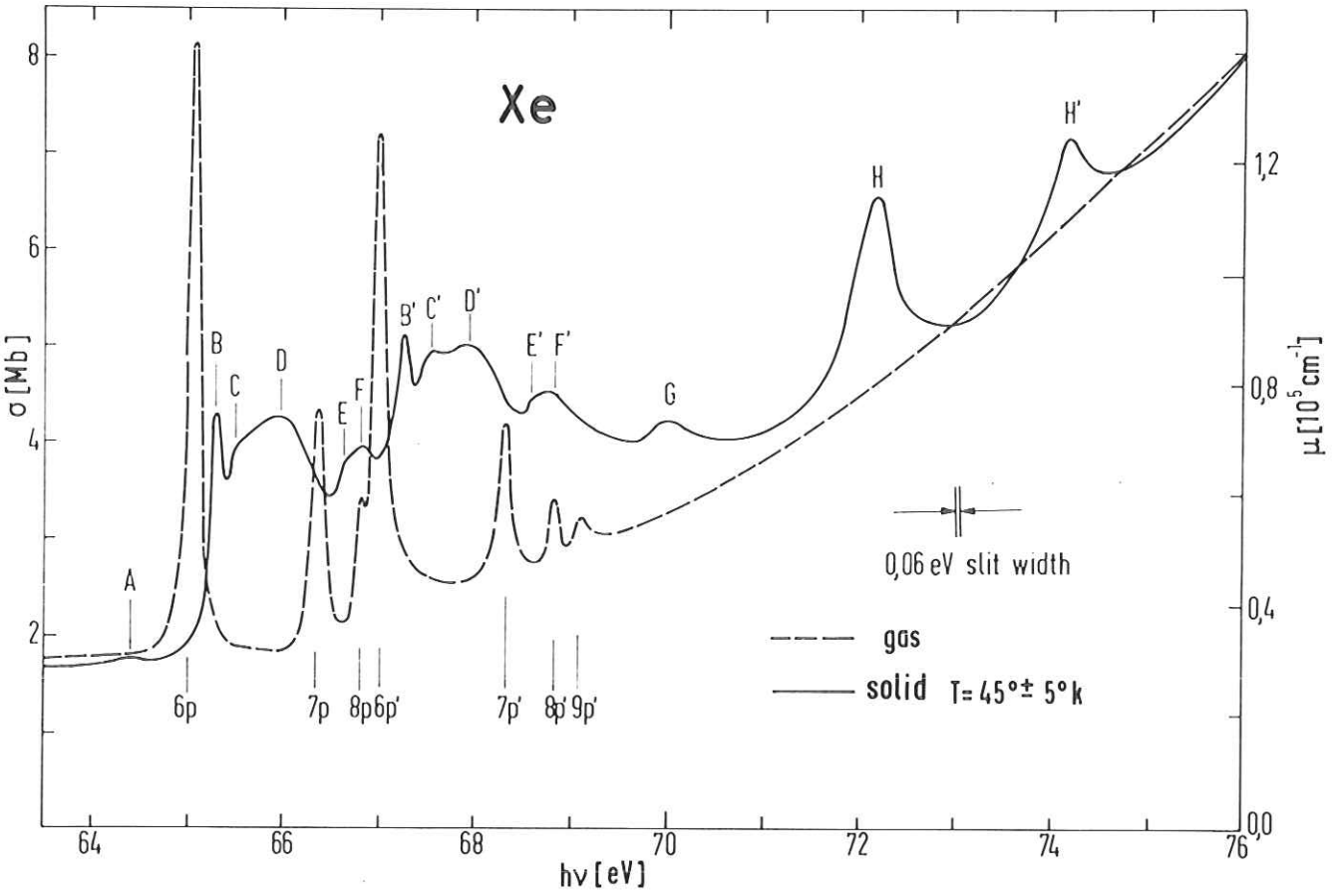

Fig. 25b

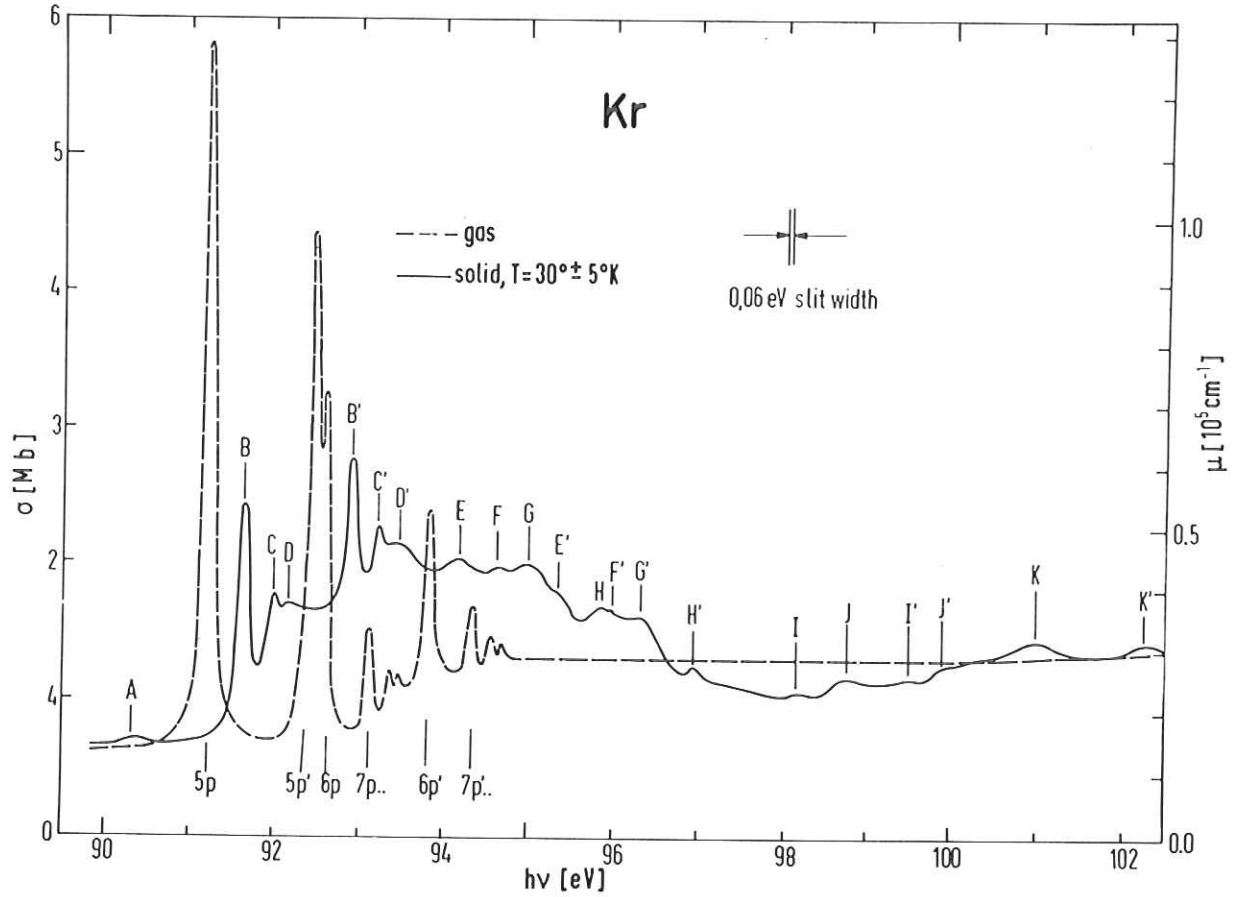

Fig. 25a

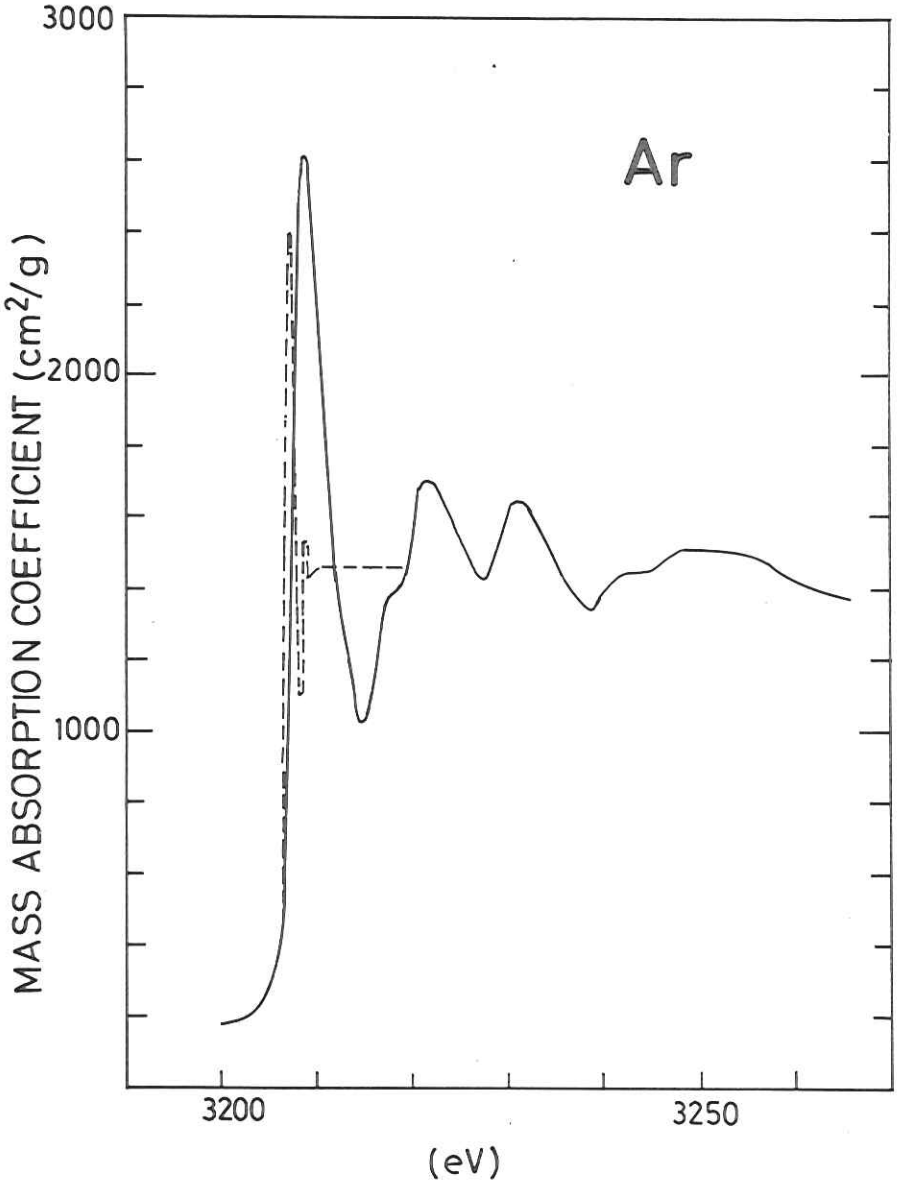

Fig. 26a

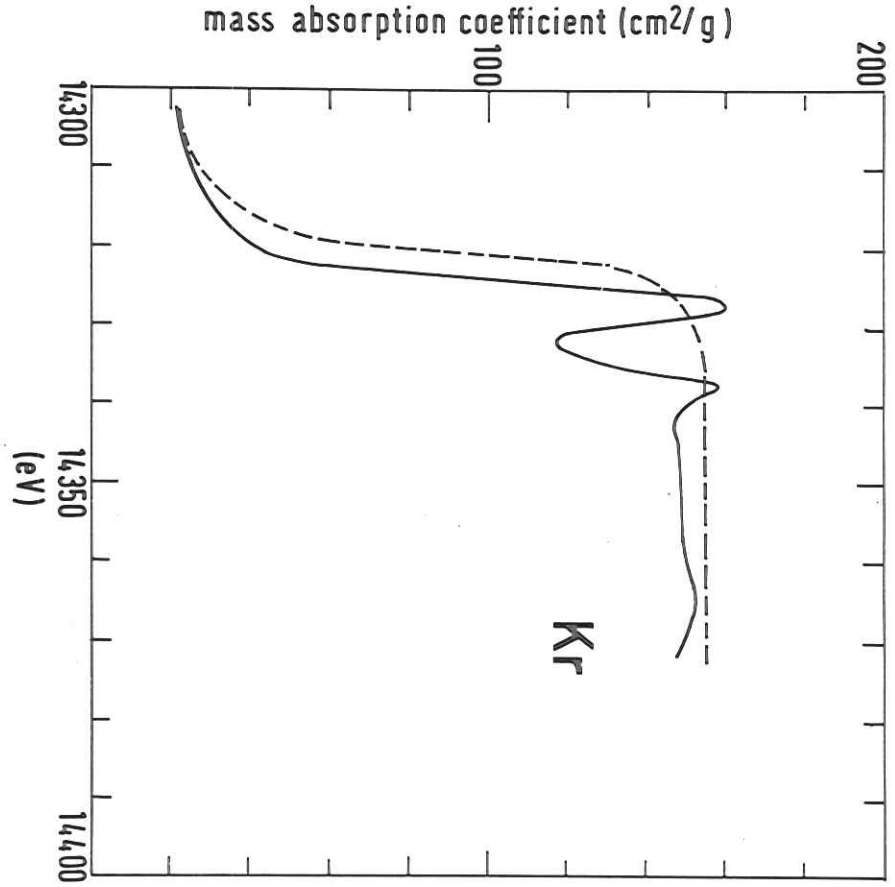

Fig. 26b

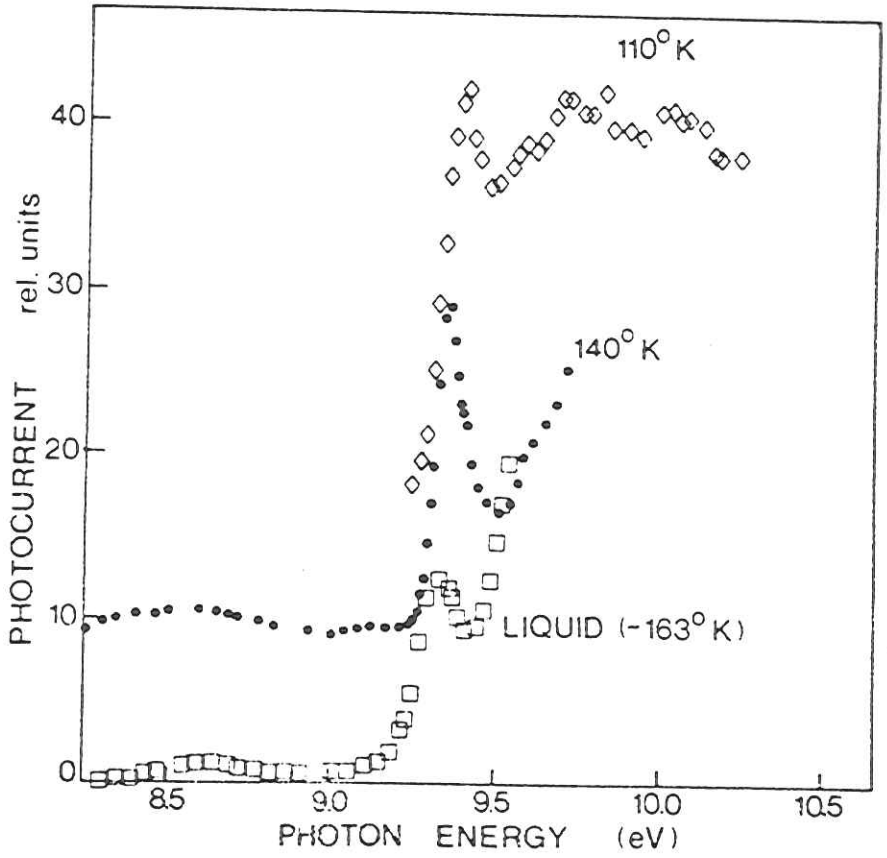
110° K
140° K
LIQUID (-163° K)
PHOTOCURRENT rel. units
PHOTON ENERGY (eV)
0
10
20
30
40
8.5
9.0
9.5
10.0
10.5

Fig. 27

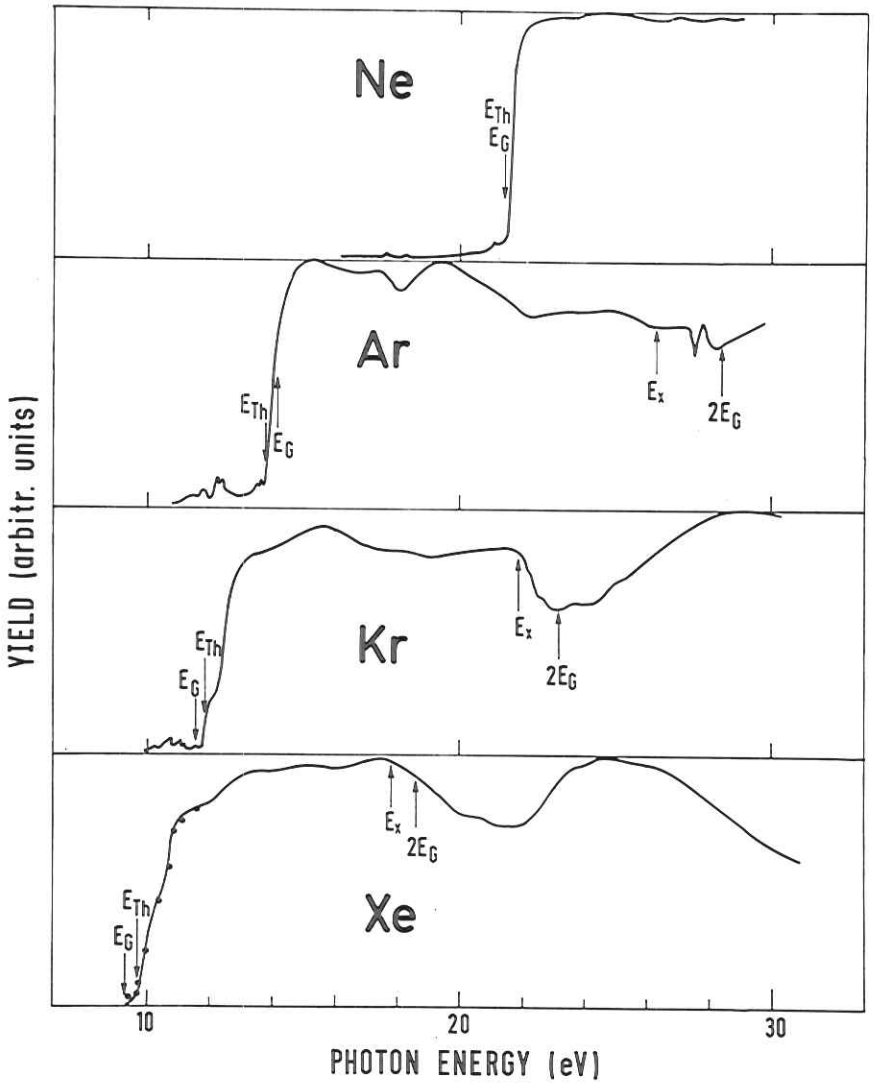
Ne
Ar
Kr
Xe
E_{Th}
E_G
E_x
$2E_G$
YIELD (arbitr. units)
PHOTON ENERGY (eV)
10
20
30

Fig. 28

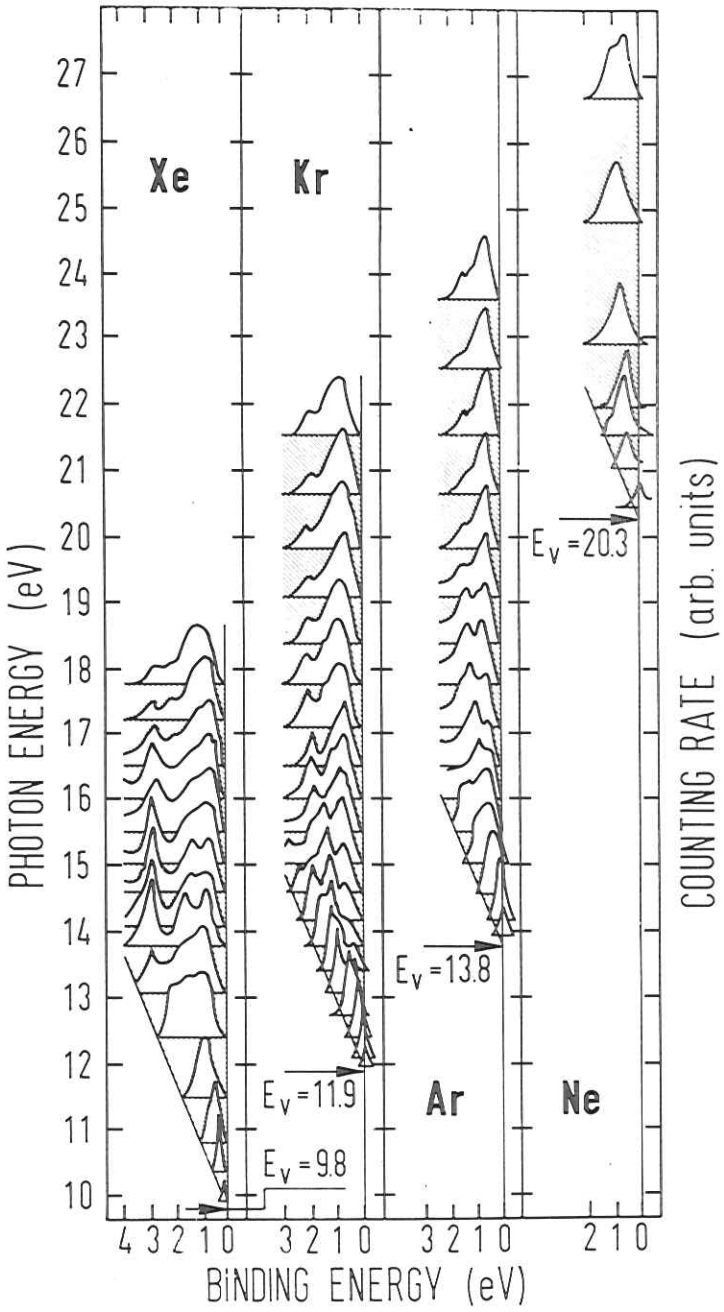
Xe
Kr
Ar
Ne
E_V = 20.3
E_V = 13.8
E_V = 11.9
E_V = 9.8
PHOTON ENERGY (eV)
BINDING ENERGY (eV)
COUNTING RATE (arb. units)

Fig. 29

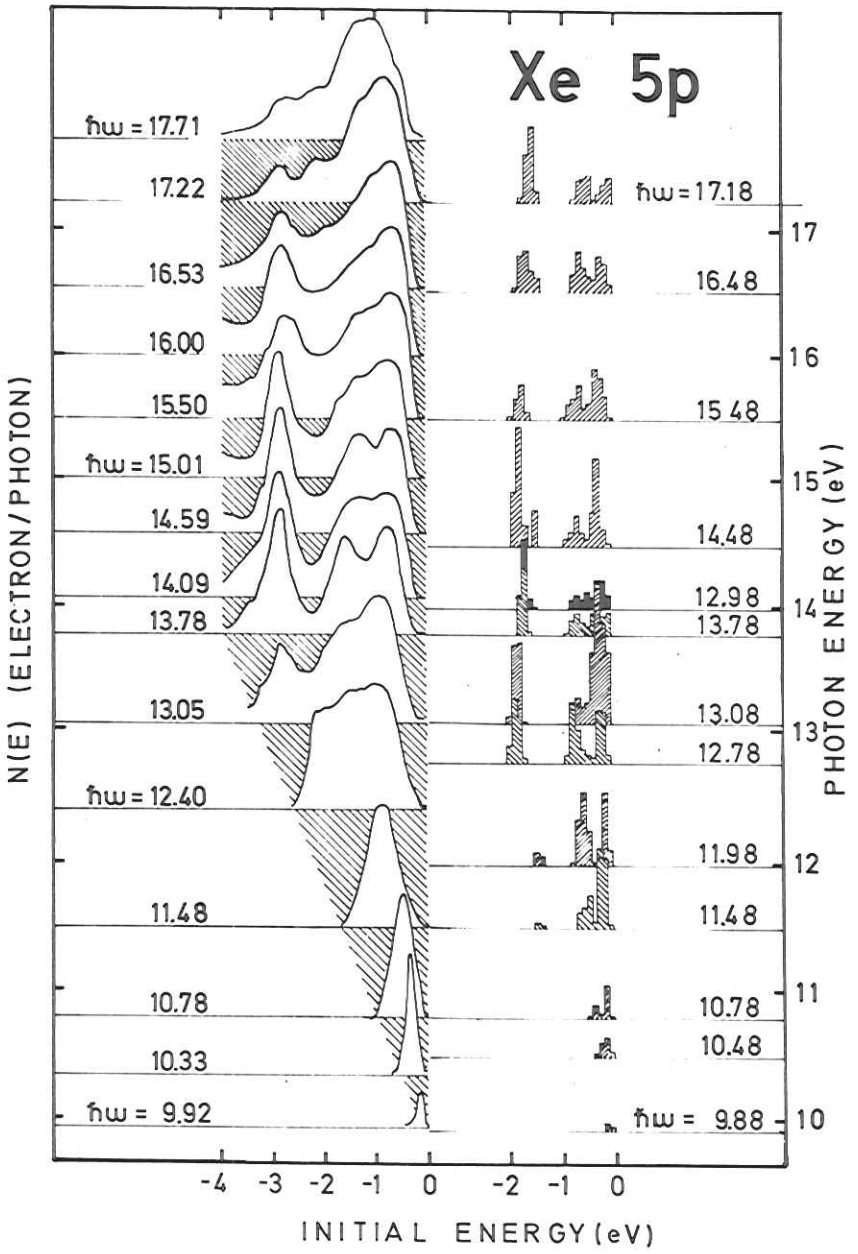
Xe 5p
ħω = 17.71
17.22
16.53
16.00
15.50
ħω = 15.01
14.59
14.09
13.78
13.05
ħω = 12.40
11.48
10.78
10.33
ħω = 9.92
ħω = 17.18
16.48
15.48
14.48
12.98
13.78
13.08
12.78
11.98
11.48
10.78
10.48
ħω = 9.88
N(E) (ELECTRON/PHOTON)
INITIAL ENERGY (eV)
PHOTON ENERGY (eV)

Fig. 30

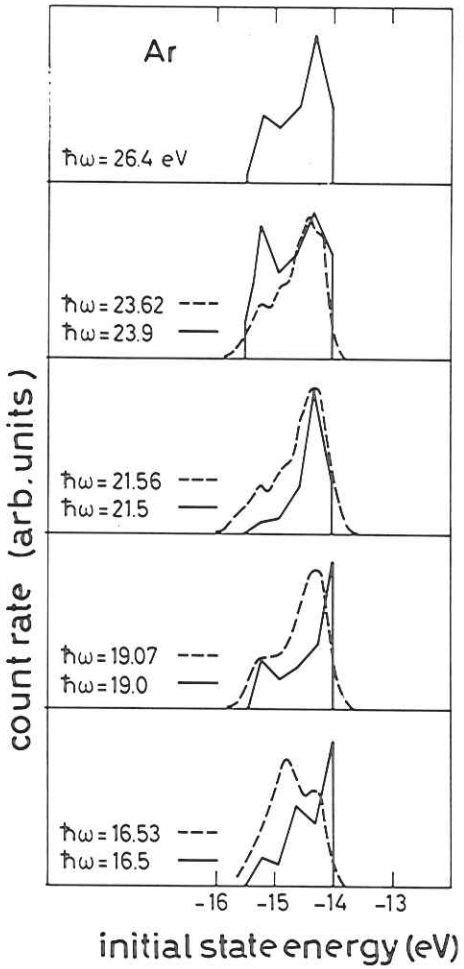
Ar
ħω = 26.4 eV
ħω = 23.62 ---
ħω = 23.9 ——
ħω = 21.56 ---
ħω = 21.5 ——
ħω = 19.07 ---
ħω = 19.0 ——
ħω = 16.53 ---
ħω = 16.5 ——
count rate (arb. units)
-16
-15
-14
-13
initial state energy (eV)

Fig. 31